UNIVERSITÀ POLITECNICA DELLE MARCHE
FACOLTÀ DI INGEGNERIA

Corso di Laurea Magistrale in Ingegneria Informatica e dell'Automazione

STUDY AND SIMULATION OF NGC SYSTEMS FOR BIOMIMETIC ROBOTS

Studio e simulazioni di sistemi NGC
Per robot marini biomorfi

Relatore:
Prof. David Scaradozzi

Candidato:
Waqas Ali Waqar

Primo Correlatore:
Ing. Nicolò Ciuccoli

Secondo Correlatore:
Ing. Daniele Costa

a.a 2019/20220

Abstract

Over the years the interest in research and exploration of the marine environment has led to significant growth in the field of autonomous submarine vehicles. The autonomy of the AUVs depends mainly on two factors: the first consists of a suitable guidance, control and navigation system, while the second factor concerns the efficiency of the propulsion system. Over the past two decades, the improvement of AUVs propulsive performance has been studied and investigated by many researchers, who have concluded that greater propulsive efficiency can be achieved by approximating the tail propulsion system of fish, given that they are highly efficient swimmers. In order to achieve this, biomimetic AUVs have been developed.

This paper reports the work done by the author during the ERASMUS internship at the CRIS (Center for Robotic and Intelligence Systems) department of the University of Limerick. The main aim of this work is to develop a simulation environment, enhanced with a three-dimensional graphical interface, for a biomimetic AUV equipped with a hybrid propulsion system. The simulation environment is implemented in the Simulink software, which provides various toolboxes such as the Virtual Reality Toolbox, that allows to create and interact with dynamic systems in a 3D virtual reality environment.

The second aim of this project is to design and implement a guidance and control system for the robot in the simulator. In particular, the AUV analysed in this work tries to imitate the appearance and approximate the swimming style of a fish belonging to the ostraciiform class and has been called GUIZZO 6.0.

Sommario

Nel corso degli anni l'interesse nella ricerca ed esplorazione dell'ambiente marino ha portato una notevole crescita nel campo dei veicoli sottomarini autonomi (AUV).
L'autonomia degli AUV dipende principalmente da due fattori: il primo consiste nella realizzazione di un sistema di navigazione, guida e controllo adatto, mentre il secondo fattore riguarda l'efficienza del sistema di propulsione.

Negli ultimi due decenni, il miglioramento delle prestazioni propulsive degli AUV è stato oggetto di studio e investigazione di molti ricercatori, i quali sono giunti alla conclusione che una maggiore efficienza propulsiva può essere raggiunta imitando il sistema di propulsione della coda dei pesci, dato che essi sono nuotatori altamente efficienti. Al fine di raggiungere tale obiettivo, sono stati sviluppati AUV biomimetici.

In questo elaborato viene riportato il lavoro svolto dall'autore, durante il periodo di tirocinio ERASMUS presso il dipartimento CRIS (Centre for Robotic and Intelligence Systems) dell' Università di Limerick. Lo scopo principale del progetto consiste nello sviluppare un ambiente di simulazione, rafforzato da una interfaccia grafica tri-dimensionale, per un AUV biomimetico dotato di un sistema di propulsione ibrida. L'ambiente di simulazione viene implementato nel software Simulink, il quale fornisce numerosi toolbox come il Virtual Reality Toolbox che consente di realizzare ed interagire con sistemi dinamici in un ambiente di realtà virtuale 3D.

Il progetto prevede, inoltre, un secondo scopo, ovvero quello di ideare ed implementare nel simulatore un sistema di guida e controllo per il robot. In particolare, l'AUV analizzato in questo lavoro cerca di imitare l'aspetto e approssimare lo stile di nuoto di un pesce appartenente alla classe ostraciiforme ed è stato chiamato GUIZZO 6.0.

Contents

Chapter 1.

Introduction

1.1 Background

In recent years, an increasingly important role in the development and advancement of modern technology has been assumed by control systems. In particular, the growth of navigation, guidance and control systems, applied to solve problems related to the aerospace field, has contributed significantly to the progress achieved in the development of modern systems and control theories.

Early success of these systems soon brought on evident progress in such different areas as industrial production, energy management and in hostile environments such as underwater one.

Navigation, guidance and control of airborne systems have been widely described in the literature; however, little attention has been paid to the issue of guidance and control of autonomous underwater vehicles. Even less interest has been shown if the autonomous underwater vehicle uses a biomimetic propulsion system.

Autonomous underwater vehicles (AUV) have been under development since 1970's. The first AUV was developed at the Applied Physics Laboratory at the University of Washington by Stan Murphy, Bob Francois and Terry Ewar in 1957 [1].

The definition commonly adopted in the nautical field for autonomous underwater vehicle is that of marine systems, independent in terms of power and intelligence [2]. In the last decade, there have been significant advances towards AUV use in operational missions, indeed, an autonomous underwater vehicle can be employed in several applications. For example, the oil and gas industry employ this vehicle to draw detailed maps of the seafloor before the installation of their infrastructures; researchers employ AUVs to acquire images and other type of data in order to document and explore oceans, lakes, underwater sites. Sometimes they have been used to find or inspect the wreckages of missing cruising boats and airplanes.

The level of autonomy achieved by AUVs and their usage are restricted by their performance in two main areas:

- Energy autonomy: The autonomous underwater vehicles have a limited battery power, which gives a limit to the time duration of their tasks; indeed, most of currents vehicles have an autonomy of just a few hours, after that the batteries need to be recharged. In order to reduce power consumption and, thus, increase the vehicle autonomy, AUVs must be provided with efficient propulsive system. A solution to improve propulsion performance of the underwater vehicle can be found in using biomimetic AUVs, which have been thoroughly investigated in the last two decades as a source of efficiency and manoeuvrability enhancement.
- Navigation autonomy: the autonomous underwater vehicles need a reliable and well-integrated navigation, guidance and control system (NGC), in which the guidance is the key element.

1.2 Fish swimming modes

In order to understand how the properties and principals that biomimetic robots must exploit for higher efficiency, it is necessary to understand, firstly, the basic morphological features common to most fish species. This section aims to give a brief introduction about the fundamental swimming mechanism found in nature.

An important role in the evolution of fish is played by two main features of water, which are incompressibility and high density. The first implies that any fish moves the surrounded water during swimming, and vice versa, while the second generates a buoyance force that counterbalance its weight, since the density of marine animal's body is sufficiently close to that of water.

In order to treat fish swimming mechanism, Figure 1.1 shows the terminologies traditionally adopted in the biomimetics field to identify the morphological features of fish.

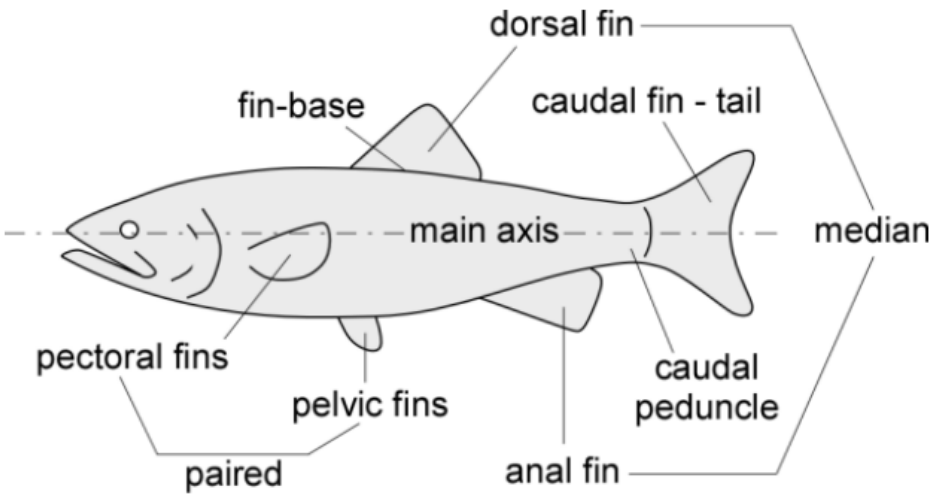

Figure 1.1: Morphological features of fish.

Figure 1.2 displays the forces acting on a swimming fish. These forces can be divided in thrust and resistance force, which act in the horizontal direction, while weight, buoyancy and hydrodynamic lift act in the vertical one. While a fish is swimming forward with a constant speed, according to the momentum conservation principle, enough thrust must be generated to balance the resistance that the fish encounters.

The main mechanisms by which transfer of momentum between the fish and surrounding water takes place are via drag, lift and acceleration reaction forces. Swimming drag consists of: skin friction between the fish and the boundary layer of water (viscous or friction drag),

pressure formed in pushing the water aside for the fish to pass (form drag) and energy loss in the vortices formed by the caudal and pectoral fins as they generate lift or thrust (vortex or induced drag). The latter two components can be jointly described as pressure drag. Lift forces are exerted on the object in a direction perpendicular to the flow direction and they originate whenever the pressure on one side of the object is greater than on the opposite side. Acceleration reaction is the additional inertial force required to accelerate the water close to a body, when the latter is in unsteady motion; the mass of water which is effectively accelerated due to this inertial force is called added mass.

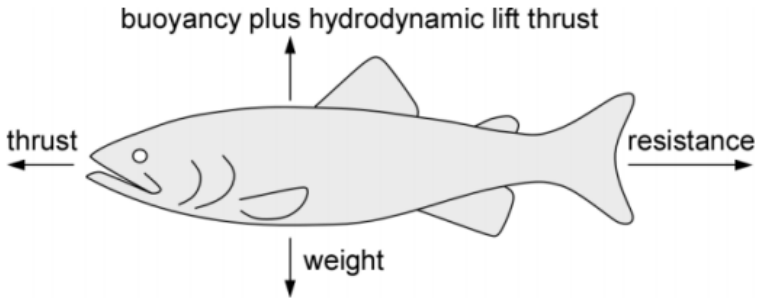

Figure 1.2: Forces acting on a swimming fish.

Drag, lift and added mass forces contribution in terms of thrust generation depends from the flow Reynolds number which is a dimensionless quantity used to predict the flow patterns. This parameter stands for the ratio of inertial over viscous forces and it is defined as:

$$Re = \frac{LU}{v}$$

Where L is a characteristic length (of either the fish body or the propulsor), U is the swimming velocity and v is the kinematic viscosity of water. For Adult fish swimming, the Reynolds number varies between 10^3 and 10^5 [3]. Figure 1.3 shows the relative contribution of the momentum transfer mechanism for swimming vertebrates, as function of Reynolds number. The shaded area corresponds to the range of adult fish swimming.

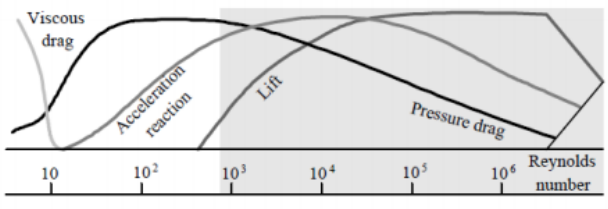

Figure 1.3: Magnitude of swimming forces as a function of the Reynolds number [3].

A classification widely used to diversify the motion of fish is based on body and/or caudal fin (BCF) locomotion and paired and/or median fin (PMF). The first refers to a swimming mode in which the fish bends its body into a backward propulsive wave, which extends to its tail up to its caudal fin. The second is like the BCF locomotion, but the bending motion is confined to their median and paired fins.

Both BCF and PMF locomotion mechanism are further classified according to the type of movement observed in the propulsive structure. The motion is said to be undulatory if a waveform is visible along the propulsive structure, while the motion is oscillatory if thrust is generated by the only oscillation about a fixed point of the propulsive structure.

The optimum design for fish morphology corresponding to a specialization for accelerating, cruising, and manoeuvring have been identified by Webb [4], as show in Figure 1.4.

However, fish are able to use both of the swimming mechanism analysed above, in fact, the experience gained in one of the two swimming modes does not exclude the possibility of using the other: indeed, many fish employ MPF locomotion for manoeuvring and stabilization and then switch to BFC thrust generation to cover long distances at constant speed.

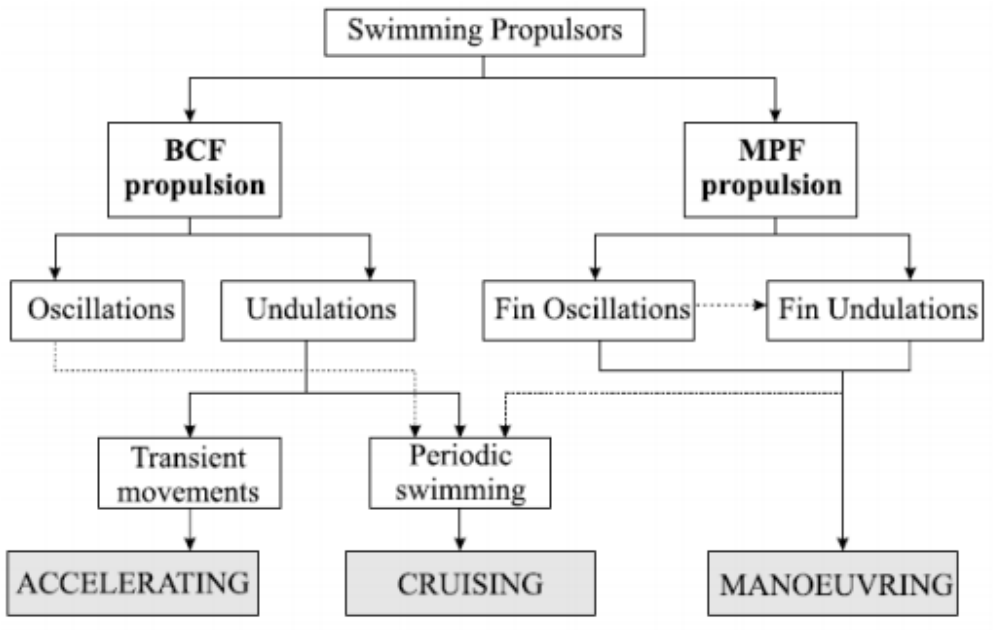

Figure 1.4: Relation between swimming locomotion and swimming functions [4].

A further classification of BCF and MPF swimmers, according to the portion of the body involved in the propulsive wave is shown in Figure 1.5, where the shade areas contribute to thrust generation.

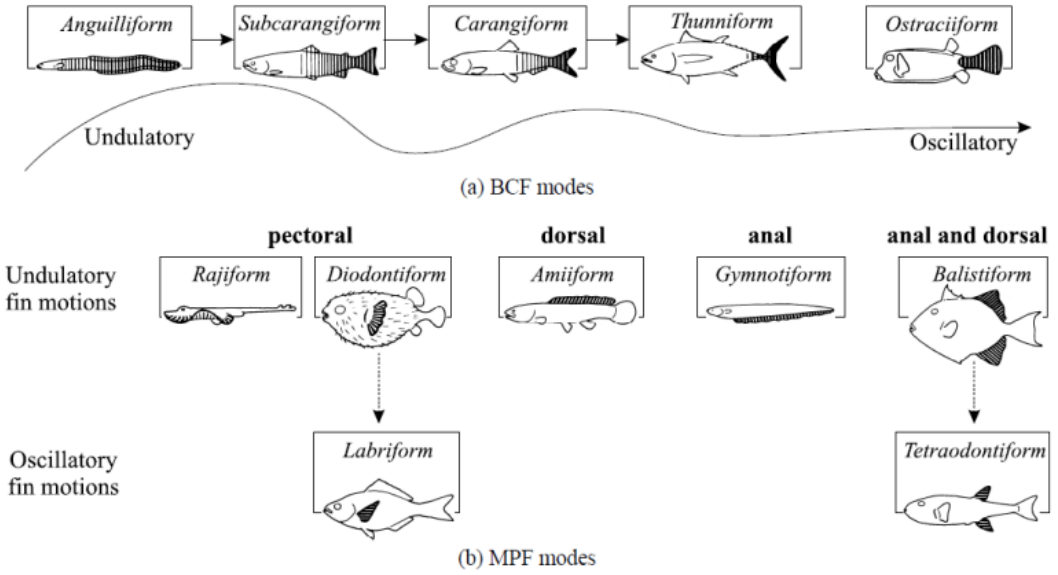

Figure 1.5: Swimming modes associated with BCF (a) propulsion and MPF (b) propulsion.

1.2.1 MPF propulsion

Undulating fins are used by a lot of fish as auxiliary propellers, as well for motion stabilization and manoeuvring. Although median and paired fins can be employed as sole source for generally slow cruising. In general fish that adopt median-pectoral fin locomotion mode can be distinguished into the following classes:

- Rajiform: the thrust generation involves the passing of the vertical undulations along the pectoral fins that are large, triangular-shaped and flexible. The amplitude of undulations increases from the anterior part to the fin tip and then tapers again towards the rear. The fins show also a flapping discipline.

- Diodontiform: the propulsion is achieved by passing undulations through the broad pectoral fins. Up to two full wavelengths may be visible across the fins, while undulations are often combined with flapping oscillating motions of dorsal and anal fins for thrust generation at higher speeds. These swimmers are not migratory, they swim into shallow water reefs.

- Amiiform: swimming is by undulations of a long-based dorsal fin, while body axis is in many cases held straight when swimming. The anal and caudal fins are missing, while the dorsal fin extends along most of the body length and exhibits many fin-rays. These swimmers are not particularly fast, a decent agility is exhibited. They are able to perform tight turning and multi-directional locomotion.

- Gymnotiform: is considered the upside-down equivalent of amiiform mode, since propulsion is reached by undulations of long-based anal fin. The dorsal fin is not present. Thanks to many individual ribs they have the complete control of the fin on the entire length because each rib has its own set of agonist and antagonist muscles. They are not migratory swimmers, due to the small body and the vulnerability to larger predators outside hunting zones.

- Balistiform: both the anal and dorsal fins undulate to generate the propulsion forces. The median fins are usually inclined relative to each other's, while the body is usually flat and compressed laterally. The caudal fin is used to enhance endurance. These swimmers are not migratory, they swim in shallow reefs.

1.2.2 BCF propulsion

In undulatory BCF modes, presented by Breder in [5], the transmission of wave take place along the fish body in the opposite direction with respect to the swimming direction. The speed of the wave must be greater than the overall forward velocity. Figure 1.6 shows the four undulatory BCF modes; The difference among the locomotion modes are related to the amplitude of the wavelength, the fraction of the body bent by the wave passage itself and the thrust generating force type. Two thrust generation mechanism have been recognized: the added-mass method, which is mainly employed by *anguilliform*, *subcarangiform*, *carangiform* model, and a lift-based (vorticity) method, which is mainly used by *thunniform* mode.

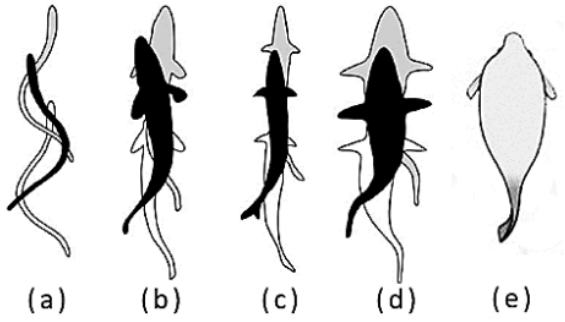

Figure 1.6: Visual diagrams to depict the body motion undulation to realize a tail oscillation. (a) Anguilliform, (b) Subcarangiform, (c) Carangiform, (d) Thunniform, (e) Ostraciiform [5].

- Anguilliform: the whole body of the fish is bent in large-amplitude undulations. Since at least a complete wavelength is always present along the fish body, the yawing moment is usually neglectable, along with any tendencies to recoil. The same features feature allows these swimmers to move backward by means of an inversion of direction of the propulsive wave.

- Sub-carangiform and Carangiform: swimmers employ the same mechanism, but with different percentage of the body involved in the undulation, i.e. one half for the former, and one third for the latter. Thus, Carangiform swimmers have a stiffer body, exhibiting a lower turning and accelerating capabilities

- Thunniform locomotion: is the most efficient BCF mode, usually described as the apex of swimming evolution. The thrust is generated thanks the caudal fin (more than 90%) through lift mechanism, the rest is produced by the added mass effect associated with the lateral undulations of the area near the peduncle. This mechanism allows the thunniform swimmers to keep high cruising speeds for long time. The slender, streamlined body the thunniform swimmers is able to minimize the drag while moving forward, while the stiff, crescent-moon shape of the caudal fin minimizes the induced drag due to lift generation

- Ostraciiform locomotion it the only purely oscillatory BCF mode. The caudal fin oscillates in a pendulum-like discipline, while the body remains rather rigid. Fish

using this mode are usually encased in inflexible bodies and forage their complex habitat by means of MPF propulsion.

A consideration must be made about fish adopting the BCF swimming mode. They leave a wake behind the tail which structure is composed by a staggered array of trailing vortices sign; these vortices have a rotational direction opposite to the one exhibited by vortices inside the drag-producing Karman vortex street wake, which propagates behind bluff objects for a specific range of the Reynolds number (Figure 1.7, (b) and (a) respectively). To characterize oscillation flow mechanism, in fluid dynamic a dimensionless parameter is used, namely the *Strouhal* number St. For a BCF swimmer it is defined as:

$$St = \frac{fA}{U}$$

Where A is the width of the wake, U the average swimming speed and f is the tail-beat frequency (Figure 1.7 (c)).

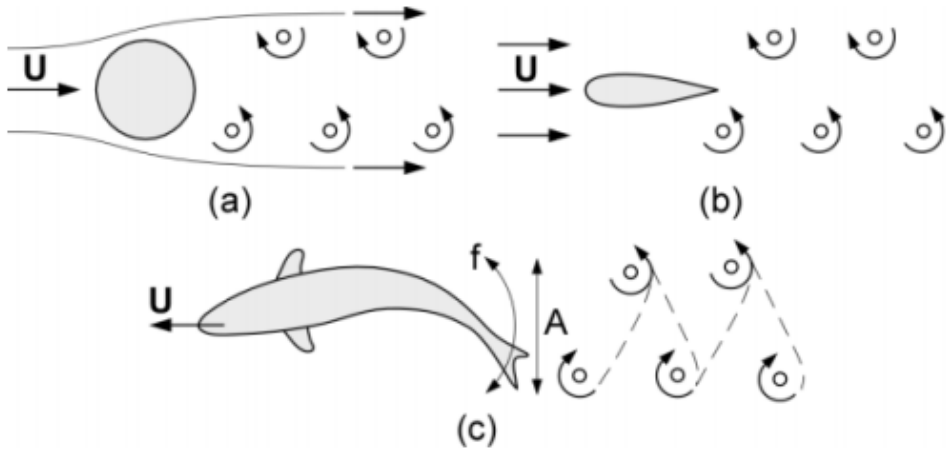

Figure 1.7: Wake structure: (a) bluff object, (b) thrust-generating foil. (c) Parameters of the Strouhal number.

1.3 State of art

A summary of the studies and the experimental results achieved so far in the development of AUV biomimetic vehicles is reported in this section (recovered from [6]). A particular attention has been paid in the motivation behind the choice of the source of bioinspiration and in the description of the biomimetic robot's propulsion system.

1.3.1 BCF swimmers

RoboTuna [7], designed at the Massachusetts Institute of Technology (MIT) can be considered as the ancestry of almost all biomimetic swimmers. In order to better understand the mechanism involved in forward BCF swimming, the robot was built as a 1.2 meters towing-tank replica of a real tuna.

Figure 1.8: RoboTuna, 1994, MIT Museum.

The reason behind the choice of tuna fish is that it is one of the fastest-swimming fish in nature and it is capable of long period of swimming at high speeds. Another important factor for which it was decided to take a tuna as a biological inspiration, is that the different subspecies of tuna presents a similar morphology, although there are differences in size. This implies the easy scalability of any design for future use as an AUV and that it was thought

that the tuna would allow a large payload because a large portion of the body would have remained rigid, thanks to the thunniform swimming mode.
A genetic algorithm was used to control the RoboTuna six links, in order to mimic the thunniform locomotion and improve efficiency.

Following the success of the RoboTuna project, MIT in partnership with Draper Laboratories developed the so-called vorticity-controlled unmanned underwater vehicle (VCUUV) using many of the techniques developed during the RoboTuna project [8]. The VCUUV was designed to be autonomous and have an on-board power supply. Once again, the morphology of a real blue fin tuna was used. However, this time the shape was scaled up to 2.4 metres in length, comparable in size with conventional AUVs in use at the time. The VCUUV's tail movement came from a simplified five-vertebrae backbone, with the four joints actively controlled by a closed-loop hydraulic system. The backbone, in turn, acted on a spline-and-rib structure. Like RoboTuna, rather than trying to seal a flexible structure, the tail was allowed to be flooded.

A direct application of the RoboTuna design can be seen in Boston Engineering's GhostSwimmer, which is a tuna based AUV, developed under commission from the US government, with advice from Barrett, for use in harbour monitoring [9].

The next generation of robotic swimmers to emerge from MIT was RoboPike [10]. The pike was chosen as a source of bioinspiration because of the rapid manoeuvring and acceleration abilities it demonstrates in nature. RoboPike's tail movement came from a further simplified four-vertebrae backbone, with the three joints actively controlled by tendons driven by waterproofed brushless d.c. servomotors mounted in the midsection of the body, which, together with the tail, was flooded. RoboPike's forward section was constructed as a single pressure vessel housing batteries and electronic subsystems.
The Japanese National Maritime Research Institute (NMRI) developed a series of further simplified link-based robotic fish, including a three-link 34 cm robotic sea bream denoted PF-300 which was built to study the turning performance [11]. The sea bream was selected as a source of bioinspiration because in nature its large side profile area and carangiform swimming style makes it an excellent fast-turning fish. The two joints were actuated directly by brushless d.c. servomotors housed in small pressure vessels; the actuation mechanism penetrated the pressure vessel through a corrugated waterproof boot. The tail itself was left

in a naked skeletal state, as it was thought that the majority of the propulsive force would be generated by the caudal fin, accurate representation of the rest of the body morphology was thought to be unnecessary.
Subsequent robot swimmers developed by NMRI, include the 65 cm four-link PF-600, the 70 cm four link PF-700, the 97 cm three-link UPF-2001, the 26 cm two-link PF-200, and the 57 cm three-link PF-550 [12]. Like PF-300, all the subsequent robot swimmers to emerge from NMRI relied on radio communication remote control, limiting them to operations on or near the surface. All were constructed with open skeletal joints; however, effort was made to approximate the profile of real fish tails by attaching moulded sections to the tail vertebra.

The Tokyo Institute of Technology developed two robotic dolphins aimed as prototypes toward the design of a biomimetically propelled AUV [13]. The first had a pneumatic actuation system, and the second a d.c. servomotor. Both robots had a three-vertebrae design 1.5 metres in length with one active joint at the top of the tail, and a passive joint at the caudal fin. By varying the stiffness of the passive joint, it was found that a wide variety of tail beat kinematics could be achieved [14].

Developers at the Istanbul Technical University also developed a robotic dolphin AUV prototype with the hope of improving upon the propulsion efficiency found in conventional AUVs [15]. The Istanbul dolphin had a four-vertebrae construction with each of the three joints actuated by an opposing bellows-type pneumatic system. The flexing tail section was covered in a waterproof membrane supported by a flexible structure to allow the tail joints to remain dry. The caudal fin was made from cast silicon in order to mimic the flexibility of a real dolphin's caudal fin.
In contrast, the University of Essex has developed a series of multi-link carangiform and subcarangiform robot swimmers [16], the latest of which, namely G9, is based on a four-vertebrae tail structure constructed using stereolithography apparatus resin. The three joints are actively controlled by three powerful d.c. servomotors [17]. In this case no specific fish was chosen as a source of bioinspiration, instead an attempt was made to capture the more generalized principles of fish morphology.

The Bei hang University Robotics Institute also developed a series of robotic fish based on nonspecific bioinspired morphology for use as unmanned underwater vehicles. SPC-II and SPC-III had a common two-joint BCF type propulsion module. The two joints were each

actuated by a 150W brushless d.c. motor, located within a sealed part of the vehicle. SPC-II had a roughly fish-like morphology designed with a large side profile area for rapid turning ability, with an overall length of 1.2 metres. Despite having a maximum depth rating of only 5 metres the SPC-II proved useful as a visual assistant for underwater archaeology [18]. SPC-III was constructed in many ways like a traditional AUV [19]. However, in place of the propeller, the two-joint BCF tail was attached.

Following on from a study that demonstrated that dead fish exposed to a harmonic stimulus could produce a forward-swimming gait, researchers at MIT have developed a simplified compliant body method for generating BCF swimming gaits in small biomimetic AUVs suitable for multi-agent survey tasks. Reports indicate that these simplified designs have proven to be fairly robust, giving good longevity. A simple d.c.-servomotor-driven mechanism embedded into a moulded silicon body can produce a travelling body wave if activated harmonically. It was found that, by doping the silicon, the body could be given a different elastic modulus and hence produce different propulsive kinematics.

In 2014, at the Essex University, *iSplash-II* [20] (Figure 1.9) was developed. It was the first robotic fish capable of outperforming real carangiform fish in terms of average maximum velocity and endurance, the duration that top speed is maintained. The lateral and thrust forces were optimized around the center of mass, generating accurate kinematic displacements and greatly increasing the magnitude of added mass.

Figure 1.9: Picture of iSplash-II.

One of the recent works of MIT is the development of the Soft Robotic Fish SoFi [21]. This robot is characterized by a hydraulic propulsion system that can perform low-to-high frequency tail actuation to achieve a range of swimming speeds and can execute turn by

adjusting the baseline deflection around which the tail undulates. The swimming mode is obtained as follows: the motor pumps water into two balloon-like chambers in the fish's tail that operate like a set of pistons in an engine. As one chamber expands, it bends and flexes to one side; when the actuators push water to the other channel, that one bends and flexes in the other direction.

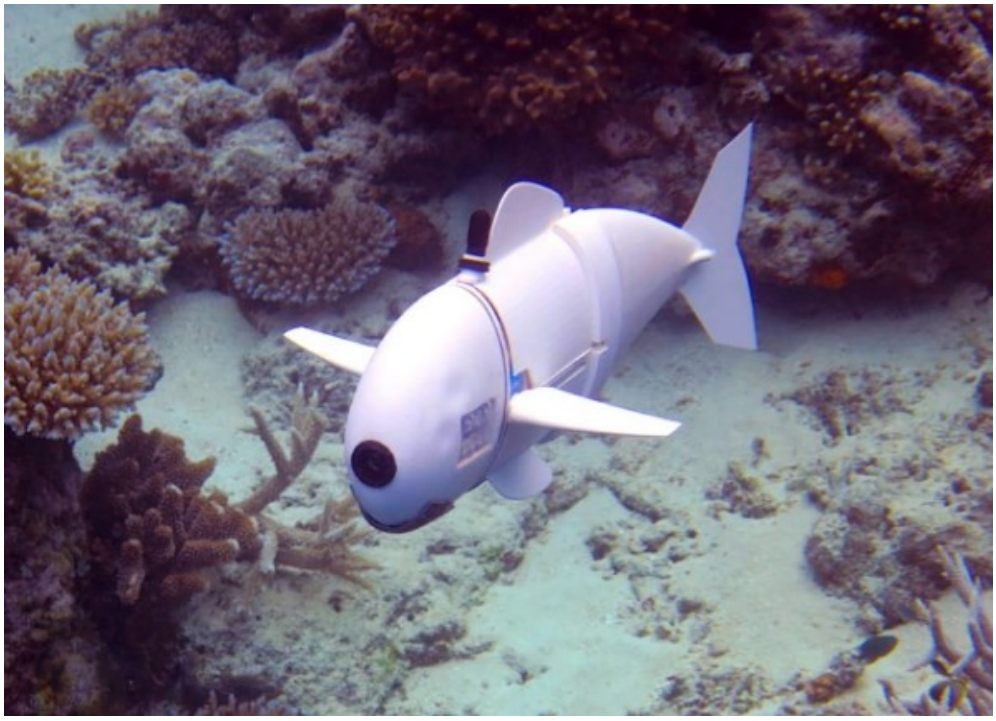

Figure 1.10: Picture of Soft Robotic Fish SoFi.

1.3.2 MPF swimmers

The excellent manoeuvrability and station-keeping ability of PMF swimmers in nature inspired Kato [22] at Tokai University to develop the robotic black bass. The black bass was chosen because in nature it is a species known to use pectoral fins for low-speed locomotion and station-keeping manoeuvres. Two servomotors for each pectoral fin allow the fins to be actuated on the yaw axis and the pitch axis respectively. By controlling the relative phase and magnitude of yaw and pitch oscillations, manoeuvring forces in the full six degrees of freedom could be achieved. The black bass project could be considered to be the equivalent for biomimetic PMF locomotion to what RoboTuna was for biomimetic BCF locomotion.

AQUA was a six-finned robot swimmer developed at McGill University [23], shown in Figure 1.11 The swimming gait was roughly based on Ostraciiform swimming, with the six

fins only actuated on the pitch axis and shaped more like flippers than wings. The AQUA project demonstrated that, by using multiple simple single-axis actuated flippers, heave, surge, pitch, roll, and yaw motions can be achieved.

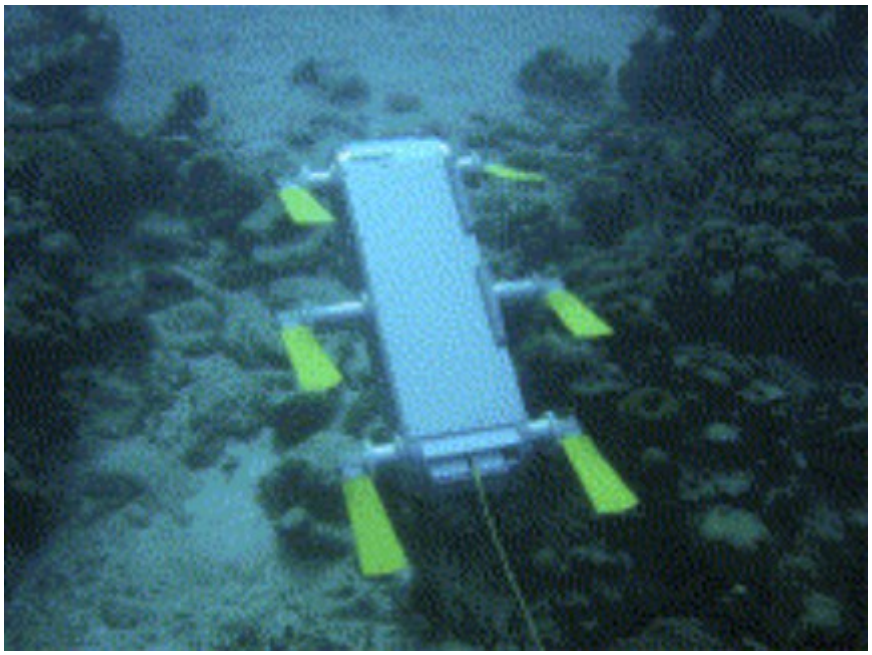

Figure 1.11: The hexapod underwater robot AQUA.

MIT researchers have also developed a multipaired fin swimming AUV [24]. Based roughly on the morphology of a sea turtle, MIT's RoboTurtle was a four-finned labriform-type swimmer. For simplicity of expansion, RoboTurtle's fins were constructed as self-contained modules [25]. Each module contained a 190 W d.c. brushed motor to provide actuation in roll, and a 15 W d.c. brushed motor to provide motion in pitch. Like the robotic black bass, manoeuvring forces were controlled by altering the phase and amplitude of oscillations.

In the commercial sector, Festo has developed manta-ray-based swimmer–glider AUVs, the AquaRay [26]. It uses a powerful hydraulic actuation system to control its wings, which have a 96 cm span. Festo have gone on to use the fin ray effect in their penguin-inspired AUVs. Festo's AquaPenguin uses two pectoral fins in a labriform mode for propulsion. Both fins are driven in the roll plane by a single shared d.c. motor, with mechanical gearing to give a synchronized roll oscillation; on each fin, pitch control is achieved using a dedicated d.c. servomotor.

Both Festo's biomimetic AUVs are shown in Figure 1.12.

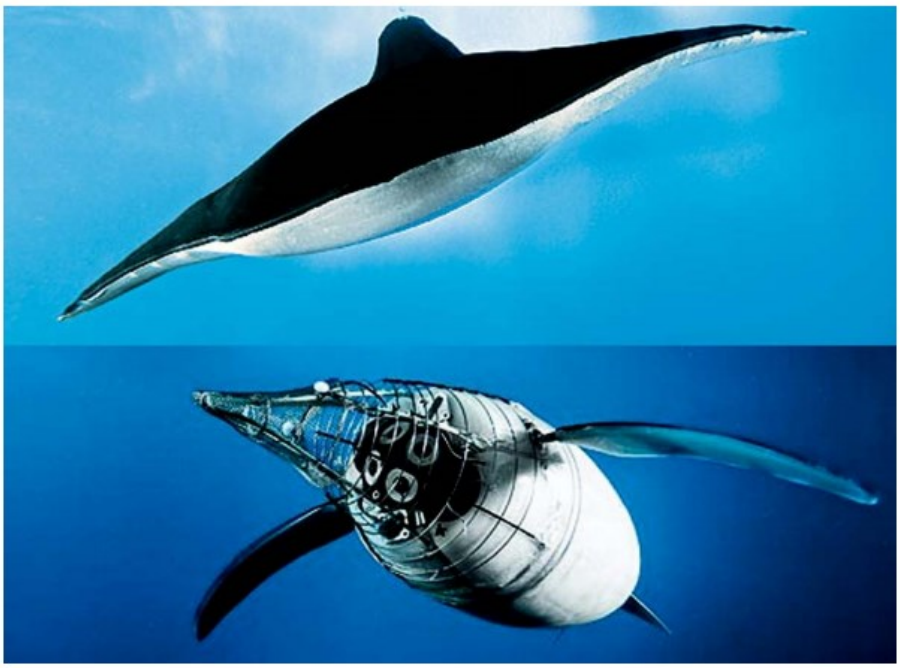

Figure 1.12: Pictures of Festo's AquaRay (top) and Festo's AquaPenguin without the outer skin (bottom).

Another manta-ray-based swimmer–glider AUVs have been developed in the commercial sector by EvoLogics. The Subsea glider is available in a variety of sizes from 1.5m up to 3.5m wingspan and incorporates a buoyancy-driven glider mechanism and a hydro-jet propulsion system for precision manoeuvring as well as the ray-like swimming motion.

1.3.3 Combined BCF and PMF swimmers

Having developed both fast efficient BCF swimming and precision-stable PMF swimming mechanisms, the natural logical progression is to combine both to create a versatile AUV platform. Although several BCF swimming robots have incorporated actuated pectoral fins for vertical lift generation, there have been relatively few attempts to incorporate more sophisticated pectoral fin manoeuvring systems into BCF swimmers.

Peking University has been developing a 1.2 metres robotic dolphin, which combines BCF and PMF swimming. The BCF motion comes from a novel adjustable amplitude Scotch yoke

mechanism driven by a 150 W d.c. brush motor, which drives the tail section [27], and a 20 W d.c. servomotor, which actively controls the caudal fin.
The PMF motion comes from pectoral fin modules, which are similar to those used on the RoboTurtle, and enable the robotic dolphin to perform station keeping and reversing manoeuvres [28].

Taiwan University's Biomimetic Autonomous Underwater Vehicle (BAUV) is a 2.4m biologically inspired swimming robot that incorporates a three-vertebrae BCF swimming mechanism, with two pectoral fins actuated in roll and pitch, to provide both high-speed BCF swimming with PMF precision manoeuvring [29].

Developers at the Chinese Academy of Science Beijing have developed a 78 cm biomimetic swimmer that uses a novel mechanical linkage system similar to that used in UPF-2001 to derive actuated control over two links from a single d.c. motor to provide BCF propulsion [30]. PMF manoeuvring comes from two pectoral fins driven by a three-motor arrangement similar to that found in Festo's AquaPenguin, giving active roll and pitch control for labriform locomotion.

1.4 Objective of the thesis

The design of a biomimetic propulsion system for an autonomous underwater vehicle tries to accomplish the task of increasing the efficiency of the propulsion system, thus decreasing the problem of the limitation of battery power.

In this thesis the design of a hybrid biomimetic robot is presented. The source of bio-inspiration of the robot is that of a fish swimming in BCF mode, however, the biomimetic robot is equipped by a hybrid propulsion system. In fact, it features both bio-inspired thruster, which drives the fins, and traditional thruster used by AUVs, that is, screw propeller.

The purpose of using a hybrid propulsion system is purely academic. The adoption of this solution allows to better analyse the efficiency, in terms of energy consumption, by the two types of propulsion systems proposed.

The main task of this work is to provide a simulation environment for the biomimetic robot with hybrid propulsion system.

The simulator is built in Simulink environment and is characterized by a 3D graphic interface, developed using the Virtual Reality Toolbox, which is a solution for viewing and interacting with dynamic systems in a three-dimensional virtual reality environment, defined using Virtual Reality Modelling Language (VRML).

Furthermore, this thesis presents a second task, that is the implementation, in the simulator, of a suitable guidance and control system for the navigation of the biomimetic robot.

- Control system: The first thing analysed is the control system, which has the task of making the robotic fish reach and maintain the desired reference. Control system must manage the two propulsion systems described above and to do this, it is necessary to use a good control strategy.

- Guidance system: After the implementation of a suitable control system, the next step is the implementation of the guidance system. The guidance system designed uses the Line of Sight (LOS) algorithm to elaborate the right heading, which is supposed to feed the steering control system, in order to reach the desired waypoint.

1.5 Thesis outline

The first part of this work was the design and development of the robotic fish prototype. Chapter 2 presents a brief overview of the robotic fish different version of prototypes up to the hybrid version, named GUIZZO 6.0; after that, the chapter describes hybrid robot's hardware in detail.

The development of the mathematical model is described in Chapter 3. This model was obtained considering the robot's body as a cylinder od radius $R$and length L. Furthermore, the non-linear mathematical model has been described in its vectorial representation, in six degrees of freedom. This chapter describes the GUIZZO 6.0 dynamics kinematics and propulsion system, then the implementation of the mathematical model in Simulink is reported.

Chapter 4 presents the navigation, guidance and control system implemented for the vehicle. Firstly, this chapter describes, in theory, NGC systems used for autonomous underwater vehicle focusing on the LOS guidance law. Secondly, the NGC system implemented for the biomimetic robotic fish is presented, focusing on the control strategies implemented. Finally, the implementation of this system in Simulink environment and the simulation results are given.

The development of the virtual underwater world for the vehicle is reported in Chapter 5. This chapter focuses on how the three-dimensional graphical interface was developed using the Virtual Reality Toolbox; and it shows the VRML built for underwater environment and for GUIZZO 6.0.

Finally, chapter 6 presents the conclusions that have been drawn from this work along with a brief overview of how the results compare with the main aims and objectives previously set out in this introduction. Possible future developments are outlined as well.

Chapter 2.

The GUIZZO 6.0 Robotic Fish

The previous chapter introduced the concept of autonomous underwater vehicle, focusing on their propulsion system and how the latter may be improved in terms of efficiency, thanks to the employment of biomimetic robots.

The aims of this project, as previously mentioned, was the development of a simulation environment, based on three-dimensional graphical interface, and the design of a suitable NGC system for a biomimetic AUV. The autonomous underwater vehicle in question is the biomimetic robotic fish GUIZZO 6.0. Therefore, before proceeding with the exposure of the work, GUIZZO 6.0 will be described.

This chapter is divided in two section:

- GUIZZO 6.0 is included in the class of prototypes developed by a group of researchers, professors and students of Università Politecnica delle Marche (UNIPM), for the OpenFISH.science project, founded by the Lab4Dive project. In the first section, the series of hybrid biomimetic underwater robots developed before GUIZZO 6.0 will be reported.
- Second section describes the 3D Model of GUIZZO 6.0. This model was imported as a .wrl format file and was used for the virtual reality world of the simulator.

2.1 From BRAVe to GUIZZO 6.0

Before describing the robotic fish on which the navigation, guidance and control system has been implemented, in this section, the prototypes of hybrid biomimetic robot, previously developed, will be reported. All these prototypes are ostraciiform swimming robot and presents a similar hybrid propulsion system. The evolution of these versions of robotic fish lead to realization of GUIZZO 6.0 design.

2.1.1 BRAVe prototype

The first prototype was named BRAVe [31], which stand for Biomimetic Research Autonomous Vehicle; BRAVe has been presented on the occasion of Student Autonomous Underwater Challenge – Europe (SAUCE-E), at the Centre of Maritime Research and Experimentation (CMRE) at La Spezia, Italy, where it has won the Innovation Award. BRAVe architecture consists of three-compartment assembly with a waterproofing case, a battery pack, and a wired communication device designed to connect the various modules. The case is a cylindrical pressure hull enclosed between two flanged sockets and sealed by o-rings. Fully assembled, the robotic fish is 1.5 meters long and has a mass of approximately 15kg. As regard the propulsion system, the vehicle is equipped by caudal fin, which was driven by a Pololu DC motor integrated with a spatial-cam kinematic joint , and three screw propellers: one allows the vehicle to change depth and the other two allows the vehicle to navigate nimbly, turning the yaw axis to adjust its heading.

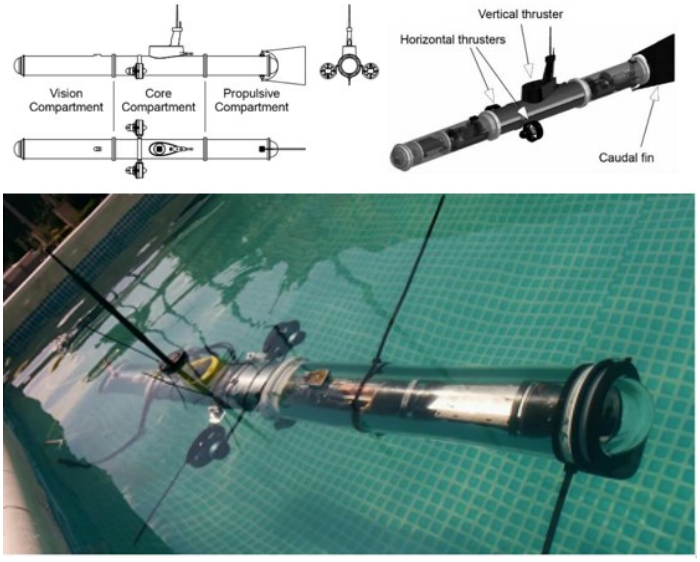

Figure 2.1: BRAVe prototype.

2.1.2 DORI prototype

The second prototype, called DORI (diminutive of "dorico", which means "from Ancona") [32], is much smaller, compact and solid, but has the same "oscillating plate" architecture of BRAVe.

The vehicle consists of the longer fore-body and the short tail section, thus resulting 0.6 meters long and has a mass of approximately 6 kg. The robotic fish was validated to safely reach 100m without water leakages or structural damages.

The body is composed by an aluminium cylindrical pressure hull, enclosed between two acetal neck flanges and a Perspex dome closes the most-forward flange. A double o-ring seal was created between the flange and the dome, in order to prevent any water leakage.

In order to minimize the pitching moment during vertical movement the vertical propeller's axis of rotation passes through the center of buoyancy of the entire vehicle. On the robot sides, two horizontal thrusters were fixed, aligned with its roll axis.
The tail section consists of a cylindrical cap manufactured by lathe from POM/acetal block.

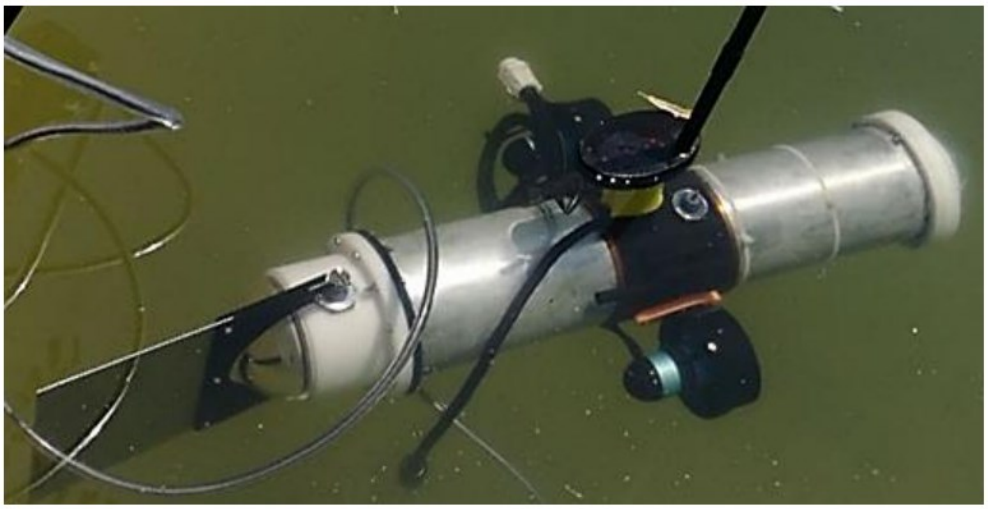

Figure 2.2: DORI prototype.

2.1.3 GUIZZO prototype

The further pursuit of an efficient propulsion system composed only by bio-inspired thrusters and the intention to create a robot aesthetically more similar to an ostraciiform swimming mode fish have led, the designers of the vehicles previously reported, to the development of GUIZZO prototype. The name GUIZZO derives from "guizzare", which is a verb that means wiggling or twisting with rapid and sudden movements. There are several versions of this prototype. Indeed, over the last three years, the first GUIZZO version has undergone small changes by researchers and students, in order to improve its structure and propulsion system. All GUIZZO versions have been designed starting from their 3D CAD models, which not only was used for the different analysis and simulation of the prototype, but also for the realization of different components that compose the robot, using a 3D STRATASYS printer.

The first version, GUIZZO 1.0 (Figure 2.3), is made up of Bosch aluminium profiles and several vertebrae, which compose the vehicle's skeleton. As for propulsion system, to change depth of the vehicle, two bio-inspired thrusters were used, consisting of fins located in the pectoral area on the sides of the body. For the advancement and heading a bio-inspired thruster, or caudal fin, was used.

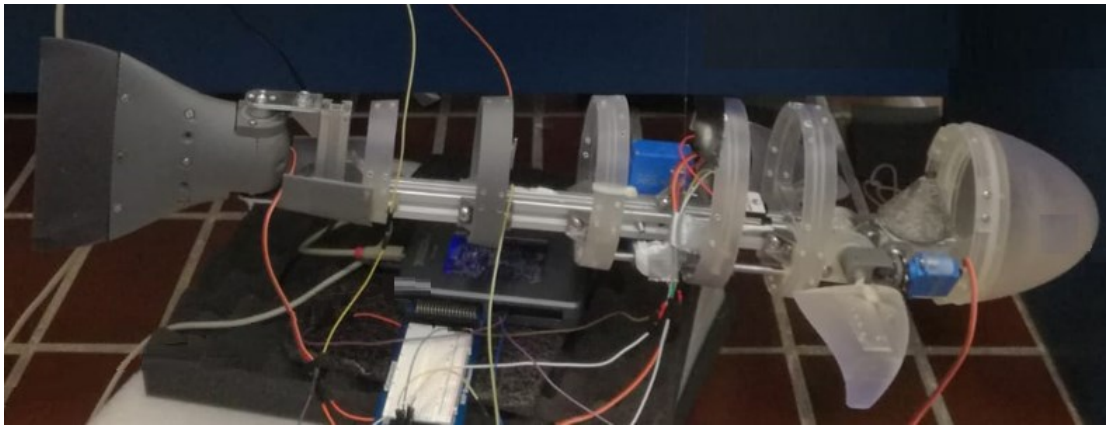

Figure 2.3: GUIZZO 1.0 prototype.

GUIZZO 1.0 caudal fin was designed with a different structure and transmission from that of BRAVe and DORI prototypes. It consisted in a fin-shaped container, in which a servomotor is incorporated. This system is connected to the stern vertebra of the vehicle via two rectangular and flat grip bars, which are fixed to the stern vertebra by means of screws. The lower grip bar is also attached to the servo shaft, while, a disk connected to the gear of

the servo is fixed on the upper grip bar. In this way the translations related to the vertebra-fin system are fixed, but at the same time rotation around the axis of the created constraint is guaranteed. When the servomotor is activated, an effort is discharged onto the grip bars, which being constrained to the stern vertebra (therefore to whole vehicle's body), induce, the servo, to start rotating around the axis of aforementioned constraint. In this way the caudal fin is set in motion, since servo and fin form a single system.

An important characteristic of GUIZZO 1.0 consists of a displacing mass of lead inserted into the fish body; the lead mass is moved, by a servo motor connected to a Scoth-Yoke mechanism, along the body to keep it in balance and therefore avoid pitching moments.

In the second version, GUIZZO 2.0, a vertical propeller for depth changes was added. The second modification consisted in the arrangement and propulsion transmission of pectoral fins. Indeed, they were oriented in such a way that an angle of 45 degrees is was formed between the body of the fish and the fins. As for their propulsion system, in the previous version the two fins were operated by means of a single servomotor combined with a cam mechanism which operated a cylindrical bar; the latter was attached on one side to the first fin and on the other side to the second fin. In version 2.0, however, each fin was operated by its servomotor. Specifically, a crankcase is used to attach the servomotor to the vehicle body and a cylindrical crankcase to join the pectoral fin and the ABS disc combined with the servo gear. In this way the cam mechanism is eliminated. Figure 2.4 shows GUIZZO 2.0 the 3D CAD model.

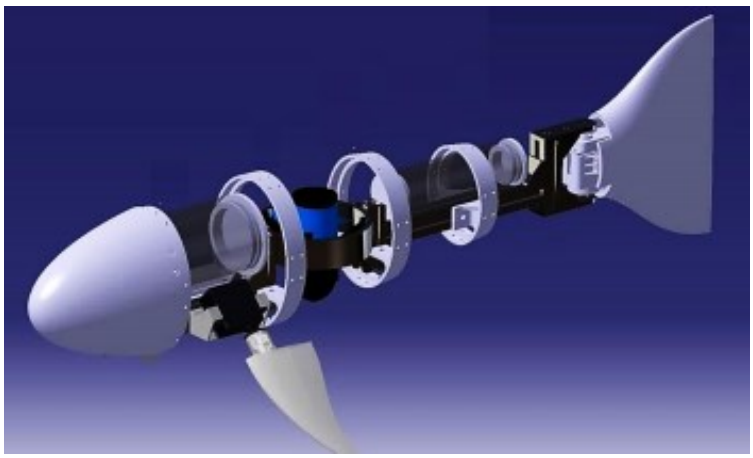

Figure 2.4: GUIZZO 2.0 3D CAD model.

From GUIZZO 2.0 to GUIZZO 4.0 (shown in Figure 2.5) the following changes have been made:

- Replacement of Bosch aluminium bars with Delrin bars.
- Elimination of the displacement mass in lead by changing the location of the vertical propeller, in such as to make its rotation axis coincide with entire vehicle's center of buoyance. Furthermore, to do this, numerous wooden parts were added.
- Addition of waterproof compartments to host electronic components.
- Choice not to use 4 different vertebrae for the body but only 2 models of them, the larger for the central part and smaller for the bow and stern of the robot.

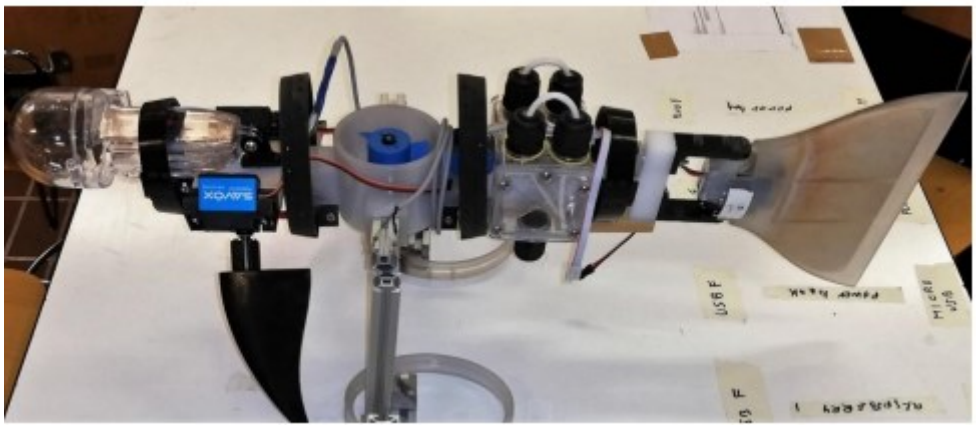

Figure 2.5: GUIZZO 4.0 prototype.

As for the GUIZZO 5.0 version, only the 3D model was made, without the development of the real model. In this version the design of the vertebrae has been further modified and the design of the motor-holder were improved. In addition, a dorsal fin was created with the intent to use it to host an antenna, which will be employed to control the vehicle remotely. Figure 2.6 shows GUIZZO 5.0 3D model assembly.

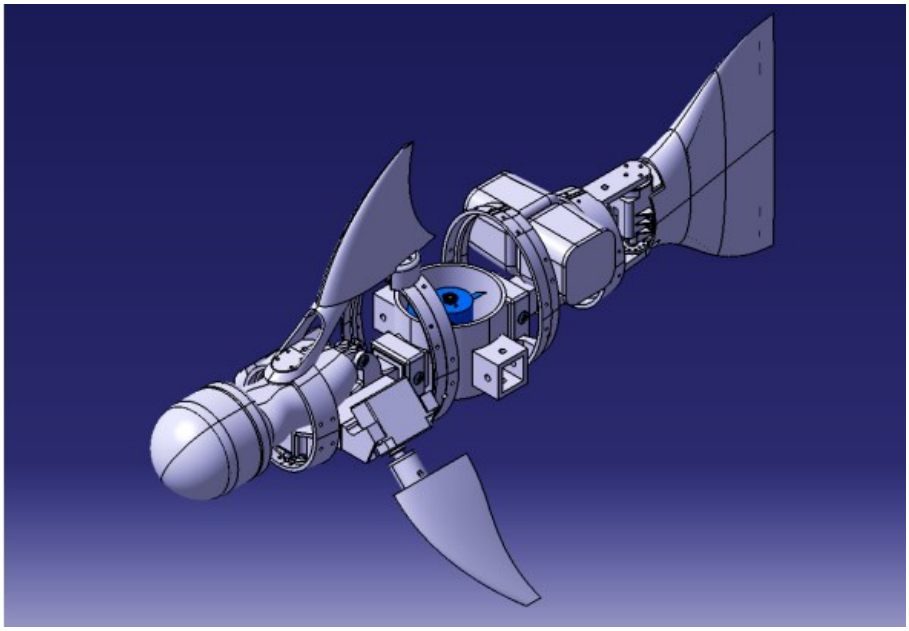

Figure 2.6: GUIZZO 5.0 3D model assembly.

Finally, GUIZZO 6.0 model is reported in this project. As mentioned above, GUIZZO 5.0 project was taken up to make this version of the vehicle. The only change made was to insert two lateral propellers for the heading and forward movement, making the complex an overactuated hybrid system. The purpose of making this version of the vehicle is purely academic. The choice to use both propellers and the bio-inspired thruster for horizontal movement is due to the research and analysis of the vehicle's behavior in terms of total energy consumption.

2.2 GUIZZO 6.0 3D CAD model

As mentioned in the previous chapter, the first aim of this work is to develop a simulation environment for the biomimetic robot, enhanced with a three-dimensional graphical interface. To obtain the latter, preparation of a 3D vehicle design was essential. In this section, the 3D model of GUIZZO 6.0 is described in detail.

The design on computer is of fundamental importance for many aspects concerning the realization of a prototype, as it allows to drastically reduce development times and costs, while maintaining the behaviour of the prototype's design very close to the real one. In fact, in the CAD (Computer Aided Design) field, the 3D model is represented unambiguously in its shapes and dimensions by reproducing the physical object to create or already existing one. It also allows to archive and use previous models, already equipped with technical quotas and statistical or dynamic calculation, on which to base a new project.

The previous version's drawings to that of GUIZZO 6.0 were created using the software CATIA V5 (Computer Aided Three-dimensional Interactive Application). This software was developed in 1977 by the French company Dassault System for internal use in the aircraft production field, and it was made public in 1998, becoming the most used software in the technical engineering industry, especially in automotive, marine and aerospace sector. CATIA V5 is also a hybrid modeller, which allows the coexistence of solid and surface representation, creating a single model. This simplifies the operations required in various activities, such as the engineering of forms.

For the realization of GUIZZO 6.0 3D model, the actual work, done by the author of this elaborate, has been to resume the previous version (GUIZZO 5.0) drawing, implemented in CATIA V5 software, and add to it the design of two propellers, including their holders. The components were placed on the vehicle's sides, centered at the same height as the pectoral fins center. The added propellers and motor holders have the same characteristic, in terms of type and size, as those of the vertical thruster and its holder; apart from their orientation, which is parallel to the main body of the robotic fish.

The 3D model of GUIZZO 6.0 developed in CATIA V5 software, with its components highlighted, is shown in Figure 2.7.

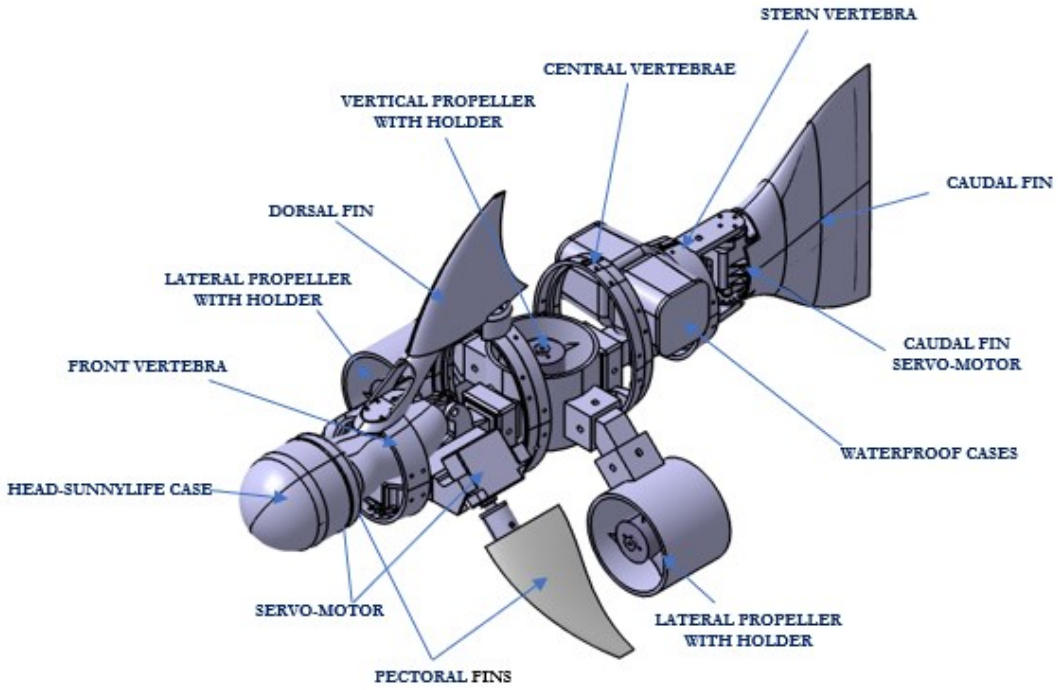

Figure 2.7: GUIZZO 6.0 3D model assembly with components high lined.

GUIZZO 6.0 model is characterized by an overall length of approximately 0.58 m. The body skeleton is made up of two profiles, which in the real model will be two polyoxometalate (POM) profiles, commonly called Delrin. The various parts, which compose the robotic fish model, are briefly described below.

- FINS
    1. **Caudal fin:**

       The caudal fin has a section in which a servomotor is lodged, so that the two become a single component. In addition, the CAD model of the caudal fin is hollow inside and open on the outside; this could be problematic in the real model, as the fin will be filled with water, increasing the overall vehicle's weight. To avoid the problem, in real model, polyurethane foam will be used to close the cavity, while ensuring a better buoyancy.

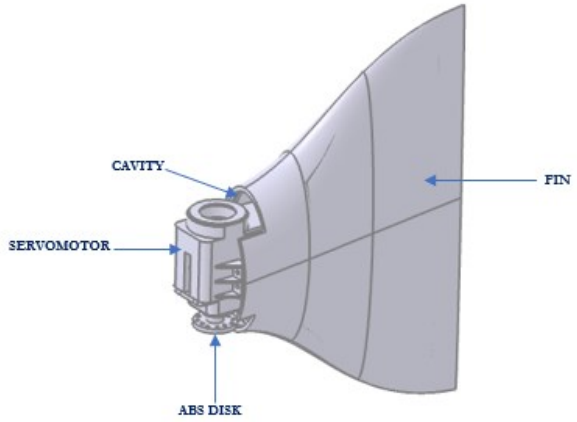

Figure 2.8: Caudal fin's 3D model.

2. **Pectoral fins:**

These fins are created basing on a NACA (National Advisory Committee for Aeronautics) profile and are located in the pectoral area of the vehicle and their main characteristic is that of being inclined with respect to the body, forming an angle of 45 degrees. Furthermore, each fin is connected to a servomotor by beans of a cylindrical part, which, specifically, connects the servomotor output ABS (acrylonitrile-butadiene-styrene) disk to the fin attachment. The design of the servomotors, used for the entire prototype reflects the real models, that is SAVOX SW1211SG. Each servo is connected to a carter which holds and connects them to the vehicle's body.

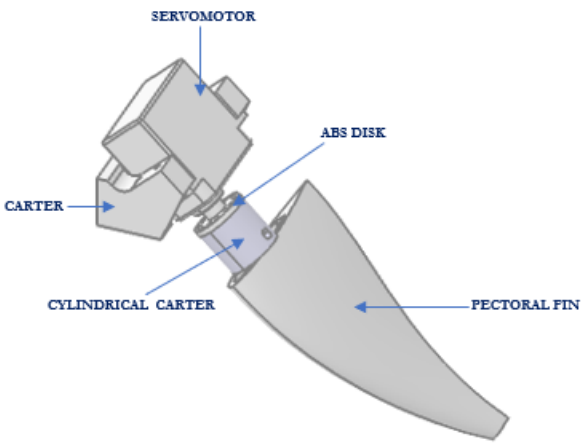

Figure 2.9: Pectoral fin 3D model.

3. **Dorsal fin:**

   The dorsal fin was created from a NACA profile and sized to the proportion of the prototype, the internal section presents a cavity to host, in real model, an antenna which could be used to control the robot remotely.

- PROPELLERS

  The prototype is equipped with three thrusters, the design of which reflect real one in size. One is used to change the robot's depth, while the other two are used for the horizontal motion (forward and heading).

  1. **Vertical propeller:**

     This propeller is located at the center part of the vehicle. In particular, propeller's axis of rotation passes through the center of buoyancy of entire vehicle. Furthermore, it is hold by a motor-holder, which presents four quadrangular holes: two are used to connect it with the vehicle's skeleton, and the other two are used to connect it with the motor-holders of the lateral propellers, by means of a Delrin bar.

  2. **Lateral propellers:**

     As mentioned before, they are inside their motor-holders, which is connected to the vertical propeller's one. Their center is situated at the same height of the pectoral fin's center. Furthermore, the axes of rotation of both is parallel to the center of buoyancy.

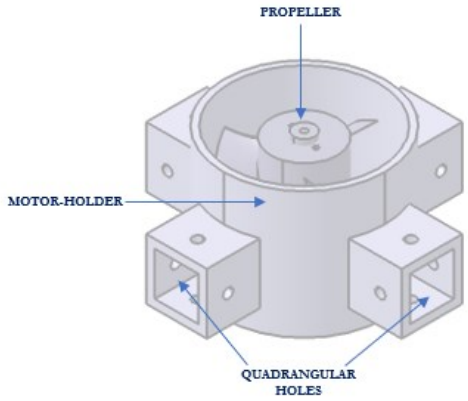

Figure 2.10: Motor-holder 3D model.

- VERTEBRAE

  The vertebrae, together with Delrin bars, act as a means of connection between the various components and, therefore, constitute the robot's skeleton. GUIZZO 6.0 has in total four vertebrae: front vertebra, two central vertebrae and stern vertebra; a consideration must be made for the last. The stern vertebra connects the caudal fin with the rest of the body, this happens thanks to two flat grip beams. The first flat beam was joined directly to the lower part of stern vertebra body and caudal fin's servomotor is screwed directly to the beam by means of an ABS disk. The upper grip beam, unlike the first, has not been joined to the vertebra body, hence, it was fixed to the vertebra by inserting it into one seat suitably created on the top of the vertebra.

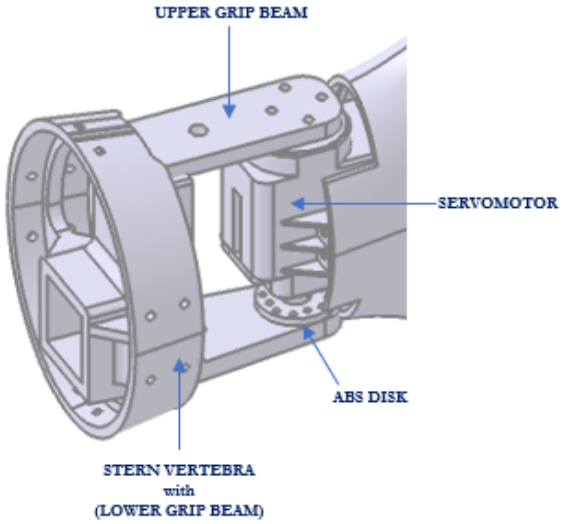

Figure 2.11: Stern vertebra 3D model.

- ACCESSORY COMPARTMENTS:

  Finally, GUIZZO 6.0 is equipped with two type of accessory compartments:

  1. **Head-SunnyLife case:** which is a waterproof camera case, SunnyLife, used for dives up to 60 meters deep. This case has been placed in the front and it can be considered as robotic fish's head.
  2. **Waterproof cases:** these two cases are set at the tail part.

All these accessory cases will be used, in the real model, to contain to contain the electronic components, so that they are not damaged due to the water in which the robot will be immersed.

The electronic items could be: any kind of sensors, for example a camera or inertial sensors (such as accelerometers and gyroscopes), an electronic board to control the robotic fish (such as ARDUINO) and connection for the actuators.

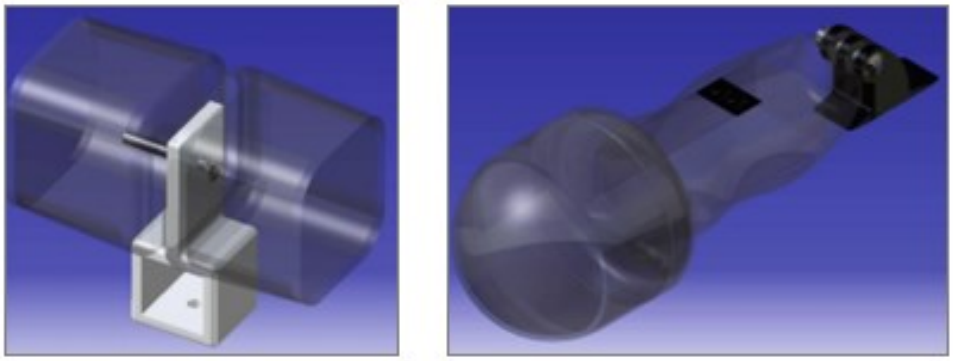

Figure 2.12: Accessory compartments 3D model.

Chapter 3.

Modelling of GUIZZO 6.0 & Propulsion System

In order to build a simulation environment and different control algorithms it is important to study and implement a dynamic model of the vehicle, including the propulsion system. This chapter describes the development of a non-linear dynamic model of GUIZZO 6.0, in six degrees of freedom (according to the theory illustrated by Fossen [33]), which is obtained by transforming into vectorial representation the mathematical model previously implemented by Ing. Daniele Costa and by Ing. Nicolò Ciuccoli, in which the body of the vehicle was approximated to a cylinder with radius R and length L [34-35].

The main reason for the development of a vectorial representation of the equation of motion is to exploit the physical properties of the model and to reduce the number of coefficients required for control. Furthermore, models based on vectorial setting are useful from a computational point of view and to perform algebraic manipulations.

Following the description of the non-linear model in vectorial setting, the implementation in Simulink environment of this is reported. The reason for using this software can be traced back to the fact that it allows you to simulate the various control algorithms that can be developed; in addition, it allows you to adopt various tools, in particular the *Simulink 3D Animation* (which includes Virtual Reality Toolbox) which offers the possibility to link Simulink models and MATLAB algorithm to 3D graphic objects in virtual reality scenes.

The chapter is organised as follows: kinematic equations are given in section 1 and dynamic equations of motion are given in section 2. Forces and moments generated by the Robotic Fish's propulsion system are described in section 3. Finally, section 4 discusses about the implementation of the dynamic model in Simulink environment, reporting also the obtained results.

3.1 Kinematics

Kinematics is a branch of physics that studies the motion of bodies treating only geometrical aspects, without taking into consideration the forces that cause motion.

The equation of motion of the marine vehicle can be written in vectorial setting according to Fossen [33] as:

$$\dot{\eta} = J_\theta(\eta)v \tag{3.1}$$

$$M\dot{v} + C(v)v + D(v)v + g(\eta) = \tau \tag{3.2}$$

Where the different matrices and vectors and their properties will be described in the following paragraphs.

3.1.1 Reference Frames

When analysing the motion of a marine robot in six degrees of freedom it is convenient to define two coordinate frames, as shown in Figure 3.1. The moving frame $\{b\}$ is fixed to the body of the craft and its origin $\{O_b\}$ is usually chosen in such a way as to coincide with the vehicle's centre of gravity. The motion of the body-fixed frame is described relative to the Earth-centered one, the North-East-Down frame $\{n\}$, which can be considered inertial, since the effects of the Earth's motion on the vehicle at low speed is negligible. The suggestion given by this consideration, is that the position and orientation of the robotic fish should be described relative to the $\{n\}$, while the linear and angular velocities should be expressed in $\{b\}$.

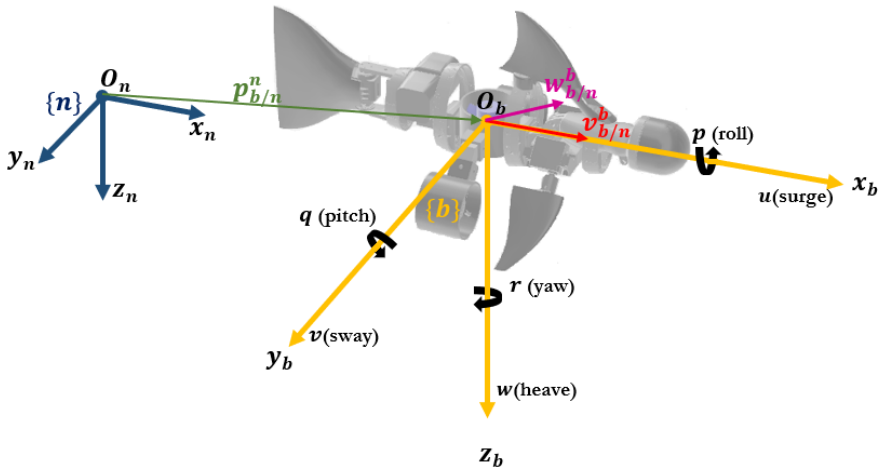

Figure 3.1: GUIZZO 6.0 reference frames: {b} (body-fixed) and {n} (NED).

The notation adopted for the vectors in $\{b\}$ and $\{n\}$ frames for the marine robot are the following:

- $v_{b/n}^{b} = \begin{bmatrix} u \\ v \\ w \end{bmatrix}$ linear velocity of the point O_b relative to $\{n\}$ expressed in $\{b\}$;
- $w_{b/n}^{b} = \begin{bmatrix} p \\ q \\ r \end{bmatrix}$ angular velocity of the point O_b relative to $\{n\}$ expressed in $\{b\}$;
- $p_{b/n}^{n} = \begin{bmatrix} x_n \\ y_n \\ z_n \end{bmatrix}$ position of O_b in the $\{n\}$ frame;
- $\Theta_{nb} = \begin{bmatrix} \phi \\ \theta \\ \psi \end{bmatrix}$ Euler angles between $\{n\}$ and $\{b\}$.

3.1.2 Kinematic equation of motion

The kinematics model describes the relationship between the two reference frames, $\{b\}$ and $\{n\}$, from a geometric point of view. These equations are described by the vectors $\boldsymbol{\eta}$ and $\boldsymbol{v}$.

$$\eta = \begin{bmatrix} \eta_1 = p_{b/n}^{n} \\ \eta_2 = \Theta_{nb} \end{bmatrix}, \quad v = \begin{bmatrix} v_1 = v_{b/n}^{b} \\ v_2 = w_{b/n}^{b} \end{bmatrix}$$

where η denotes the position and attitude of the craft, in which the position vector $p_{b/n}^{n}$ is the distance between NED frame and the body-fixed frame expressed in the NED coordinate frame ($\{n\}$), Θ_{nb} is the Euler angles vector and v denotes linear and angular velocity vector.

EULER PARAMETERS REPRESENTATION (UNIT QUATERNION)

When vectorial notation is applied for the description of non-linear equations of motion, for rigid bodies in six degrees of freedom, it is possible to observe that these equations assume a systematic structure. In fact, these can generally be divided into equations that describe the translational motion and those that describe the rotational motion. While for the position it is frequently used a vector of size 3×1 relative to the axes of reference x y and z, for the representation of the attitude there are different ways. The most commonly used is the representation by Euler angles, which consists of three parameters: roll angles (ϕ), pitch (θ), and yaw (ψ).

If the vectors v_1 and v_2 are given, then it is possible to find the tempo derivate of the position and attitude vectors, η_1 and η_2, using the following transformation:

$$\begin{bmatrix} \dot{\eta_1} \\ \dot{\eta_2} \end{bmatrix} = \begin{bmatrix} J_1(\eta_2) & 0_{3\times3} \\ 0_{3\times3} & J_2(\eta_2) \end{bmatrix} \begin{bmatrix} v_1 \\ v_2 \end{bmatrix} \tag{3.3}$$

where $\boldsymbol{J_1(\eta_2)}$ and $\boldsymbol{J_2(\eta_2)}$ are the transformation matrices.

The representation of orientation by Euler angles is very common thanks to their easy physical interpretation and to the fact that they can be measured directly by the sensors (gyros). There are, however, some disadvantages that arise due to the presence of singular points [36], characteristic of the angular representation: it can be noted, in fact, that the transformation matrix $J_2(\eta_2)$ turns out to be undefined due to pitch angles $\theta = \pm 90°$ and becomes ill conditioned when the pitch angle reaches $\pm 90°$. For the marine robot, which could operate near these singularities, it can be problematic.

An alternative to Euler angle representation is the four-parameter method based on unit quaternion $\boldsymbol{(q)}$ [37], which is an extension of complex numbers. A quaternion unit can be defined as:

$$q = [q_0 \quad q_1 \quad q_2 \quad q_3]^T \tag{3.4}$$

Let β denote the principal angle and λ the main axis associated with Euler's theorem, which states that the different rotations around the different axes passing through a fixed point are equivalent to a single rotation around an axis passing through this fixed point. The Euler parameters representing orientation are defined as:

$$q = [\,\vec{q} \quad q_3\,]^T = [q_1 \quad q_2 \quad q_3 \quad q_0]^T \tag{3.5}$$

where:

$$\vec{q} = [q_1 \quad q_2 \quad q_3]^T = \lambda \sin\frac{\beta}{2} \tag{3.6}$$

$$q_0 = \cos\frac{\beta}{2}, \quad 0 \le \beta < 2\pi \tag{3.7}$$

The Euler parameters satisfy the constraint of quaternion units, that is:

$$\|q\| = 1 \iff q_1^2 + q_2^2 + q_3^2 + q_0^2 = 1 \tag{3.8}$$

The transformation relative to $\boldsymbol{\dot{\eta}_1}$ and $\boldsymbol{v_1}$ can be expressed as:

$$\dot{\eta}_1 = R_b^n(q)v_1 \tag{3.9}$$

where $R_b^n(q) = \begin{bmatrix} 1-2(q_2^2+q_3^2) & 2(q_1q_2-q_3q_0) & 2(q_1q_3+q_2q_0) \\ 2(q_1q_2-q_3q_0) & 1-2(q_1^2+q_3^2) & 2(q_2q_3-q_1q_0) \\ 2(q_1q_3-q_2q_0) & 2(q_2q_3-q_1q_0) & 1-2(q_1^2+q_2^2) \end{bmatrix}$. (3.10)

Before defining $\boldsymbol{\dot{\eta}_2}$ the **Skew-Symmetrical** ($\boldsymbol{S}$) is introduced [37]. One of the advantages of vectorial representation is, in fact, the possibility of using some system properties such as Skew-Symmetric.

This operator is define as $\boldsymbol{S} = \left(\begin{bmatrix} a \\ b \\ c \end{bmatrix}\right) \triangleq \begin{bmatrix} 0 & -c & b \\ c & 0 & -a \\ -b & a & 0 \end{bmatrix}$ con $S: \Re^3 \rightarrow \Re^{3\times3}$.

An important property of $\boldsymbol{S}$ is the following: given two vectors in $\Re^3$, $\mathbf{v} = \begin{bmatrix} a \\ b \\ c \end{bmatrix}$ e $\mathbf{w} = \begin{bmatrix} d \\ e \\ f \end{bmatrix}$,

then their vectorial product can be expressed as:

$$\boldsymbol{v}\times\boldsymbol{w} = \begin{bmatrix} a \\ b \\ c \end{bmatrix} \times \begin{bmatrix} d \\ e \\ f \end{bmatrix} \triangleq \begin{bmatrix} bf-ce \\ cd-af \\ ae-db \end{bmatrix} = \begin{bmatrix} 0 & -c & b \\ c & 0 & -a \\ -b & a & 0 \end{bmatrix} \begin{bmatrix} d \\ e \\ f \end{bmatrix} = \boldsymbol{S}(\mathbf{v})\mathbf{w} \tag{3.11}$$

Angular velocity transformation, $\boldsymbol{\dot{\eta}_2}$, is defined as:

$$\dot{\eta}_2 = \dot{q} = T_q(q)v_2 \tag{3.12}$$

where

$$T_q(q) = \frac{1}{2}\begin{bmatrix} -\vec{q}^T \\ q_0 I_{3\times3} + S(\vec{q}) \end{bmatrix} = \frac{1}{2}\begin{bmatrix} -q_1 & -q_2 & -q_3 \\ q_0 & -q_3 & q_2 \\ q_3 & q_0 & -q_1 \\ -q_2 & q_1 & q_0 \end{bmatrix} \tag{3.13}$$

In this way, the Euler parameters representation is defined for any valid unit quaternion and singularity is avoided (typical of a three-parameter representation).

Therefore, the kinematics equation can be expressed by means of the Euler parameters (unit quaternion) as follows:

$$\begin{bmatrix} \dot{p}_{b/n}^{n} \\ \dot{q} \end{bmatrix} = \begin{bmatrix} R_b^n(q) & 0_{3\times3} \\ 0_{4\times3} & T_q(q) \end{bmatrix} \begin{bmatrix} v_{b/n}^{b} \\ w_{b/n}^{b} \end{bmatrix} \Leftrightarrow \dot{\eta} = J_q(\eta)v \tag{3.14}$$

Dynamics

The dynamics consists in the analysis of the forces and moments that cause the motion of a rigid body, in this case GUIZZO 6.0.

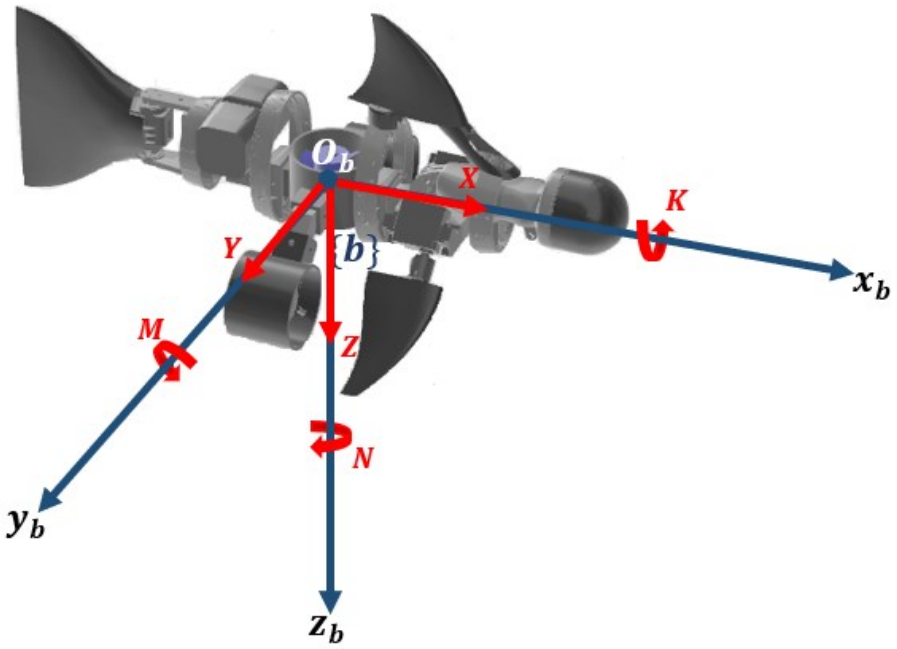

Figure 3.2: forces and moments which causes robotic fish motion.

3.2.1 Dynamic equation of motion

In general, when the body-fixed frame's origin O doesn't coincide with the centre of gravity (CG), the dynamic equation of motion of a rigid body with six degrees of freedom can be written in compact form as [33-37-38]:

$$M_{RB}\dot{v} + C_{RB}(v)v = \tau_{RB} \tag{3.15}$$

M_{RB} is the inertia matrix of the rigid body, it is constant, symmetric and positive definite, i.e. $\dot{M}_{RB} = 0$ and $M_{RB} = M_{RB}^T > 0$, moreover it has a unique parametrization, of the type:

$$M_{RB} = \begin{bmatrix} mI_{3\times3} & -mS(r_G) \\ mS(r_G) & I_0 \end{bmatrix} \tag{3.16}$$

where m is the marine vehicle's mass and $r_G = \begin{bmatrix} x_G \\ y_G \\ z_G \end{bmatrix}$ is a 3×1 vector that denotes the distance of the centre of gravity CG with respect to the body-fixed frame, $I_{3\times3}$ is the identity

matrix (3×3), $I_0 = \begin{bmatrix} I_x & -I_{xy} & -I_{xz} \\ -I_{yx} & I_y & -I_{yz} \\ -I_{zx} & -I_{zy} & I_z \end{bmatrix}$ is inertia tensor of the robotic fish with respect to the body-fixed frame $\boldsymbol{(I_0 = I_0^T > 0)}$.

$C_{RB}(v)$ is a skew-symmetrical parametrization of the rigid-body Coriolis and centripetal matrix ($C_{RB}(v) = -{C_{RB}}^T(v) > 0$) and it's defined as:

$$C_{RB}(v) = \begin{bmatrix} 0_{3\times3} & -mS(v_1) - mS(S(v_2)r_G) \\ -mS(v_1) - mS(S(v_2)r_G) & mS(S(v_1)r_G) - S(I_0 v_2) \end{bmatrix} \quad (3.17)$$

τ_{RB} is the general the external forces vector, including control and hydrodynamic forces and moments.

These expressions are simplified since we consider the centre of gravity coinciding with the origin of the body-fixed frame. Therefore, the components of the distance vector r_G will be equal to zero, obtaining the following results:

$$M_{RB} = \begin{bmatrix} mI_{3\times3} & 0_{3\times3} \\ 0_{3\times3} & I_0 \end{bmatrix} = \begin{bmatrix} m & 0 & 0 & 0 & 0 & 0 \\ 0 & m & 0 & 0 & 0 & 0 \\ 0 & 0 & m & 0 & 0 & 0 \\ 0 & 0 & 0 & I_x & -I_{xy} & -I_{xz} \\ 0 & 0 & 0 & -I_{yx} & I_y & -I_{yz} \\ 0 & 0 & 0 & -I_{zx} & -I_{zy} & I_z \end{bmatrix} \quad (3.18)$$

$$C_{RB}(v) = \begin{bmatrix} 0_{3\times3} & -mS(v_1)) \\ -mS(v_1)) & -S(I_0 v_2) \end{bmatrix} \quad (3.19)$$

3.2.2 Forces and moments acting on GUIZZO 6.0

The equation, described in the previous paragraph, represents the motion of the rigid body in an empty space, while in the case of marine vehicles, the hydrodynamic forces, that is the forces and moments caused by the presence of a fluid (water) in which the vehicle is submerged, must also be considered.

These hydrodynamic forces acting on the vehicle can be divided into: disturbances caused by the environment (wind, waves, sea currents), restoring forces due to gravity and buoyancy forces, and finally the forces related to the added mass due to the surrounding fluid inertia

and the potential damping induced by the energy dissipated by the waves generated on the surface.

Considering the set of forces described above, the equation of motion of the marine robot with 6 degrees of freedom in body-fixed frame can be written, in compact form, as follows [37]:

$$\underbrace{\left(\boldsymbol{M_{RB}} + \boldsymbol{M_A}\right)}_{\boldsymbol{M}}\dot{\boldsymbol{v}} + \underbrace{\left(\boldsymbol{C_{RB}(v)} + \boldsymbol{C_A(v)}\right)}_{\boldsymbol{C(v)}}\boldsymbol{v} + \boldsymbol{D(v)v} + \mathbf{g}(\boldsymbol{\eta}) = \boldsymbol{\tau_E} + \boldsymbol{\tau} \qquad (3.20)$$

Where:

- $\boldsymbol{M}$ is inertia matrix (including added mass)
- $\boldsymbol{M_{RB}}$ is inertia matrix of the rigid body
- $\boldsymbol{M_A}$ is added mass matrix
- $\boldsymbol{C(v)}$ is Coriolis and centripetal matrix (including added mass))
- $\boldsymbol{C_{RB}(v)}$ is Coriolis and centripetal matrix of the rigid body
- $\boldsymbol{C_A(v)}$ is added-mass Coriolis and centripetal matrix
- $\boldsymbol{D(v)}$ is total hydrodynamic and centripetal matrix
- $\mathbf{g}(\boldsymbol{\eta})$ is vector of restoring (gravitational and buoyant) forces and moments
- $\boldsymbol{\tau_E}$ is vector of environmental forces and moments
- $\boldsymbol{\tau}$ is vector of propulsion forces and moments (exerted by the thrusters)

The forces and moments that can be identified are:

1) Hydrodynamic rigid-body-like added mass forces and moments $-M_A\dot{v}$,
2) Hydrodynamic Coriolis-like added mass forces and moments $-C_A(v)v$,
3) Hydrodynamic damping and lift forces and moments $-D(v)v$,
4) Restoring (gravitational and buoyant) forces and moments $-\mathrm{g}(\eta)$,
5) Environmental forces and moments τ_E, which are null (thus, $\tau_E = 0$),
6) Propulsion forces and moments τ (will be analysed in the next chapter)

ADDED MASS

When a rigid body is moving in a fluid, it is necessary to consider the additional inertia of the fluid that surrounds the body, which is accelerated by its movement. This added mass, however, must not be considered as an amount of fluid connected to the vehicle in such a way that the vehicle and the fluid represent a new system having a mass greater than the old system, but must be understood as the forces induced by pressure due to a forced harmonic motion of the body, which is proportional to the acceleration of the same [38].

The hydrodynamic force along the x_b axis due to linear acceleration in the direction of the axis considered is defined as:

$$X_A = -X_{\dot{u}}\dot{u}\ , \quad \text{where} \quad X_{\dot{u}} = \frac{\partial X}{\partial \dot{u}}\ . \tag{3.21}$$

In the same way it is possible to define the remaining 36 components of the forces and moments $[X \quad Y \quad Z \quad K \quad M \quad N]^T$ to the six linear and angular accelerations $[\dot{u} \quad \dot{v} \quad \dot{z} \quad \dot{p} \quad \dot{q} \quad \dot{r}]^T$.

These elements define the added mass matrix $M_A \in \mathfrak{R}^{6\times 6}$. In general, all the elements of the matrix are non-null. However, given that the motion of the vehicle occurs at reasonably low speeds and having assumed the body of the vehicle as a cylinder, most of the hydrodynamic effects do not affect the resulting motion. This property is valid also for $C_A(v)$ and $D(v)$.

Therefore, the following form is obtained:

$$M_A = \begin{bmatrix} M_{11} & M_{12} \\ M_{21} & M_{22} \end{bmatrix} = \left[\begin{array}{ccc:ccc} X_{\dot{u}} & 0 & 0 & 0 & 0 & 0 \\ 0 & Y_{\dot{v}} & 0 & 0 & 0 & 0 \\ 0 & 0 & Z_{\dot{w}} & 0 & 0 & 0 \\ \hdashline 0 & 0 & 0 & K_{\dot{p}} & 0 & 0 \\ 0 & 0 & 0 & 0 & M_{\dot{q}} & 0 \\ 0 & 0 & 0 & 0 & 0 & N_{\dot{r}} \end{array}\right], \text{ where } \ M_A = M_A^T > 0,\ \dot{M}_A = 0 \tag{3.22}$$

$$C_A(v) = \begin{bmatrix} 0_{3\times 3} & -S(M_{11}v_1 + M_{12}v_2) \\ -S(M_{11}v_1 + M_{21}v_2) & -S(M_{21}v_1 + M_{22}v_2) \end{bmatrix} =$$

$$\begin{bmatrix} 0 & 0 & 0 & 0 & -Z_{\dot{w}}w & Y_{\dot{v}}v \\ 0 & 0 & 0 & Z_{\dot{w}}w & 0 & -X_{\dot{u}}u \\ 0 & 0 & 0 & -Y_{\dot{v}}v & X_{\dot{u}}u & 0 \\ 0 & -Z_{\dot{w}}w & Y_{\dot{v}}v & 0 & -N_{\dot{r}}r & M_{\dot{q}}q \\ Z_{\dot{w}}w & 0 & -X_{\dot{u}}u & N_{\dot{r}}r & 0 & K_{\dot{p}}p \\ -Y_{\dot{v}}v & X_{\dot{u}}u & 0 & -M_{\dot{q}}q & -K_{\dot{p}}p & 0 \end{bmatrix}$$

where $C_A(v) = C_A^T(v) > 0,\ \dot{C}_A(v) = 0$ (3.23)

HYDRODYNAMIC DAMPING

In general, the damping of a marine vehicle in high speed motion is highly nonlinear and coupled. A possible approximation can be made considering that the marine robot has an uncoupled motion, where the second order terms are negligible, obtaining a structure of the matrix $\boldsymbol{D(v)}$ composed by only linear and quadratic damping terms that appear on the diagonal:

$$D(v) = -\begin{bmatrix} X_u + X_{u|u|}|u| & 0 & 0 & 0 & 0 & 0 \\ 0 & Y_v + Y_{v|v|}|v| & 0 & 0 & 0 & 0 \\ 0 & 0 & Z_w + Z_{w|w|}|w| & 0 & 0 & 0 \\ 0 & 0 & 0 & K_p + K_{p|p|}|p| & 0 & 0 \\ 0 & 0 & 0 & 0 & M_q + M_{q|q|}|q| & 0 \\ 0 & 0 & 0 & 0 & 0 & N_r + N_{r|r|}|r| \end{bmatrix}$$

(3.24)

Furthermore considering the vehicle body as a cylinder, it has been assumed that the linear damping terms are null, that is $X_u = Y_v = Z_w = K_p = M_q = N_r = 0$.

$$D(v) = -\begin{bmatrix} X_{u|u|}|u| & 0 & 0 & 0 & 0 & 0 \\ 0 & Y_{v|v|}|v| & 0 & 0 & 0 & 0 \\ 0 & 0 & Z_{w|w|}|w| & 0 & 0 & 0 \\ 0 & 0 & 0 & K_{p|p|}|p| & 0 & 0 \\ 0 & 0 & 0 & 0 & M_{q|q|}|q| & 0 \\ 0 & 0 & 0 & 0 & 0 & N_{r|r|}|r| \end{bmatrix} \quad (3.25)$$

RESTORING FORCES

When a rigid body is completely or partially immersed in a fluid, two other forces must be considered: gravitational force and buoyancy force. The first f_g is induced by the weight W and acts through the centre of gravity $r_G = \begin{bmatrix} x_G \\ y_G \\ z_G \end{bmatrix}$ of the robotic fish. The latter f_B is induced by buoyance B and acts through the centre of buoyancy $r_B = \begin{bmatrix} x_B \\ y_B \\ z_B \end{bmatrix}$ of the robot.

Let m denote the mass of the vehicle, Δ the volume of the fluid moved, g the acceleration of gravity and ρ the density of the water, it follows:

$$W = mg \tag{3.26}$$

$$B = \rho g \Delta \tag{3.27}$$

these act along z_b axis, the first with a positive sign while the second with a negative sign. Furthermore, by applying the transformation matrix according to the Euler angle, restoring force in respect to the body-fixed frame can be defined as follows:

$$\mathrm{g}(\eta) = \begin{bmatrix} (W-B)\sin\theta \\ -(W-B)\cos\theta\sin\phi \\ -(W-B)\cos\theta\cos\phi \\ -(y_g W)\cos(\theta)\cos(\phi) + (z_g W)\cos(\theta)\sin(\phi) \\ (z_g W)\sin(\theta) + (x_g W)\cos(\theta)\cos(\phi) \\ -(x_g W)\cos(\theta)\sin(\phi) + (y_g W)\sin(\theta) \end{bmatrix} \tag{3.28}$$

By hypothesis $W = B$ e $x_g = y_g = 0$:

$$\mathrm{g}(\eta) = \begin{bmatrix} 0 \\ 0 \\ 0 \\ (z_g W)\cos(\theta)\sin(\phi) \\ (z_g W)\sin(\theta) \\ 0 \end{bmatrix} \tag{3.29}$$

3.2 Propulsion system

The propulsion system can be described by the following equation in vectorial notation:

$$\boldsymbol{\tau = \tau_{HT1\&HT2} + \tau_{HT3} + \tau_{VT2\&HT3} + \tau_{VT1}} \tag{3.30}$$

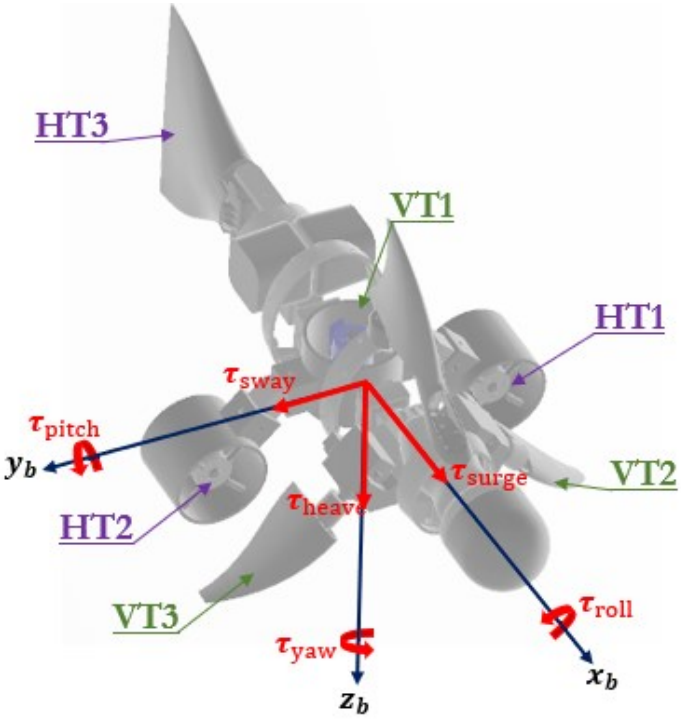

Figure 3.3: Forces and moments $\tau = [\tau_{surge} \quad \tau_{sway} \quad \tau_{heave} \quad \tau_{roll} \quad \tau_{pitch} \quad \tau_{yaw}]^T$ exerted by the actuators HT1, HT2, HT3, VT1, VT2 e VT3.

Before proceeding with the description of GUIZZO 6.0 propulsion system, the various actuating components which allow the motion of the vehicle in question are listed below. As shown in the Figure 3.3, the marine robot is composed of a total of six actuators, of which three, or HT1, HT2 and VT1 are propellers; while the remaining three are bio-inspired thrusters composed by servomotors that activate the movement of the robot's fins, in particular VT2 and VT3 set the pectoral fins in motion. VT3 on the other hand, is responsible for implementing the caudal fin. A useful subdivision that can be made for the description of the biomimetic robot's propulsion system is to group the actuators according to two types of motion: the horizontal one (surge, sway, yaw) and the vertical one (heave, roll, pitch). According to this subdivision, the actuators can be grouped into HT1, HT2, HT3, which deal with horizontal movement; and VT1, VT2, VT3 which deal with vertical movement.

3.3.1 Propulsion exerted by caudal fin (HT3)

Numerical analysis and modelling of caudal fin's propulsion were performed by Ing. Daniele Costa in [34]. The result of the study carried out is as follows: the dynamic characterization of actuator HT3 is a function of the Strouhal number St, aa dimensionless parameter traditionally used to characterize the oscillating flows phenomena. This parameter is defined as:

$$St = \frac{fA}{U} = f\frac{2c}{U}\tan\theta_0 \tag{3.31}$$

where A is the width of the wake that separates from the fin, c is the value of the mean fin's chord, $U = [u \quad v \quad w]^T$ is the module of the robotic fish's linear speed, f is the oscillation frequency of the fin and θ_0 is the amplitude of oscillation. The actuator efficiency has been studied as the Strouhal number changes, allowing to model the behaviour of the hydrodynamic forces and torque within a period of oscillation, i.e. as a function of the angular position θ of the fin:

$$\theta = \theta_0 \cos(2\pi f t) + \bar{\theta} \tag{3.32}$$

Where $\bar{\theta}$ is the mean value of θ and represents the contribution that allows the robotic fish to steer (yaw).

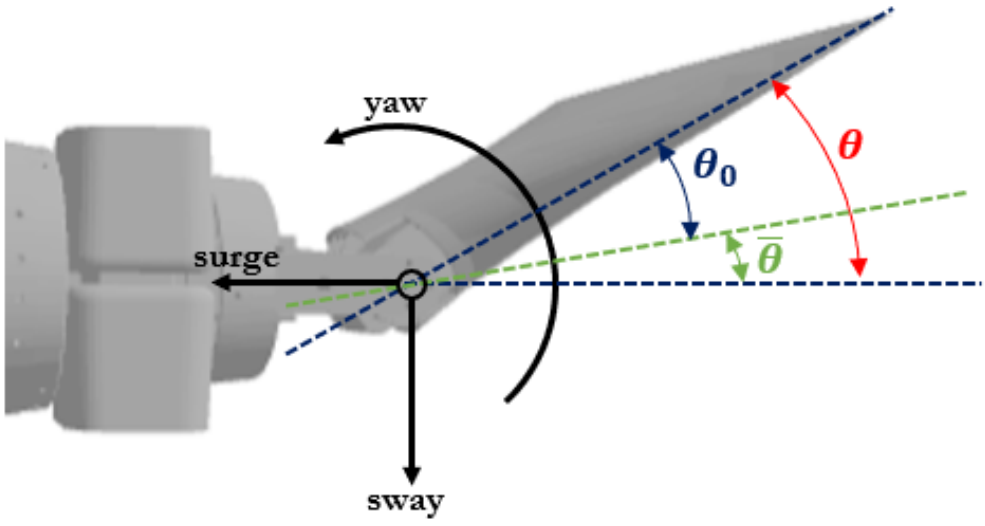

Figure 3.4: Propulsive forces and torque decomposition.

Moreover, interpolating the simulation data, force and moments have been obtained:

$$F_{surge} = \frac{1}{2}\rho U^2 S[(a_0 + a_1 St + a_2 St^2) + (b_0 + b_1 St + b_2 St^2)\, sin(4\pi ft\ + \phi_{surge})]$$

$$F_{sway} = \frac{1}{2}\rho U^2 S[sin(2\pi ft\ + \phi_{sway})\, c_2 St^2]$$

$$M_{yaw} = \frac{1}{2}\rho U^2 S[sin(2\pi ft\ + \phi_{yaw})\, d_2 St^2] \tag{3.33}$$

where S is the foil area, ρ is the water density and the angles ϕ_{surge}, ϕ_{sway}, ϕ_{yaw} are due to the flow separation phenomena.

Considering the contribution of the steering angle, it is possible to report the forces previously described in the body-fixed frame, through the following transformation:

$$\tau_{surgeHT3} = F_{surge}\, cos(\bar{\theta}) - F_{sway}\, sin(\bar{\theta})$$

$$\tau_{swayHT3} = F_{surge}\, sin(\bar{\theta}) - F_{sway}\, cos(\bar{\theta}) \tag{3.34}$$

$$\tau_{yawHT3} = M_{yaw} - \frac{1}{4}\rho U^2 SL[(a_0 + a_1 St + a_2 St^2)] sin(\bar{\theta})$$

In compact form the following is obtained:

$$\tau_{HT3} = \begin{bmatrix} \tau_{surgeHT3} \\ \tau_{swayHT3} \\ 0 \\ 0 \\ 0 \\ \tau_{yawHT3} \end{bmatrix} \tag{1.35}$$

3.3.2 Propulsion exerted by pectoral fins (VT2 and VT3)

One of the mechanical characteristics of the marine robot examined, is that of having two lateral fins allocated in the pectoral area oriented at 45°. These are responsible of underwater vehicle's lift and affect the depth (vertical movement), the pitch and roll angles. Furthermore, the lifting force and the torques created by the two fins are highly dependent on robotic fish linear velocity.

$$L_{fin} = \frac{1}{2}\rho c_L S_{fin}(\delta_s - \beta_e)v_e^2$$
$$M_{fin} = x_{fin}L_{fin} \tag{3.36}$$

where c_L is fin lift coefficient, S_{fin} is the fin planform area, δ_s is the angle of the fin referred to the hull of the vehicle, β_e the effective angles of attack of fin zero plane, v_e the effective speed of the fins and x_{fin} is the axial position of the fin expressed in body-fixed frame.

Based on the equations just described, the following can be formulated:

Let δ_{VT2} and δ_{VT3} denote the angles, respectively of the fins VT2 and VT3, referring to the hull of the vehicle, $[x_{fin} \quad -y_{fin} \quad z_{fin}]$ the point where VT2 is located and $[x_{fin} \quad y_{fin} \quad z_{fin}]$ the point where VT3 is located, both with respect to body-fixed frame, and let $\alpha = 45°$ be the orientation of the two fins, then the actuation of the fins produces two forces, $F_{VT2}\}$ and F_{VT3}:

$$F_{VT2} = \frac{1}{2}\rho c_L S_{fin}(u^2\delta_{VT2} + uw - x_{fin}uq)$$
$$F_{VT3} = \frac{1}{2}\rho c_L S_{fin}(u^2\delta_{VT3} + uw - x_{fin}uq) \tag{3.37}$$

Which can be decomposed into four components in the reference system {b} by means of the inclination angle α:

$$Z_{VT2} = F_{VT2}\cos\alpha$$
$$Y_{VT2} = F_{VT2}\sin\alpha$$
$$Z_{VT3} = F_{VT3}\cos\alpha \tag{3.38}$$
$$Y_{VT3} = F_{VT3}\sin\alpha$$

Generating the following moments:

$$\begin{aligned} K_{VT2} &= -y_{fin}Z_{VT2} - z_{fin}Y_{VT2} \\ K_{VT3} &= y_{fin}Z_{VT3} - z_{fin}Y_{VT3} \\ M_{VT2} &= x_{fin}Z_{VT2} \\ M_{VT3} &= x_{fin}Z_{VT3} \\ N_{VT2} &= x_{fin}Y_{VT2} \\ N_{VT3} &= x_{fin}Y_{VT3} \end{aligned} \tag{3.39}$$

In this way the following vector of forces and moments is obtained:

$$\tau_{VT2\&VT3} = \begin{bmatrix} 0 \\ \tau_{swayVT2\&VT3} \\ \tau_{heaveVT2\&VT3} \\ \tau_{rollVT2\&VT3} \\ \tau_{pitchVT2\&VT3} \\ \tau_{yawVT2\&VT3} \end{bmatrix} = \begin{bmatrix} 0 \\ Y_{VT2} + Y_{VT3} \\ Z_{VT2} + Z_{VT3} \\ K_{VT2} + K_{VT3} \\ M_{VT2} + M_{VT3} \\ N_{VT2} + N_{VT3} \end{bmatrix} \tag{3.40}$$

Example 1 Figure 3.5 (Forces and torques generated by the fins)

Considering that the robotic fish is moving in the direction of the axis x_b, with a positive speed u, and that the fins VT2 and VT3 are actuated with angles $\delta_{VT2} = \delta_{VT3} > 0$, then some lifting force will be exerted on the body. This force can be decomposed into F_{VT2} and F_{VT3} which will both have a component parallel to the y_b axis and the other parallel to the z_b axis. Since the angles of the fins referring to the hull of the vehicle are positive and equal, the components Y_{VT2} and Y_{VT3} will have the same intensity but in the opposite direction and therefore, added together, the resulting force parallel to the y_b axis will be zero ($Y_{VT2} + Y_{VT3} = 0$). Furthermore these forces generate the moments M_{VT2} and M_{VT3} whose resultant will be greater than 0, while the moments K_{VT2}, K_{VT3}, N_{VT2} and N_{VT3} will be null, since they depend on the lifting force component parallel to the y_b axis.

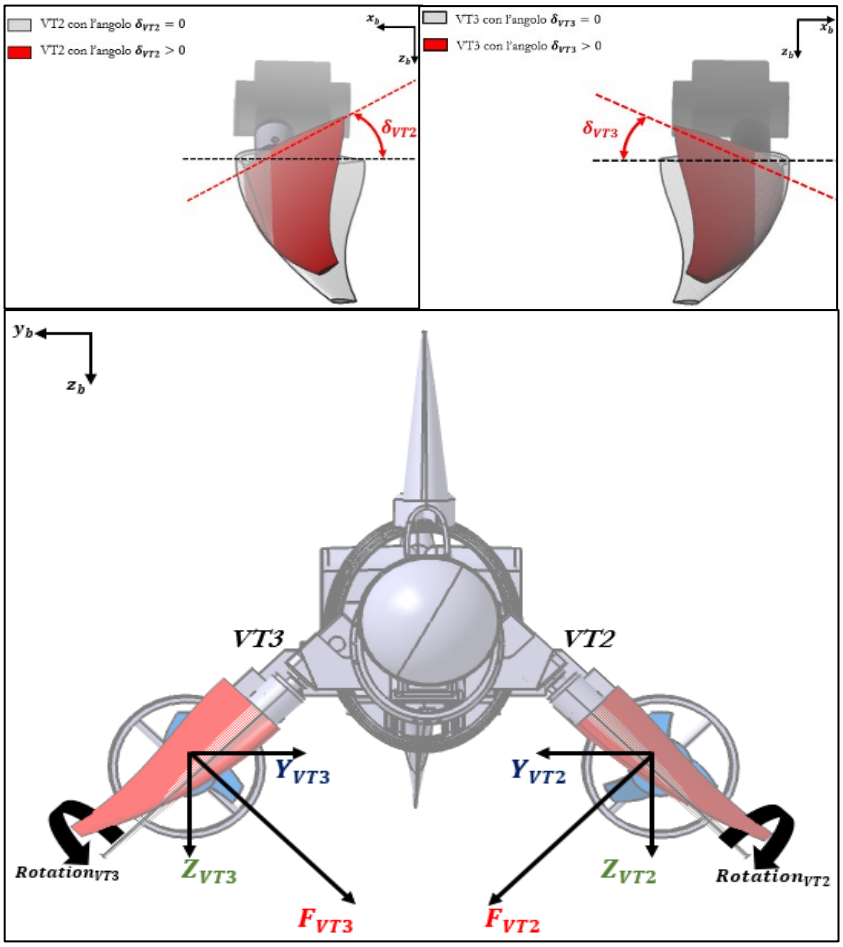

Figure 3.5: Force and torque generated by VT2 e VT3 with angles $\delta_{VT2} = \delta_{VT3} > 0$.

3.3.3 – Propeller modelling (HT1, HT2 and VT1)

GUIZZO 6.0, as previously seen, is equipped with three propellers, 2 for horizontal movement (HT1 and HT2) and one for vertical movement (VT1). The forces and torques exerted by these propellers can be modelled in the same way (Figure 3.6). In fact, each propeller exerts a thrust T (force) and torque Q_e (moment). Depending on the rotation of the motors, the direction of the vectors T and Q_e can be the same (for a rotation of the propeller in a clockwise direction) or opposite (counter-clockwise rotation). The thrust T generates torque equal to $Q_r = r \times T$, such that total torque exerted by the propeller is given by $Q = Q_e + Q_r$. The vector $r[r_x \quad r_y \quad r_z]^T$ determines the position of the thrust T point of attack.

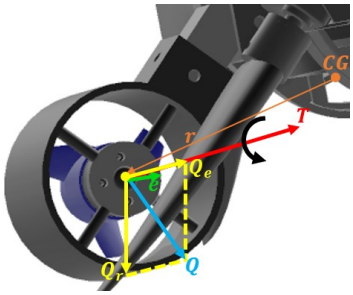

Figure 3.6*: HT2* Force and torque decomposition.

Given a general description of the thruster propulsion system, we can now, characterize the forces and torques exerted by each of them, dividing those that affect the horizontal motion from those that are responsible for the vertical motion of the robot.

PROPULSION HT1 E HT2

Forces and torques vector generated by HT1 and HT2 thrusters can be defined as follows:

$$\tau_{HT1\&HT2} = \begin{bmatrix} T_{HT1} + T_{HT2} \\ Q_{HT1} + Q_{HT2} \end{bmatrix} = \begin{bmatrix} e_{HT1} & e_{HT2} \\ S(r_{HT1})e_{HT1} & S(r_{HT2})e_{HT2} \end{bmatrix} \begin{bmatrix} K_{HT1} & 0 \\ 0 & K_{HT2} \end{bmatrix} \begin{bmatrix} n_{HT1} \\ n_{HT2} \end{bmatrix} \tag{3.41}$$

The following table shows the meaning of the terms in the equation:

	HT1	***HT2***
Thrust:	T_{HT1}	T_{HT1}
Total torque:	$Q_{HT1} = Qe_{HT1} + Q_{rHT1}$	$Q_{HT2} = Qe_{HT2} + Q_{rHT2}$
Position vector of thrust's point of attack	r_{HT1}	r_{HT2}
Unit vector of thrust direction	e_{HT1}	e_{HT2}
Thrust coefficient	K_{HT1}	K_{HT2}
Propeller rotation speed	n_{HT1}	n_{HT2}

Table 3.1: HT1 and HT2 Parameters

PROPULSION VT1

As regards the vertical thruster VT1, the vector of the forces and torques generated by it, is described by the following equation:

$$\tau_{VT1} = \begin{bmatrix} T_{VT1} \\ Q_{HT1} \end{bmatrix} = \begin{bmatrix} e_{VT1} \\ S(r_{VT1})e_{VT1} \end{bmatrix} K_{VT1} n_{VT1} \tag{3.42}$$

Where T_{VT1} is the thrust exerted by VT1, Q_{HT1} is VT1 total torque, r_{VT1} is the position vector of the exerted thrust's point of, and e_{VT1} is the vector that represents the direction of the thrust, K_{VT1} is the thrust coefficient and n_{VT1} is the rotation speed of VT1.

3.3 Mathematical model implementation in Simulink

GUIZZO 6.0 mathematical model examined in this chapter has been implemented in Simulink environment, a software for modelling, simulation and analysis of dynamic systems closely integrated with MATLAB.

The use of this software can be traced back to various reasons. Firstly, this software is widely used in an academic level; secondly, the use of this environment is intuitive due to its graphical programming nature, making complex simulator quite simple. Finally, there is the possibility to automatically compile the models created in languages suitable for real-time applications.

3.4.1 Simulation software Block description

This paragraph will briefly describe the graphical programming implemented for robotic fish dynamic model's simulation.

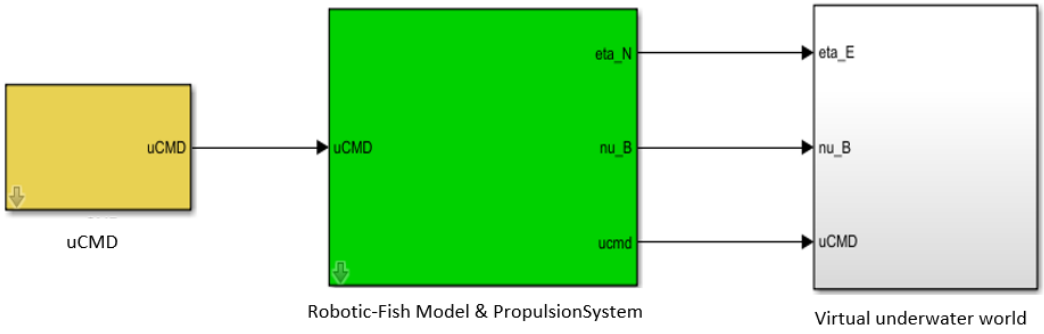

Figure 3.7: Simulation software block diagram.

The software implemented consists of three main blocks:

- *uCMD* block (in yellow), where direct controls (percentage) for the various marine robot actuators are implemented
- *Robotic-Fish Model & PropulsionSystem* block (green), where the implementation of the robotic fish dynamic model is contained
- *Virtual underwater world* (grey) This block will be explored in chapter 5.

uCMD **BLOCK**

This block contains the direct command, in percentage, for the robot various actuators. These commands are seven in total:

1) f_uHT3 controls HT3 oscillation frequency
2) Theta_uHT3 controls HT3 steering angle
3) uHT1 controls HT1 rotation speed
4) uHT2 controls HT2 rotation speed
5) uVT1 controls VT1 rotation speed
6) uVT2 controls VT2 angle referring to the hull of the vehicle
7) uVT3 controls VT3 angle referring to the hull of the vehicle

While for f_uHT3 the control range is from 0 to 1, for the rest of the commands the range of values that they can assume is from -1 to 1. Furthermore, for the f_uHT3 and Theta_uHT3 commands the scaling factor function is used which reports the values expressed as a percentage in values respectively of the frequency and of the steering angle that the caudal fin can assume.

Scaling factor function:

This function is represented by a trivial equation of the straight line passing through two point, and it can be written as:

$$y = \frac{(x - x_1)}{(x_2 - x_1)}(y_2 - y_1) + y_1$$

Where x_1, x_2 are the minimum and maximum values of the input and y_1, y_2 are the minimum and maximum values of the output that we want, x is the input and y is the desired output.

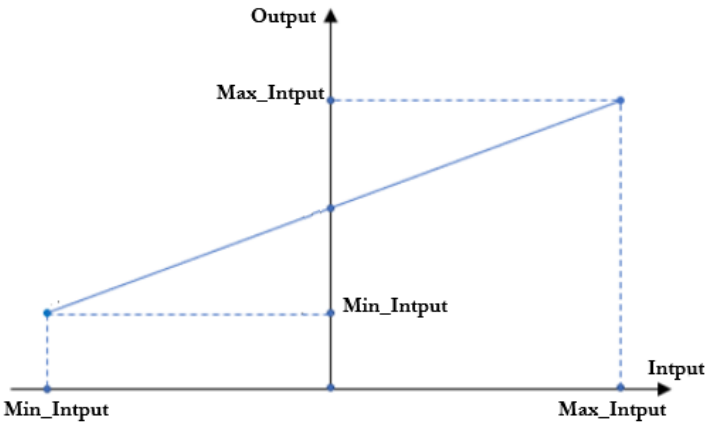

Figure 3.8: Straight line equation passing through two points (graph).

Mask Editor:

The *uCMD* block is also equipped with a mask. In Simulink, you can insert a mask on the blocks that consists in a custom user interface that hides the block's content. The Mask Editor dialog box helps to create and customize the mask adding various feature on it.

In this case, the mask consists on a control panel in which, it is possible to insert the values of the control commands as shown in the figure.

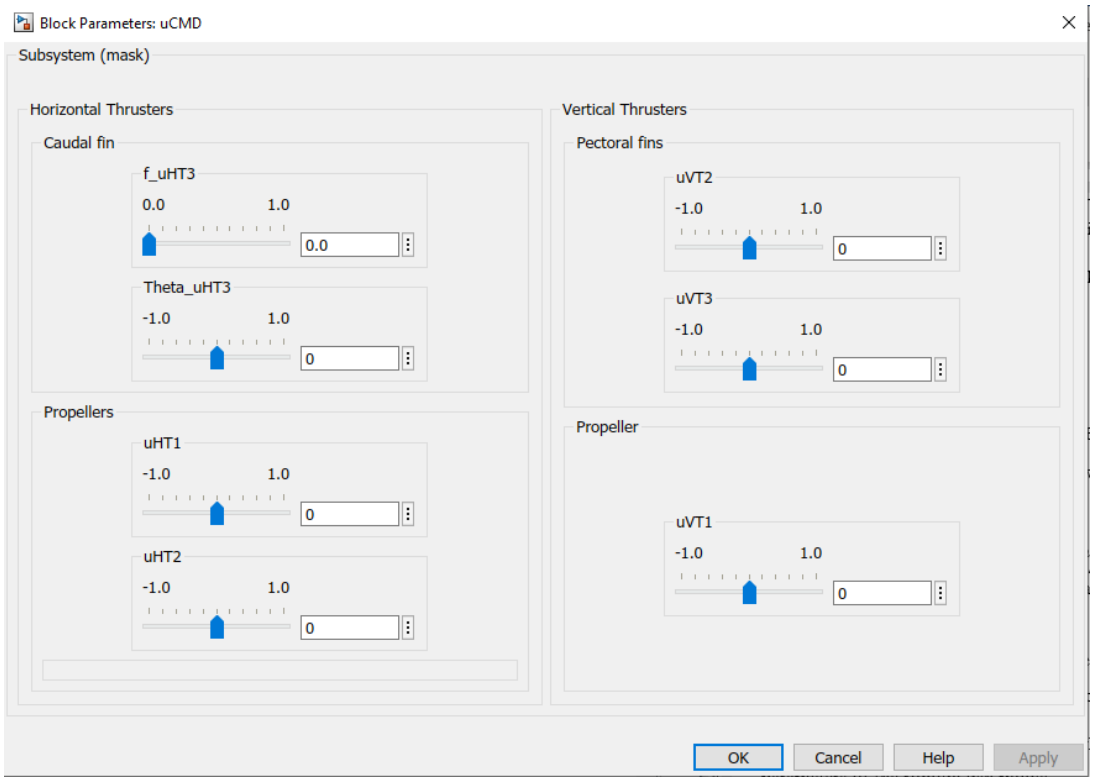

Figure 3.9: *uCMD* Mask block parameter

Robotic-Fish Model & PropulsionSystem **Block**

The examined block takes as input the vector containing the commands in percentage for different actuators and returns three outputs:

- the position vector eta_N $=[p_{b/n}^{n} \quad q]^{T}=[x_n \quad y_n \quad z_n \quad q_0 \quad q_1 \quad q_2 \quad q_3]^{T}$ referred to the reference system {n}, where the attitude is represented by quaternions.
- the velocity nu_B = $\boldsymbol{v} = [v_{b/n}^{b} \quad w_{b/n}^{b}]^{T}=[u \quad v \quad w \quad p \quad q \quad r]^{T}$ referred to the reference system integrated with the marine vehicle;
- the vector of the ucmd commands.

This block is characterized by a mask in which, it is possible to insert and /or modify the different initial parameters of the robotic fish model.

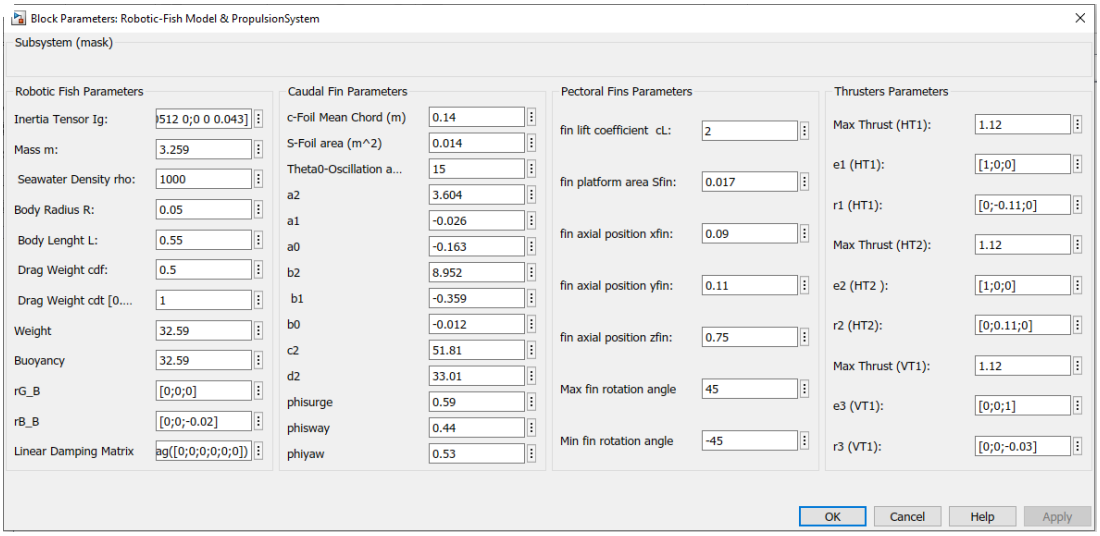

Figure 3.10: *Robotic-Fish Model & PropulsionSystem* Mask block parameter

The *Robotic-Fish Model & PropulsionSystem* block, is composed of two sub-blocks: *Propulsion System* and *RF Dynamics and Kinematics*. The first takes as input the vector of the actuators commands (uCMD) and the vector of the robotic fish speed referred body-fixed frame (nu_B) and outputs the vector of the ucmd commands and the vector of forces generated by the propulsion system, that is: Tau_B = $\tau = [\tau_{surge} \quad \tau_{sway} \quad \tau_{heave} \quad \tau_{roll} \quad \tau_{pitch} \quad \tau_{yaw}]^{T}$. The

second block, on the other hand, takes as input the vector generated by the first, Tau_B, and returns the vectors nu_B and eta_N as outputs.

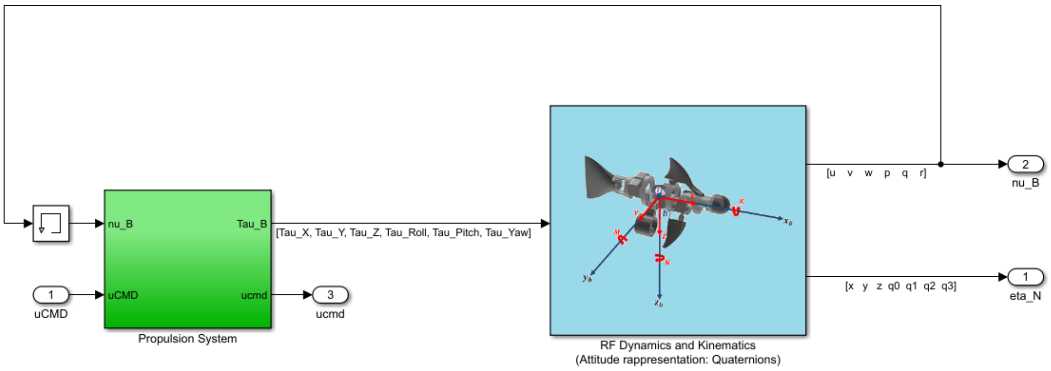

Figure 3.11: *Robotic-Fish Model & PropulsionSystem* Simulink block diagram

Propulsion System:

In this block, the equations representing the propulsion system are implemented, these can be schematized using the block diagram shown in Figure 3.12.

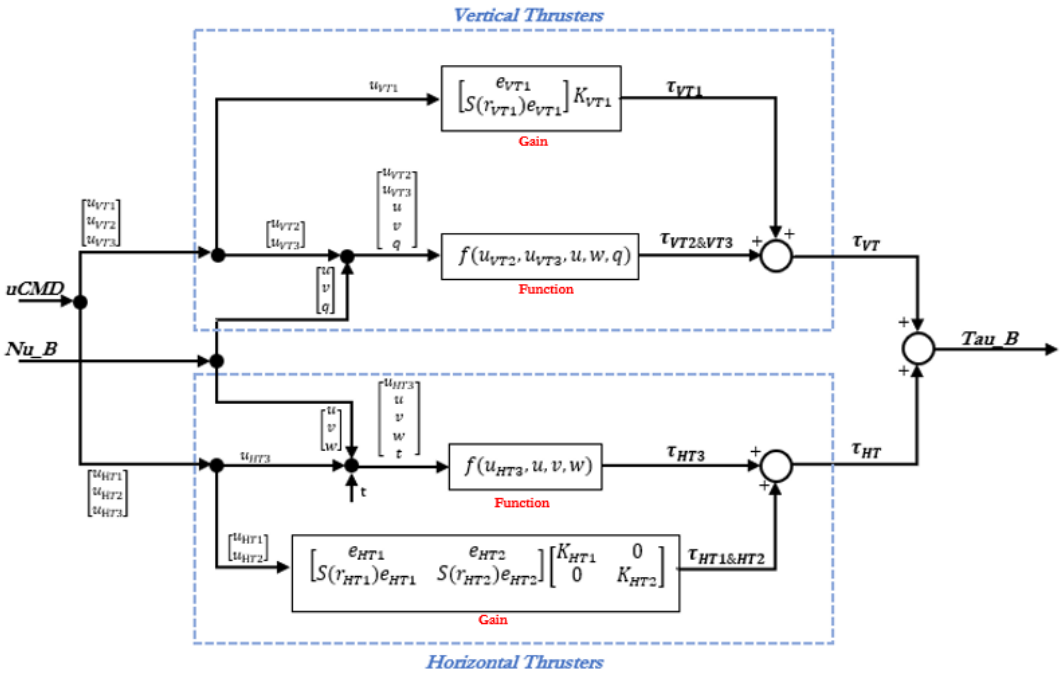

Figure 3.12: *Propulsion system* block diagram.

RF Dynamics and Kinematics

In this block, instead, the equations of dynamics and kinematics that make up the mathematical model of the robotic fish are implemented. The equations in question are schematized by the block diagram shown in Figure 3.13.

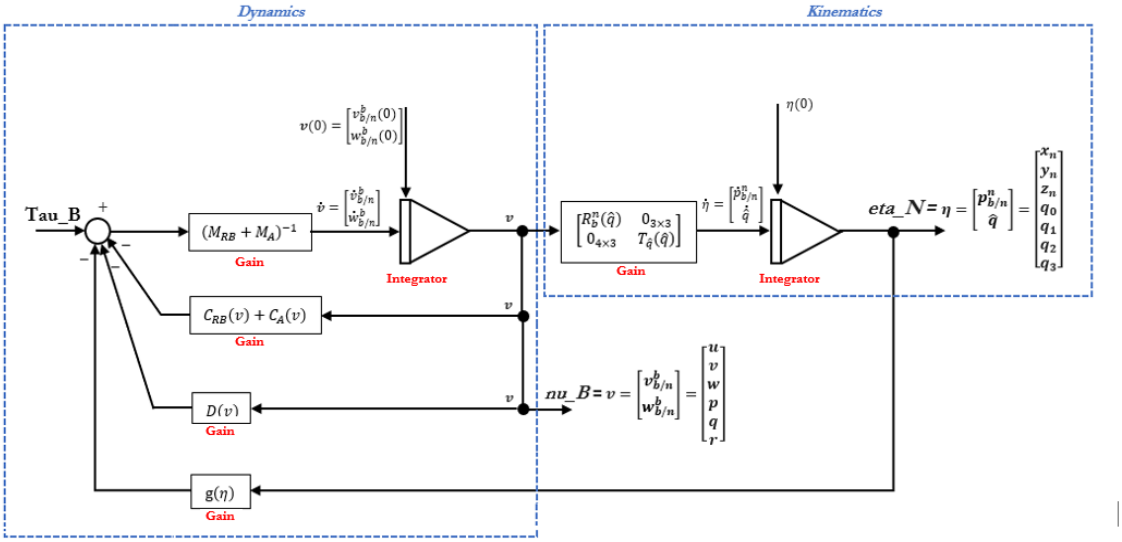

Figure 3.13: *RF Dynamic and Kinematics* block diagram.

3.4.2 Simulation results

In this chapter the dynamic model of the robotic fish has been illustrated and how it has been implemented in the Simulink software. Before proceeding with the study and implementation of a control law, it is interesting to analyse the behaviour of the simulated vehicle by controlling it directly with commands to operate the individual actuators.

In this paragraph the results obtained from the simulated tests, by activating the individual actuators with direct commands, will be discussed, in particular the bio-inspired thrusters, Caudal Fin and the Pectoral Fins.

CAUDAL FIN HT3

HT3 thruster can be actuated by controlling the frequency f of oscillation of the fin and by controlling the angle $\bar{\theta}$ that allows the vehicle to steer. These are controlled by commands f_uHT3 (range [0 1]) and Theta_uHT3 (range [-1 1]).

The first test carried out is shown in the Figure 3.14, which represents the results obtained during straight-forward navigation simulation. The robot surge velocity is plotted as a function of time at different thruster oscillation frequencies. Here a constant speed is reached when the propulsive force is balanced from the viscous resistance.

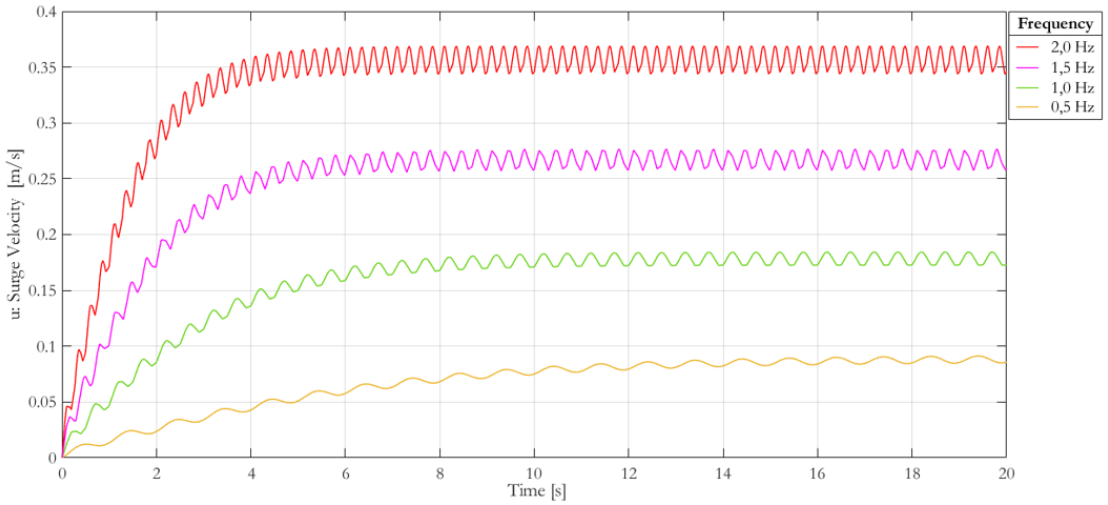

Figure 3.14: GUIZZO 6.0 Surge velocity with different oscillation frequencies of the Caudal Fin.

Focusing on the 2 Hz oscillation frequency, the graph shows the behavior of the moving vehicle.

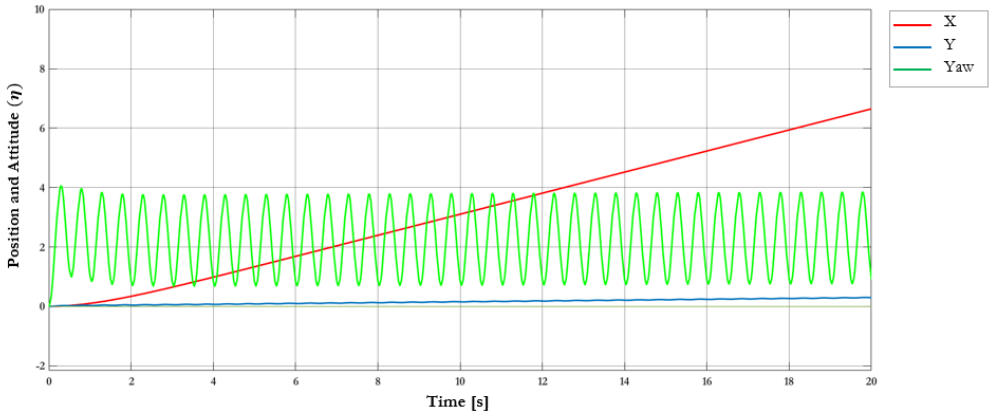

Figure 3.15: GUIZZO 6.0 position and attitude at $f = 2Hz$.

This behaviour is due to the caudal fin forces produced, shown in Figure 3.15. The surge force $\boldsymbol{\tau_{surgeHT3}}$ is a sinusoidal wave, which even if in some strectches is negative has a positive average value, while the sway force $\boldsymbol{\tau_{swayHT3}}$ and the generate torque $\boldsymbol{\tau_{yawHT3}}$ are wave with zero mean, thus producing a positive displacement only on the axis direction.

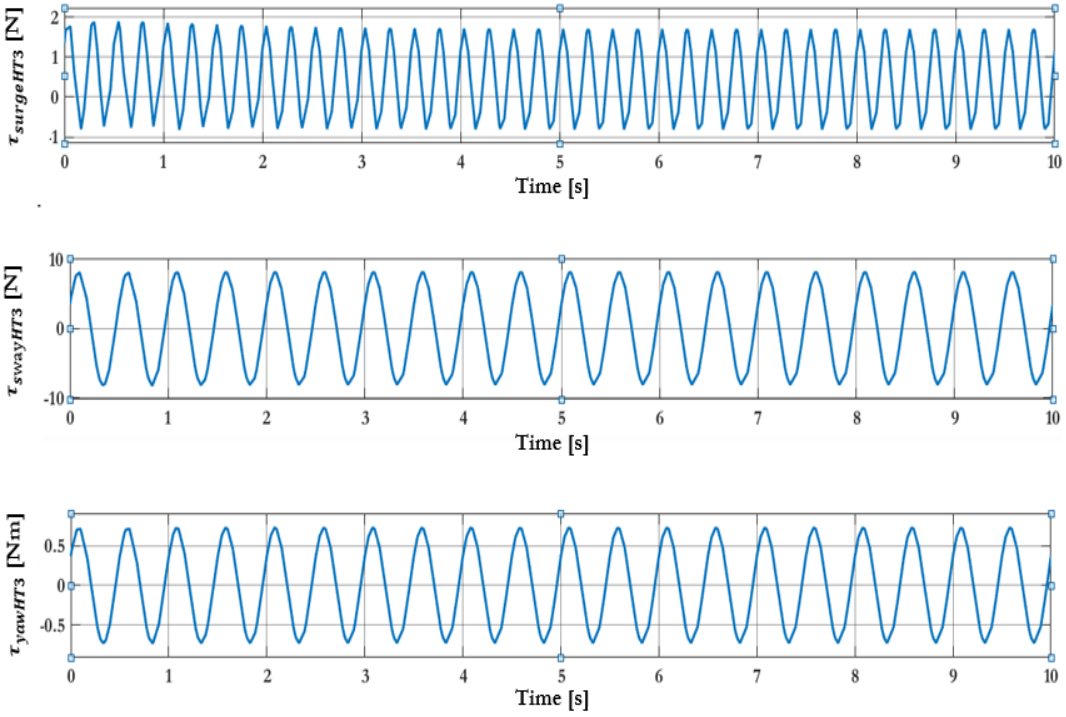

Figure 3.16: HT3 Forces and moments generated at $f = 2Hz$.

The second test carried out is by controlling HT3 not only with the oscillation frequency of the fin but also with the angle $\bar{\theta}$. This, by hypothesis, is assumed with values ranging from -60° to 60°, thus that the angular position of the fin, in modulus, is not higher than 90° to prevent damage to the mechanical structure of the fish.

Figure 3.17 shows the behaviour of the vehicle with a frequency of 2 Hz and with Theta_uHT3 command value equal to 1, i.e. with a steering angle $\bar{\theta}$ of 60 degrees. It is possible to notice that even if the steering contribution is maximum, the robotic fish cannot assume a rotation without there being a movement of the vehicle in the direction of the X and Y axes.

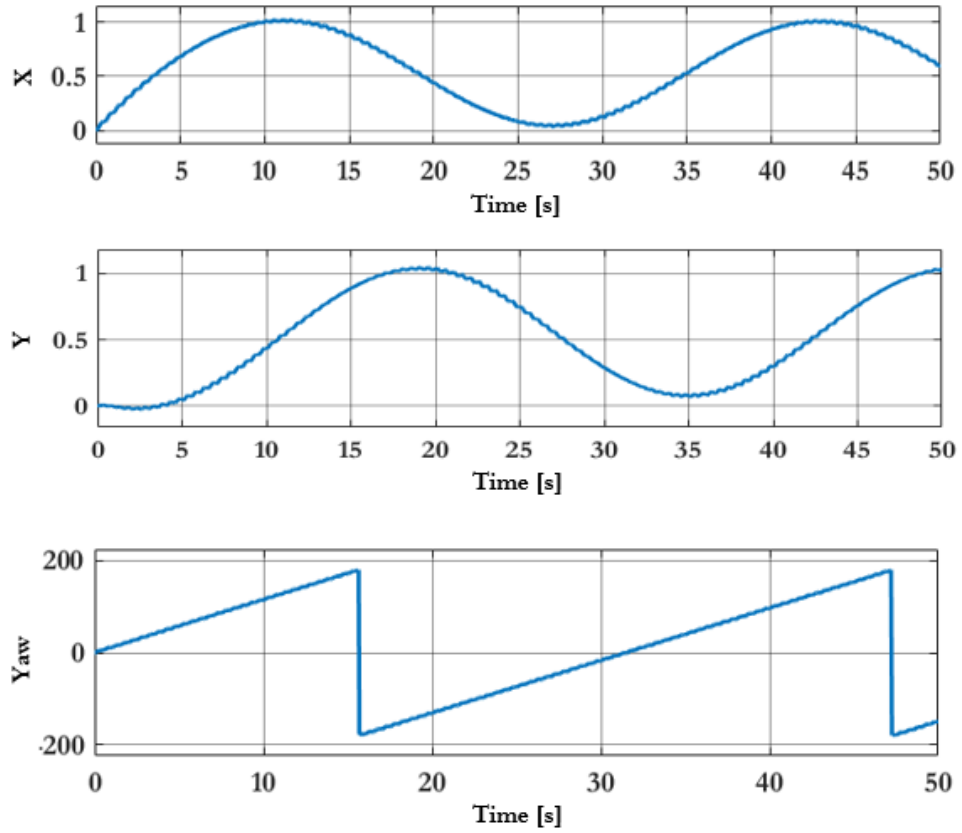

Figure 3.17: GUIZZO 6.0 behaviour with $f = 2Hz$ and $\bar{\theta} = 60°$.

This behaviour is due to the resulting forces shown in Figure 3.18, where it is possible to note that in addition to τ_{yawHT3} also $\tau_{swayHT3}$ has a non-zero average value producing a displacement from the initial position of the fish.

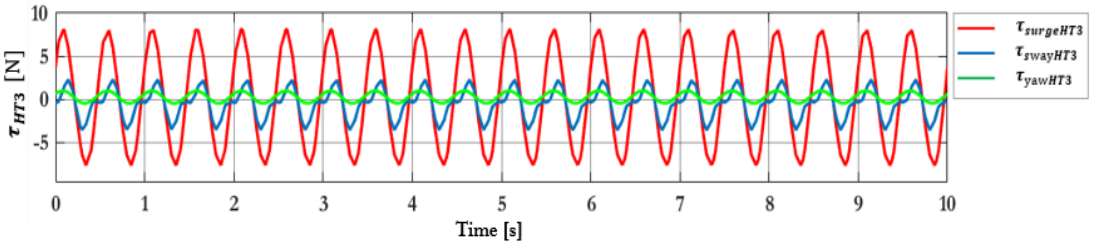

Figure 3.18: HT3 Forces and moments generated at $f = 2Hz$ and $\bar{\theta} = 60°$.

A rotation without changing the initial position of the vehicle can be obtained by means of HT1 and HT2 thrusters with $uHT1 = -uHT2$.

Figure 3.19 shows the behaviour of the underwater vehicle controlled with $uHT1 = 1$ and $uHT2 = -1$, in which the only variation obtained is that of the yaw attitude; while Figure 3.20 shows the resulting speed u of the robotic fish controlled with $uHT1 = uHT2 = 1$, where constant speed is reached when the propulsive force is balanced from the viscous resistance.

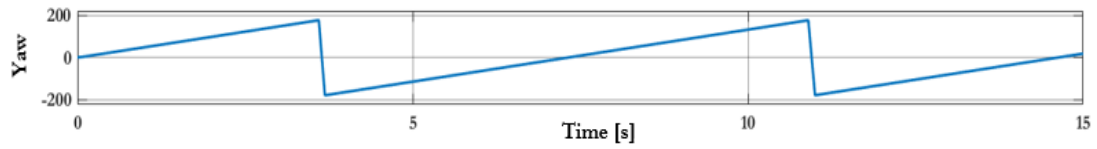

Figure 3.19: GUIZZO 6.0 rotation with uHT1= 1 and uHT2= −1.

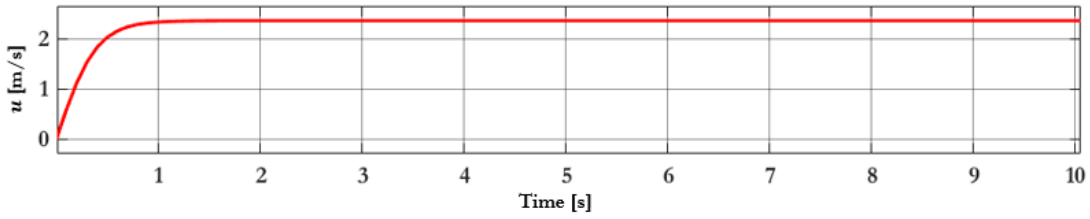

Figure 3.20: GUIZZO 6.0 straight forward speed with uHT1= 1 and uHT2= 1.

LATERAL FINS VT2 VT3

When the robotic fish is in horizontal motion it is also possible to control the depth using the side fins. These will also be responsible for changing the pitch and roll angles of the vehicle.

The fins are activated by uVT1 and uVT2 commands; the behaviour of the robotic fish moving forward by means of the caudal fin with an oscillation frequency of 2 Hz and with uVT1 = uVT2 = 1 is shown in figure.

The commands in question refer to the angles $\boldsymbol{\delta_{VT2}, \delta_{VT3}}$ relative to the hull of the fish. These angles are supposed to be: $-45° \leq \delta_{VT2} \leq 45°$ and $-45° \leq \delta_{VT3} \leq 45°$.

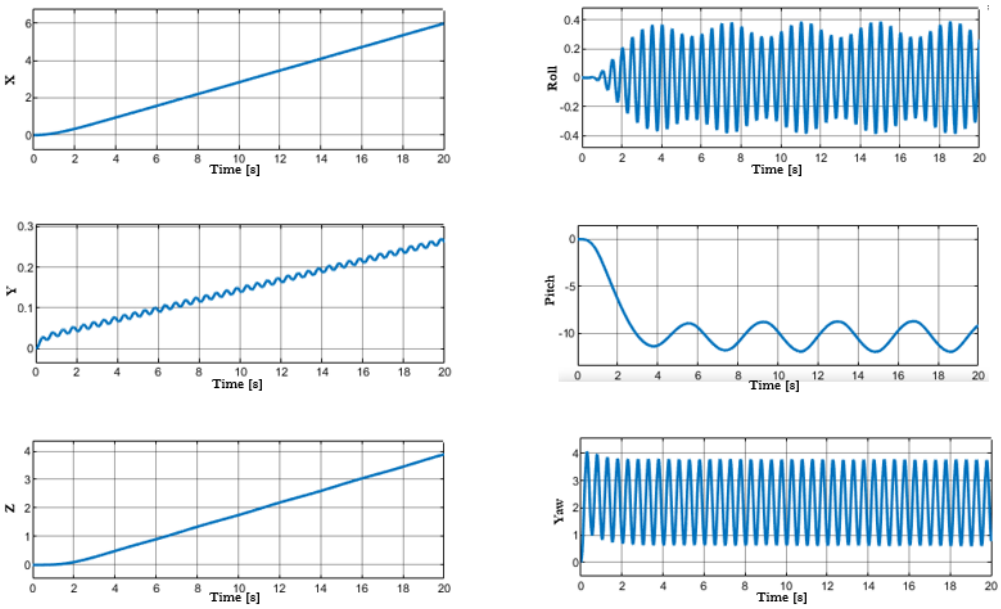

Figure 3.21: Robotic Fish Position and attitude at $f = 2Hz$ and with $\delta_{VT2} = \delta_{VT3} = 45°$.

As can be seen from Figure 3.21, in addition to the movement along the direction of the axis x caused by the caudal fin, the marine vehicle is moving vertically along and has an important variation of the pitch angle.

This is caused by the forces and moments, which are shown in Figure 3.22, generated by the lateral fins VT1 and VT2.

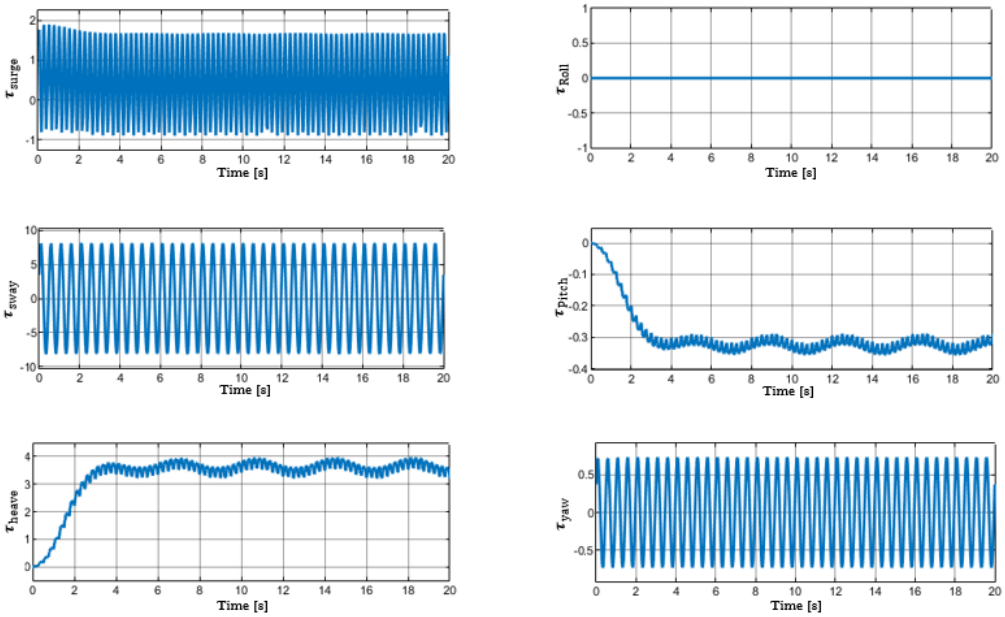

Figure 3.22: Robotic Fish Forces and moments generated at $f = 2Hz$ and with $\delta_{VT2} = \delta_{VT3} = 45$

Chapter 4.

Navigation, Guidance and Control System

This chapter deals with the problem of navigation, guidance and control of a marine vehicle, in particular it focuses on the control and guidance strategies developed to manoeuvre the biomimetic robot examined, GUIZZO 6.0.

Once the above-mentioned concepts have been described in theory, the implementation of the NGC system in Simulink is reported and the obtained results are discussed.

In detail, this chapter is organised as follows. An overview of the navigation, guidance and control system is given in section 4.1. Section 4.2 discusses, from a theoretical point of view, about the guidance law that is used for autonomous underwater vehicle's NGC system; while, the application in the case of GUIZZO 6.0 of the mentioned system is reported in section 4.3. Finally, the implementation of the NGC system in Simulink software and the simulation results are given in section 4.4.

4.1 NGC System

NGC system can be considered as the brain of the vehicle, in fact it is responsible for directing the propulsive forces and stabilizing the vehicle along the provided references with the specified accuracy. The terms navigation, guidance and control can be defined as [33]:

- **Navigation** is the process of determining vehicle's location with respect to some reference system, it measures the instantaneous states of the craft, which are used by the guidance system to generate the optimum trajectory and steering commands to achieve the specified target. The measurement of the vehicle's states (position/attitude, course, distance travelled and in some cases velocity and acceleration) is usually done by using a global navigation system (GNSS) combined with motion sensors (accelerometers and gyros).
  In this thesis, since we only deal with the simulation environment, the vehicle's states are derived directly from the mathematical model of the robotic fish described in the previous chapter.

- **Guidance** is the process for guiding a vehicle toward a given point, which in general may be moving. Guidance system represents a basic methodology that collects and processes the information provided by the navigation system and human operator and then feeds the results to the motion control system.
  Guidance system plays a vital role in bringing autonomy to the system. Many different guidance laws have been employed exploiting various design concept over the year; in particular, the guidance technology of missile is a mature field with an abundance of guidance laws already implemented in real systems. Among the current techniques used by most high-speed missiles today the most popular is the line-of-sight (LOS) guidance, which will be used for the study and implementation of the NGC system for the robotic fish examined.

- **Control** or motion control is a system which calculates the forces and moments that act upon the vehicle and processes all the information given by the navigation and guidance system to satisfy specific control objectives. These objectives are for

instance to maintain or move to a desired position with a predefined orientation. It is possible to distinguish between three main control objectives:

1. Setpoint regulation: It is the most basic control objective and it consists on a constant value (for example constant depth, trim, heel and speed control) provided by a human operator as input. In order to achieve the setpoint the controller that can be used is a simple regulator.

2. Trajectory-tracking control: In this case, the control objectives are the reference position and velocity that should be reached in a desired time and the corresponding feedback controller is a trajectory-tracking controller. Tracking control can be used for course-changing manoeuvres, speed changing and attitude control.

3. Path-following control: It consists in following a predefined path independent of time, so there are no time constraints.

Constructing the control algorithm involves the design of feedback and feedforward control laws. The outputs from the navigation system, position, velocity and acceleration are used for feedback control while feedforward control is implemented using signals available in the guidance system and other external sensors.

4.2 Guidance law

The design of an appropriate guidance law allows to solve the main problem in bringing autonomy to any vehicle. A guidance system which generates suitable trajectories to be followed represent the key element for truly autonomous operations.

4.2.1 Introduction

As mentioned before, all autonomous vehicle must be provided of a navigation, guidance and control system, which should work in agreement with each other as follows: the navigations system provides information related to the target, which is processed by the guidance system to generate reference signals; while the control system is responsible for keeping the vehicle course as specified by the guidance. Imperfections in one system degrade the efficiency of others.

There are different definitions of a guidance system, the father of inertial navigation, Charles Stark Draper, states: *"Guidance depends upon fundamental principles and involves devices that are similar for vehicles moving on land, on water, under water, in air, beyond the atmosphere with the gravitational field of earth and in space outside this field"* [39].

A rudimentary guidance and control system for a vehicle is shown in Figure 4.1, in which the guidance system receives inputs from all the sensor on-board and generate the reference signals or set points for the control system.

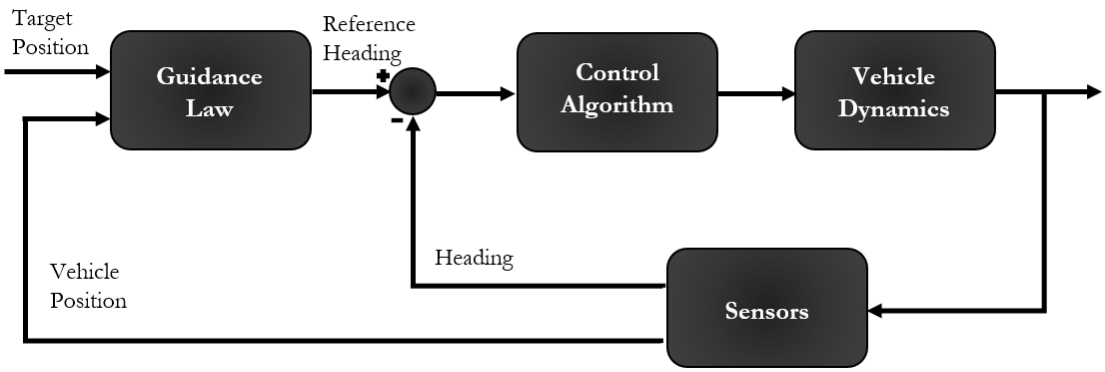

Figure 4.1: Scheme of the guidance and control system for a generic vehicle.

Guidance issues are mainly determined by the environment conditions and the location and nature of the target, which corresponds to the condition as to whether the target is stationary, moving or manoeuvring. The target location is imperative as it determines the heading to be followed by the vehicle, however, the accuracy of the system depends on the environment conditions.

As mentioned in section 4.1, the guidance technology of missiles is a mature field with an abundance of guidance laws already implemented in real systems. Currently, the popular terminal guidance laws involve line-of-sight (LOS) guidance, LOS rate guidance, command-to-line-of-sight (CLOS) guidance, proportional navigation (PNG) [40], and optimal guidance laws based on liner quadratic theory [41-42].

From the previous guidance laws directly comes the guidance technique used on autonomous underwater vehicles. In the following will be presented the LOS guidance law, which is the law used for the NGC system for the robotic fish, object of study of this work.

4.2.2 Line-Of-Sight Guidance

In general, line-of-sight (LOS) guidance is classified as a three-point guidance scheme: stationary reference point, interceptor and the target. The interceptor is supposed to achieve an intercept by moving along the LOS vector between the reference point and the target.
The most widely used scheme in the field of autonomous underwater vehicles is the waypoint law by line of sight. This guidance is achieved by a heading command to vehicle's steering system to approach the line of sight between the current position of the vehicle and the waypoint to be reached.
This guidance strategy can be used for path following, in the case guidance is achieved by splitting into several waypoints to be reached in the exact order. In this case, a LOS vector is defined as the conjunction of the current position of the vehicle and the waypoint to be achieved.
For 2-D horizontal plane motions, it is possible to consider a straight-line path defined by two waypoints
$p_k = [x_k, y_k]^T$, $p_{k+1} = [x_{k+1}, y_{k+1}]^T \in \mathbb{R}^2$; and a path-fixed reference frame with origin in rotated by a positive angle:

$$\alpha_k = atan2(y_{k+1} - y_k \ , x_{k+1} - x_k \ ) \tag{4.1}$$

Relative to x_E axis. The vehicle has the following coordinates in this new reference frame:

$$\begin{bmatrix} s(t) \\ e(t) \end{bmatrix} = \begin{bmatrix} cos\,\alpha_k & -sin\,\alpha_k \\ sin\,\alpha_k & cos\,\alpha_k \end{bmatrix} \begin{bmatrix} x_{k+1} - x_k \\ y_{k+1} - y_k \end{bmatrix} \tag{4.2}$$

where $s(t)$ is the along-track distance (tangential to path) while $e(t)$ is the cross-track error (normal to path). For path-following purpose, only $e(t)$ is relevant, since if is null, the vehicle has converged to the straight path. In order to guarantee that $e(t) \to 0)$, both course angle and heading can be used.

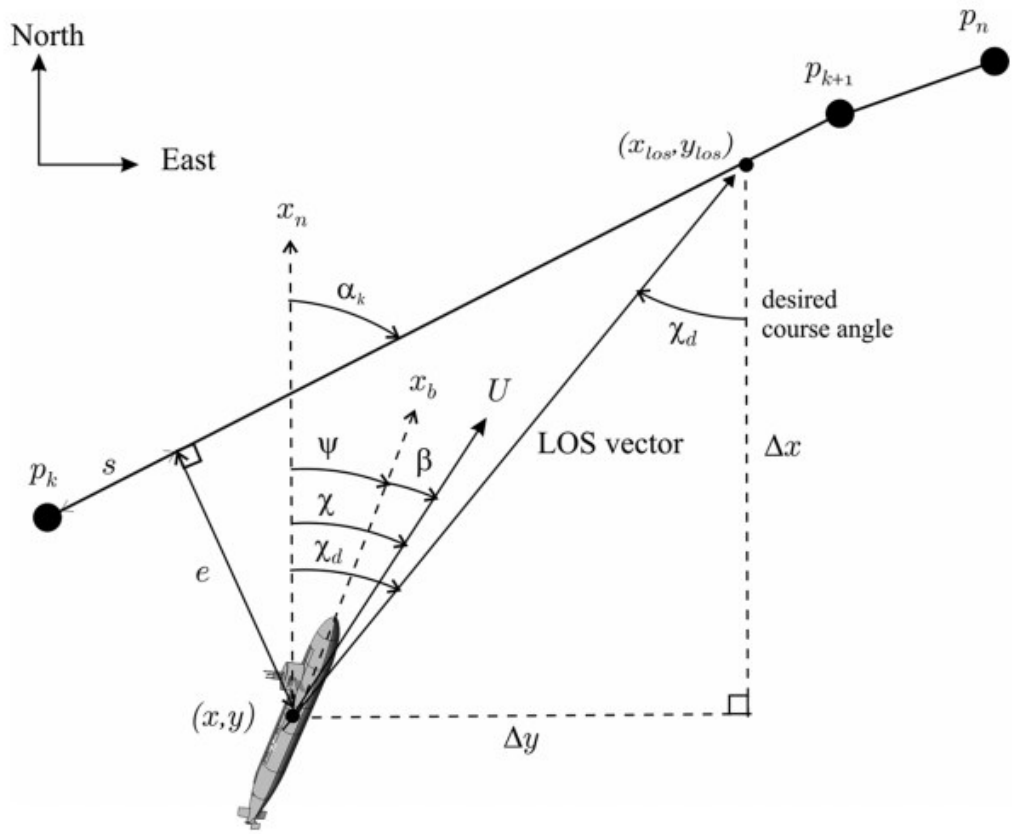

Figure 4.2: General scheme for LOS Guidance [33].

In Fossen [33] are defined two steering methods which essentially operate by the same principle. These two different guidance principles are:

- Encloser-based steering
- Lookahead-based steering

The first consists in defining a circle with radius R centered in the vehicle position. If the radius is big enough, it will intersect the straight path:
the intersection point near p_{k+1} will be called $p_{los} = [x_{los}, y_{los}]^T$ and correspond to the desired direction of travel. This direction is defined as:

$$\chi_d(t) = atan2(y_{los} - y(t)\,, x_{los} - x(t)\,) \tag{4.3}$$

The lookahead-based steering consists in dividing the desired course angle in two parts:

$$\chi_d(e) = \chi_p + \chi_r(e) \tag{4.4}$$

where $\chi_p = \alpha_k$ is the path-tangential angle, while $\chi_r(e) = arctan\frac{-e(t)}{\Delta(t)}$ is the velocity-path relative angle. This term ensures that the velocity is directed toward a point on the path that is located in the lookahead distance $\Delta(t) > 0$ ahead of the direction projection of the vehicle position on the path. It can be noticed, from the figure, that the enclosure-based technique is a lookahead-based approach a time-varying Δ from 0 to R:

$$\Delta(t) = \sqrt{R^2 - e^2(t)} \tag{4.5}$$

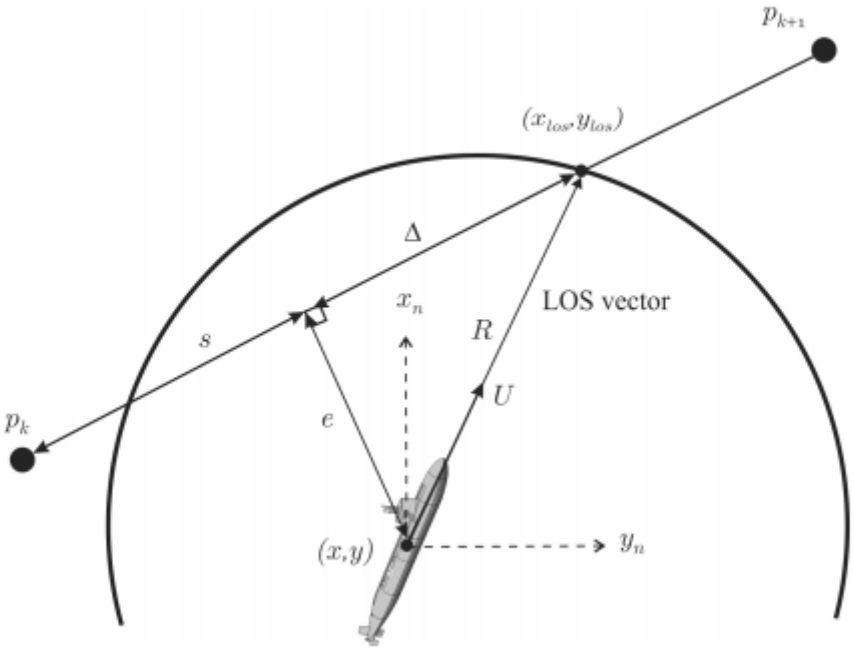

Figure 4.3: LOS Guidance in the case of a lookahead scheme [33].

4.3 NGC System application for GUIZZO 6.0

Previously, the navigation, guidance and control system of an autonomous underwater vehicle has been described in theory. In this section the implementation of the NGC system applied to the real case of the biomimetic robot examined, GUIZZO 6.0, will be reported. As mentioned before, the description of the navigation system will be omitted, therefore this work will focus on only the guidance law and control system implemented for the robotic fish.

4.3.1 GUIZZO 6.0 Guidance Law

In this paragraph will be presented a simple employment of the robotic fish with a combined LOS-waypoints guidance. The waypoint guidance is a simple but efficient guidance strategy used in a wide range of applications.

The k-th waypoint position can be defined in a 3-D space as $[x_k, y_k, z_k]$, to achieve the waypoint, in this work, a new guidance law will be introduced, which addresses the problem separating the horizontal plane (x-y plane) from the depth.

- x-y plane: in this case the LOS guidance strategy for a two-dimensional space is used, in which the goal is to reach the x and y coordinates of the k-th waypoint, basically $p_k = [x_k, y_k]^T$. To achieve the goal, guidance law calculates the distance D between k-th waypoint position $[x_k, y_k]$ and the vehicle's position at time t $[x(t), y(t)]$:

$$\boldsymbol{D = \sqrt{(x_k - x(t))^2 + (y_k - y(t))^2}} \tag{4.6}$$

The calculated distance will be fed to the surge force controller.

In order to achieve the k-th waypoint, is necessary to calculate the steering reference. The steering law will have the structure of an enclosure-based technique:

$$\boldsymbol{\psi_d(t) = atan2(y_k - y\,(t)\,, x_k - x(t)\,)} \tag{4.7}$$

($atan2$ is a function which returns an angle value within a range $[-\pi, \pi]$)

where $\psi_d(t)$ is the desired heading at time t, $[x_k, y_k]$ is the position, in the 2D space of the k-th waypoint, while $[x(t), y(t)]$is the position of the fish at time t. $\psi_d(t)$ will be then fed to the steering force controller.

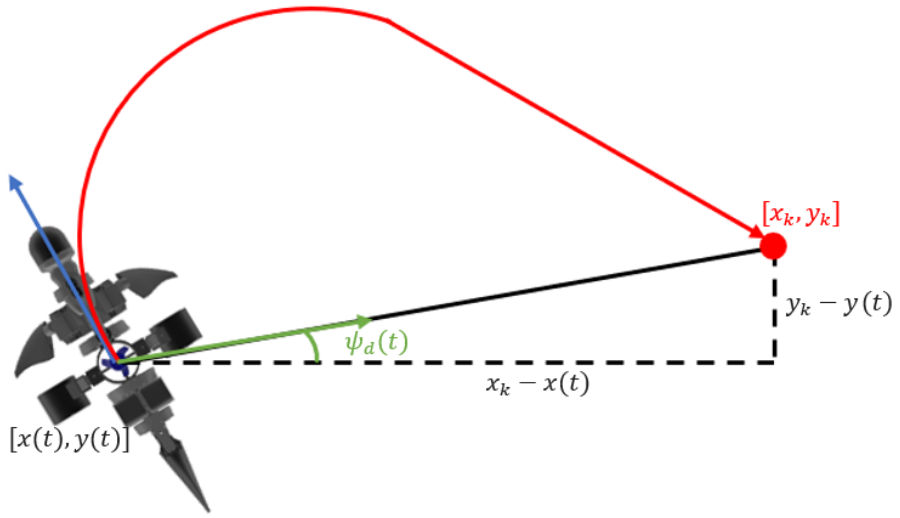

Figure 4.4: LOS Guidance scheme GUIZZO 6.0.

- Depth: in this case the guidance system will not do any operation, thus will fed directly the z coordinate of the k-th waypoint, z_k, to the heave controller

4.3.2 GUIZZO 6.0 Motion Control system

PID CONTROL SYSTEM

The motion control system developed for the marine vehicle is a PID control system. This choice has been made since the PID controller is one of the most common control systems, thanks to its implementation simplicity, and it has been deeply analysed in the literature. In this work the vehicle is assumed to be in an environment without any king of disturbances, and without any noises in robotic position and attitude measurements.

Before proceeding to the analysis and description of the motion control system implemented, some considerations must be made regarding the actuators that are used to operate the GUIZZO 6.0.

As seen in the chapter 3, the vehicle is equipped with a total of six actuators: lateral propellers (HT1 and HT2) and caudal fin (HT3) are responsible of horizontal motion; vertical propeller (VT1) and pectoral fins (VT2 and VT3) are responsible of the vertical motion (depth).

These actuators are controlled by the following command:

1. f_uHT3 controls caudal fin (HT3) oscillation frequency
2. Theta_uHT3 controls caudal fin (HT3) steering angle
3. uHT1 controls lateral propeller (HT1) rotation speed
4. uHT2 controls lateral propeller (HT2) rotation speed
5. uVT1 controls vertical propeller (VT1) rotation speed
6. uVT2 controls pectoral fin (VT2) angle referring to the vehicle's hull
7. uVT3 controls pectoral fin (VT3) angle referring to the vehicle's hull

In addition, the motion control system that will be described consists in controlling the command signals of the actuators, to reach the desired references, through three outputs:

1. τ_X surge force, which is responsible of surge motion control;
2. τ_N yaw moment, which is responsible of steering control;
3. τ_Z heave force, which is responsible of depth control.

The considerations that have been made regarding the motion control system are the following:

- The human operator is given the opportunity to use the lateral propellers or the caudal fin to control the surge motion. Then τ_X will generate the command signals either for the rotation speed of the lateral propellers (u_HT1 and uHT2) or for the oscillation frequency of the caudal fin (f_uHT3).

- As for heading control, for a simplicity matter, only the lateral propellers are used. Then, the steering controller output τ_N will only generate command signals uHT1 and uHT2 and not Theta_uHT3; therefore, caudal fin will not be used for steering.

- The last consideration is made on depth control; in this case it is automatically decided whether to use the vertical propeller or the lateral fins. If the vehicle does

not move along the horizontal plane, therefore the lateral propellers and the caudal fin are off, the depth control output generates the command signal for the rotation speed of the vertical propeller VT1. Otherwise the command signal is generated to operate the pectoral fins VT2 and VT3.

To generate actuator's command signals, starting from the output of the control system, the control allocation module is introduced. This will be analysed later.
After listing the condition under which the motion control system is described, it is possible, now, to delve into the PID controller used.

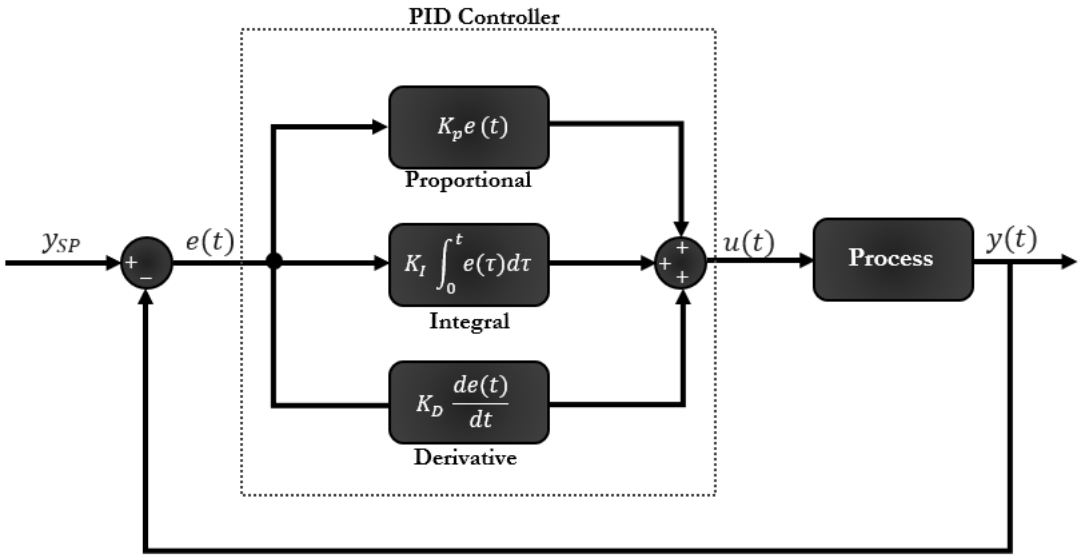

Figure 4.5: Generic PID controller structure.

Figure 4.5 shows the classic scheme of a PID controller where $y(t)$ is the measured process variable, y_{SP} the reference variable, $u(t)$ is the control signal and $e(t) = y_{SP} - y(t)$ is the control error. The control signal is thus a sum of three elements: the P-term, which is proportional to the error; the I-term which is proportional to the integral of the error; the D-term which is proportional to the derivative of the error.

PID controller is also characterized by three parameters: proportional gain K_P, integral gain K_I and derivative gain K_D. To get good controller these gains must be properly tuned. In order to tune the PID gains, the following rules can be applied, while looking at the response of the controlled system to a step reference input:

- Proportional control: Larger values of the proportional gain mean a decrease in the rise time and in the steady-state error. However, it leads to an increase in the overshoot
- Integral control: Larger values of the derivative gain lead to an increase in the stability of the system, still it leads to the signal noise amplification.
- Derivative control: Larger values of the integral gain imply steady state errors are eliminated more quickly. On the other hand, larger values lead to a larger overshoot and to a decrease in the stability of the system.

For GUIZZO 6.0 motion control system, only Proportional and Derivative controller (PD) has been used. Indeed, integral control is used to cancel the steady-state error on a step reference, or when the proportional controller is not enough, or ontrodeces a large overshoot and oscillatory motion with little damping. In particular, the control system consists in three decoupled PD controllers: surge force PD controller, heading PD controller, and depth PD controller.

S***urge Force Controller:***

As mentioned above, surge force controller consists in two cases: the first case occurs when human operator decides to actuate the vehicle only with lateral propellers, while the second case occurs when human operator selects the caudal fin to operate the vehicle.
Based on the actuator's selection, the controller gains will also be different. For this reason, it was decided to build two separate PD controllers: one to generate the command signal for the rotation speed of the propellers and the other to generate the command for the caudal fin's oscillation frequency.
The surge force controller can be defined as follows:

$$\begin{cases} \tau_X = K_{Px\_prop} D(t) + K_{Dx\_prop} \dfrac{dD(t)}{dt} & \text{for lateral propellers} \\ \tau_X = K_{Px\_fin} D(t) + K_{Dx\_fin} \dfrac{dD(t)}{dt} & \text{for caudal fin} \end{cases} \tag{4.8}$$

Where D is the distance between the waypoint and the actual vehicle's position calculated by the guidance law. K_{Px_prop} and K_{Dx_prop} are the PD controller gains in case the propellers are actuated and K_{Px_fin} and K_{Dx_fin} are the PD controller gains in case the fin is actuated. PD gain's tuning was done analytically.

Heading (Steering) Controller:

The steering PD controller can be defined as:

$$\tau_N = K_{PN}\psi_{error}(t) + K_{DN}\frac{d\psi_{error}(t)}{dt}$$
$$\psi_{error}(t) = \psi_D(t) - \psi(t) \tag{4.9}$$

where $\psi_D(t)$ is the steering angle calculated by the guidance-law, $\psi(t)$ is the vehicle's yaw angle at time t, K_{PN} and K_{DN} are the steering PD controller's gains.

Depth Controller

Depth PD controller can be defined as:

$$\tau_Z = K_{PZ}z_{error}(t) + K_{DZ}\frac{dz_{error}(t)}{dt}$$
$$z_{error}(t) = z_{rif} - z(t) \tag{4.10}$$

where z_{rif} is the waypoint's z coordinate to achieve, $z(t)$ is the vehicle's z-axis position at time t, K_{PZ} and K_{DZ} are the depth PD controller's gains.

CONTROL ALLOCATION

In general, for marine craft in n DOF it is necessary to distribute the generalised control forces $\tau \in \mathbb{R}^n$ to the actuators in terms of control inputs $u \in \mathbb{R}^r$. If $r > n$ this is an overactuated control problem while $r < n$ is referred to as underactuted control.
Computation of u from τ is a typical Control Allocation problem, which in its simplest form is unconstrained while physical limitations such as input amplitude and rate saturations imply that a constrained problem must be solved.

For robotic fish we have that $n = 3$ and r =7. Moreover, the control allocation problem can be formulated in the following way:

$$u(t) = T^{+}\,\tau(t) \quad \text{with} \quad u_{min} \leq u(t) \leq u_{max} \tag{4.11}$$

Where $u(t)$ is the vector of control inputs, $u = [u_{f\_HT3}\ u_{\theta\_HT3}\ u_{HT1}\ u_{HT2}\ u_{VT1}\ u_{VT2}\ u_{VT3}]^T$,at time t; $\tau(t)$ is the control forces vector, $\tau = [\tau_X \quad \tau_N \quad \tau_Z]^T$, at time t; $T^{+} \in \mathbb{R}^{r \times n}$ is the force coefficients pseudoinverse matrix, that will have the following form:

$$T^{+} = \begin{bmatrix} T_{11} & T_{12} & T_{13} \\ T_{21} & T_{22} & T_{23} \\ T_{31} & T_{32} & T_{33} \\ T_{41} & T_{42} & T_{43} \\ T_{51} & T_{52} & T_{53} \\ T_{61} & T_{62} & T_{63} \\ T_{71} & T_{72} & T_{73} \end{bmatrix}$$

Therefore, the solution to the control allocation problem simply consists in solving the system of equations:

$$\begin{cases} T_{11}\tau_X + T_{12}\tau_N + T_{13}\tau_Z = u_{f\_HT3} \\ T_{21}\tau_X + T_{22}\tau_N + T_{23}\tau_Z = u_{\theta\_HT3} \\ T_{31}\tau_X + T_{32}\tau_N + T_{33}\tau_Z = u_{HT1} \\ T_{41}\tau_X + T_{42}\tau_N + T_{43}\tau_Z = u_{HT2} \\ T_{51}\tau_X + T_{52}\tau_N + T_{53}\tau_Z = u_{VT1} \\ T_{61}\tau_X + T_{62}\tau_N + T_{63}\tau_Z = u_{VT2} \\ T_{71}\tau_X + T_{72}\tau_N + T_{73}\tau_Z = u_{VT3} \end{cases} \quad \text{with saturation limit } u_{min} \leq u_i \leq u_{max}$$

For the considerations previously made, it was decided to use three different configurations of the pseudoinverse matrix T^{+}:

- The first configuration is used when the human operator decides to select only the lateral propellers (HT1 and HT2) to operate the vehicle along the horizontal plane. For depth, however, pectoral fins are used. Hence the pseudoinverse matrix will have the following form:

$$T_1^+ = \begin{bmatrix} 0 & 0 & 0 \\ 0 & 0 & 0 \\ 1 & 1 & 0 \\ 1 & -1 & 0 \\ 0 & 0 & 1 \\ 0 & 0 & 1 \\ 0 & 0 & 0 \end{bmatrix}$$

In this case the set of equations to solve is:

$$\begin{cases} u_{f\_HT3} = 0 \\ u_{\theta\_HT3} = 0 \\ u_{HT1} = \tau_X + \tau_N \\ u_{HT2} = \tau_X - \tau_N \\ u_{VT1} = 0 \\ u_{VT2} = \tau_Z \\ u_{VT3} = \tau_Z \end{cases} \text{ with the saturation limit } u_{min} \leq u_i \leq u_{max}$$

- The second configuration is used when it is chosen by the human operator to actuate the vehicle for the surge motion by means of the caudal fin (HT3), while the lateral propellers are used to steer. However, also in this case the pectoral fins are used for the depth. Hence:

$$T_2^+ = \begin{bmatrix} 1 & 0 & 0 \\ 0 & 0 & 0 \\ 0 & 1 & 0 \\ 0 & -1 & 0 \\ 0 & 0 & 1 \\ 0 & 0 & 1 \\ 0 & 0 & 0 \end{bmatrix}$$

The set of equations to be solve is:

$$\begin{cases} u_{f\_HT3} = \tau_X \\ u_{\theta\_HT3} = 0 \\ u_{HT1} = \tau_N \\ u_{HT2} = -\tau_N \\ u_{VT1} = 0 \\ u_{VT2} = \tau_Z \\ u_{VT3} = \tau_Z \end{cases} \text{ with the saturation limit } u_{min} \leq u_i \leq u_{max}$$

- The last configuration is used when the surge force control, τ_X, is null. In this case all the actuators are switched off, since $\tau_X = 0$ means that the reference expressed only in x and y coordinates (horizontal plane) has been reached. However, given that

the horizontal plane control is divided by the depth control, it could happen that the z coordinate of the reference has not yet been reached, in which case the control system automatically activates the vertical propeller (VT1) to reach the target.

In this case the pseudoinverse matrix will be:

$$T_3^+ = \begin{bmatrix} 0 & 0 & 0 \\ 0 & 0 & 0 \\ 0 & 0 & 0 \\ 0 & 0 & 0 \\ 0 & 0 & 0 \\ 0 & 0 & 0 \\ 0 & 0 & 1 \end{bmatrix}$$

A final consideration to make regarding the x-y plane is that it is not always possible to reach the exact point of the reference for various reasons, for example due to the presence of noise in the measurement of the vehicle's position, or due to disturbances acting on the vehicle itself due to the surrounding environment (sea current, waves and other disturbances). The implementation of a good robust controller could be a solution to the above-mentioned problem. In our case, however, it was decided to approach a different method, namely that of identifying a region defined by a circle of radius ε inside which the reference is considered to have been reached. To do this, once the vehicle enters the circle of radius ε, all the actuators responsible for x-y plane motion are turned off. Thus, the third configuration of the matrix is used if $\tau_X \leq \varepsilon$.

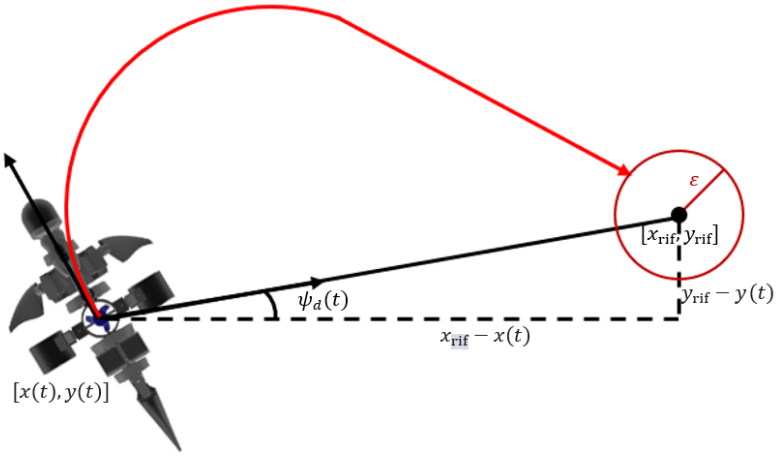

Figure 4.6: LOS Guidance scheme for GUIZZO 6.0 with circle of radius ε.

4.4 NGC system implementation in Simulink

This section briefly describes the implementation of GUIZZO 6.0 guidance and control navigation system in the Simulink software. Then the results obtained by the simulation software are reported, focusing on some cases and discussing some problems that have been addressed

4.4.1 Simulation software structure

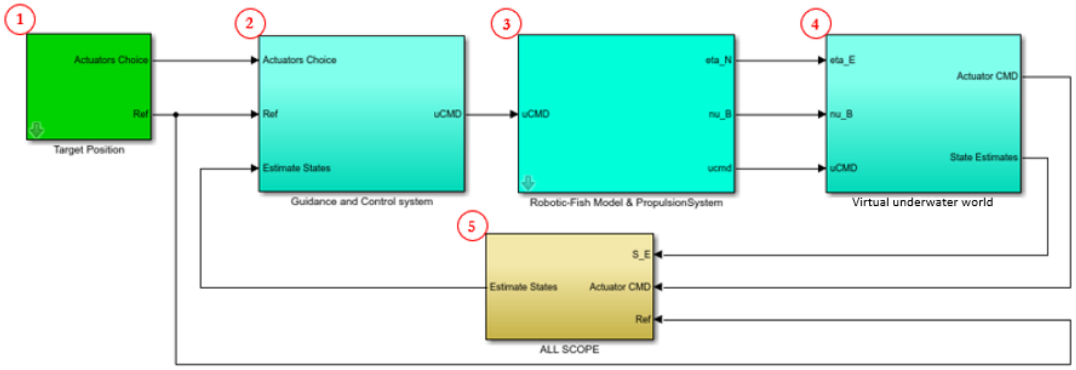

Figure 4.7: NGC Robotic Fish Simulink block diagram.

.

As shown in the Figure 4.7, the simulation software is characterized by a total of five subsystems:

1. Target Position:

   This subsystem is characterized by a mask that acts as a "control panel" that can be used by human operator. The control panel mainly provides for the management of three types of operations:

   - By means of a radio button, it is possible to choose how the vehicle is actuated, i.e. "normal" operation which involves the use of the caudal fin for surge motion, the lateral propellers for steering. "Only propeller" operation, where the propellers are used for both surge motion and steering.
   - The second operation also consists of a radio button that allows you to choose the type of target to be reached. "Way-Point Position" consist in choosing the x y z coordinate of the reference, essentially it consists of a set-

point. "Way-Points bases Path" it allows you to choose Path consisting of a multiple waypoint that can be generated from the "Waypoints generator" block, which is simply a Simulink block that creates a group of signals ("Signal Builder").

- The last operation can be carried out if "Way-Point Position" is chosen and consists in entering the x y z reference to be reached (Xr, Yr, Zr).

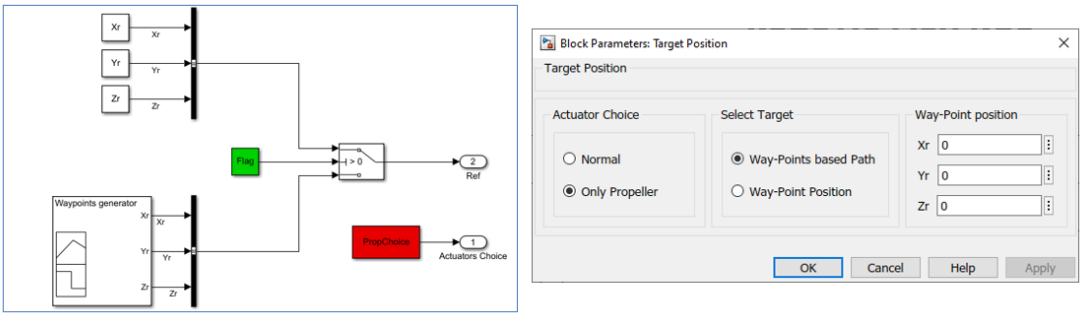

Figure 4.8: "Target Position" block diagram with mask.

2. Guidance and Control system:

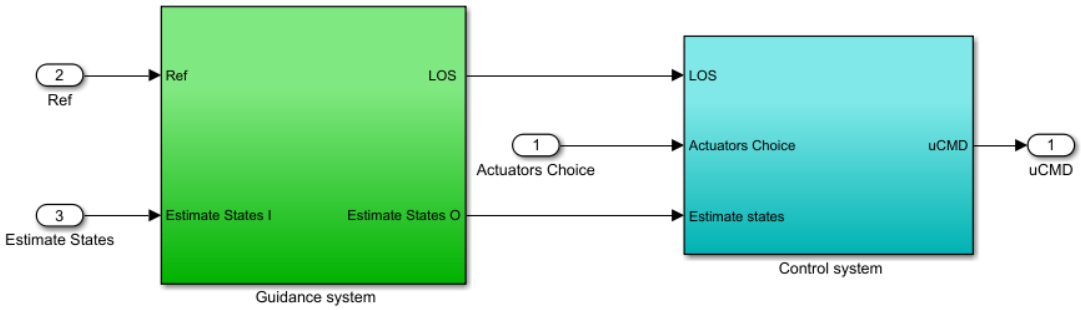

Figure 4.9: "Guidance and Control system" block diagram.

This subsystem is divided into two other sub-blocks: "Guidance system" and "Control System".

- In the first sub-block, the LOS guidance law, described in section 4.3.1, is implemented. This block takes as input the "ref" vector consisting of Xr Yr

and Zr and as a second input takes the vector "Estimate States" containing the position, the orientation, the linear and angular velocities of the robot at the current time by selecting only the x y z coordinates of the current position of the vehicle (X Y Z). As output it returns the vector, "LOS" composed of the distance, D, calculated by the "Distance" block, the yaw angle, Yaw_d, calculated by the "LOS law" block and the difference between Zr and Z, that is Ze. Furthermore, it returns as second output the "Estimate States" vector.

To calculate the angle Yaw_d the Unwrap Simulink block is also used; this block unwraps the input by adding or subtracting appropriate multiples of π to remove phase discontinuities. Unwrap block is used whenever the vehicle is performing with a yaw angle around $+\pi$ (or $-\pi$); in this case "atan2" block shifts from $+\pi$ to $-\pi$ (or $-\pi$ to $+\pi$), thus creating a discontinuity point.

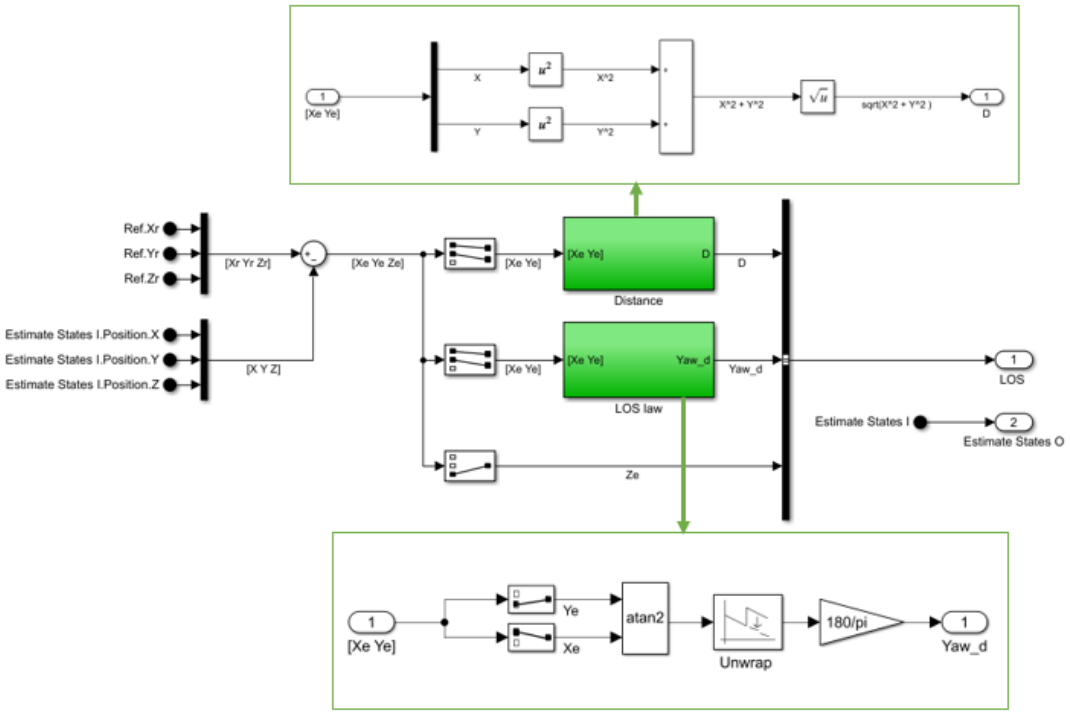

Figure 4.10: "Guidance system" block diagram.

- The second sub-diagram takes as input the vectors returned by the guidance system block, "LOS" and "Estimate States", it also takes as input the "Actuators Choice" variable. In addition, the "Control System" block is, in turn, made up of two other subsystems, "Control Law" and "Control allocator".

  The "Control law" block contains the PD controller described in the paragraph. The "Actuator Choice" variable assumes value 0 when, in the control panel of the "Target Position" block, "normal" operation is selected, while it assumes value 1 if "Only Propeller" operation is selected. This variable is used to select between the two PDs of the surge force TX.

  As output, the "Control Law" block returns the vector "Tin" formed by surge force TX, by steering moment TN, and by the depth force TZ.

  The "Control Allocator" block takes as input the "Tin" vector and the "Actuator Choice" variable and outputs the "uCMD" vector formed by the control signals of the robotic fish actuators.

  In this block the control allocation strategy described in the paragraph is implemented. In the "Pseudoinverse choice" block the different force coefficients matrices are defined (T_1^+,T_2^+, T_3^+) and one of them is selected according to the logic described in the paragraph.

  The "Saturation limits" block is used to set the saturation limits for each actuator command signal.

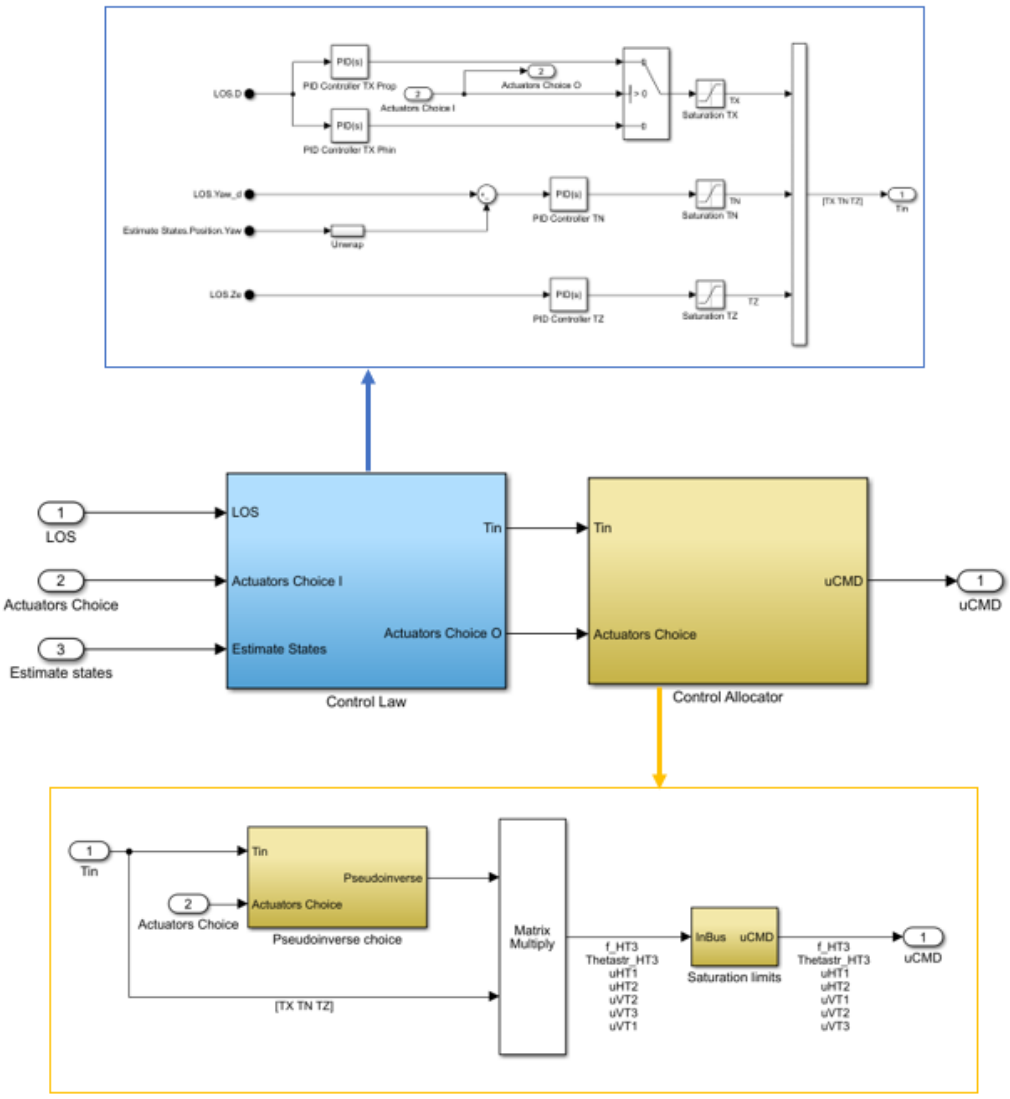

Figure 4.11: "Control system block diagram".

3. Robotic-Fish & PropulsionSystem: A thorough analysis of this subsystem has been reported in chapter 3.
4. Virtual underwater world: This subsystem will be described in chapter 5.
5. ALL SCOPE: This subsystem contains all the graphs relating to the position, orientation, linear velocity and angular velocities of the robotic fish. In addition, it contains the graphics of the control signals of the actuators with which the vehicle is equipped.

4.4.2 Simulation results

The simulation results, presented in this section, can be divided into two types of tests carried out. The first case concerns the test performed by giving as target to reach a waypoint in the x-y plane without considering the depth. The second test performed consists in giving as target to achieve a waypoint-based path characterized by a total of four waypoints. In this case, the depth also varies.

- FIRST CASE: X-Y PLANE

  The first case test concerns the behaviour of the vehicle only in the horizontal plane and therefore the depth is considered constant, equal to zero. The waypoint to reach is $[x_r = 5 \quad y_r = 5 \quad z_r = 0]^T$, moreover the radius of the circle within which the target is considered reached is $\varepsilon = 0.2$ (the unit of measurement of the values just provided is the meter).

  Figure 4.12 a) shows the x-y plane path of the vehicle when "normal" operation is selected (caudal fin for surge motion and lateral propellers for steering).

  It is possible to note that, although the actuators are turned off when the vehicle reaches the circle with radius ε, the reference is passed. At this point, to reach the reference again, the vehicle's actuators are reactivated again.

  This happens because the propulsion forces are greater than the frictional force; so that, even if the actuators turn off, the fish continues to move.

  This phenomenon occurs considerably if only the lateral propellers are used to actuate the robot (Figure 4.12 b), as the propulsion force of the propellers is greater than that exerted by the caudal fin.

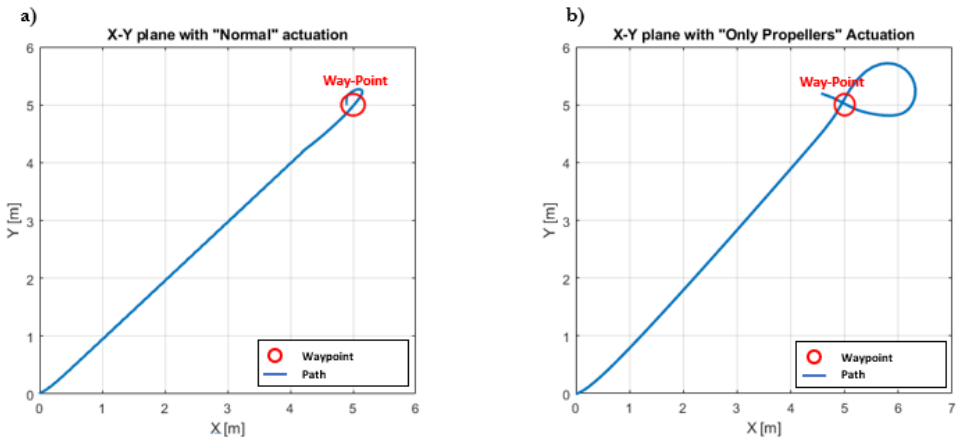

Figure 4.12: GUIZZO 6.0 Path X-Y plane with waypoint $[x_r = 5 \quad y_r = 5 \quad z_r = 0]^T$.

One method of solving this type of problem is to change the gains of the surge motion PD controller, specifically, to increase the derivative value. This, however, implies that the vehicle reaches the goal in longer times.

Instead, the method adopted is to use the lateral propellers to brake the vehicle, reversing the direction of rotation.

To do this, a circle of radius ξ is chosen, where $\xi < \varepsilon$, and when $\tau_x \leq \xi$ then, in the control allocation, a fourth configuration of the force coefficient pseudoinverse matrix is used; in which the lateral propellers are turned on with inverted direction of rotation, or with negative force coefficients:

$$T_4^+ = \begin{bmatrix} 0 & 0 & 0 \\ 0 & 0 & 0 \\ -1 & 0 & 0 \\ -1 & 0 & 0 \\ 0 & 0 & 0 \\ 0 & 0 & 0 \\ 0 & 0 & 1 \end{bmatrix}$$

The pseudoinverse matrix T_4^+ is used both in the case of "Only Propellers" and in the case of "Normal". In this way the lateral propellers are used as brake.

Note that the surge motion control and depth control are treated separately, therefore the force coefficient for the vertical propeller VT1 remains unchanged.

The Figure 4.13 shows the path of the marine vehicle with waypoint equal to $[x_r = 5 \quad y_r = 5 \quad z_r = 0]^T$ and $\varepsilon = 0.2$ and $\xi = 0.05$ (the unit of measurement of the values just provided is the meter).

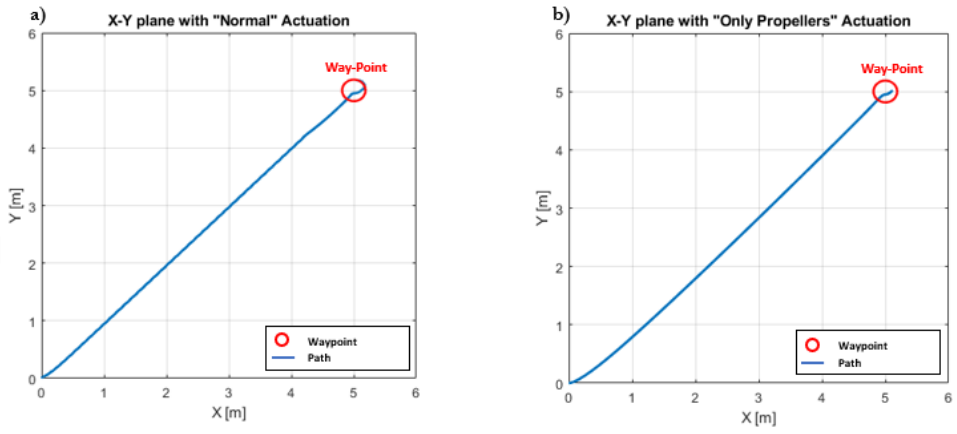

Figure 4.13: Robotic Fish Path X-Y plane with waypoint $[x_r = 5 \quad y_r = 5 \quad z_r = 0]^T$ with break system

- SCOND CASE: WAPOINT BASED PATH

  The second test that is reported is to give the marine robot as a target to achieve a waypoint-based path, consisting of a total of four waypoints:

  1. Waypoint1→ $[x_r = 5 \quad y_r = 0 \quad z_r = 2]^T$
  2. Waypoint2→ $[x_r = 5 \quad y_r = 5 \quad z_r = 4]^T$
  3. Waypoint3→ $[x_r = 0 \quad y_r = 5 \quad z_r = 6]^T$
  4. Waypoint4→ $[x_r = 0 \quad y_r = 0 \quad z_r = 8]^T$

  The "Signal Builder" Simulink block was used to generate the four waypoints. The Figure 4.14 shows the signals that the block mentioned above generates.

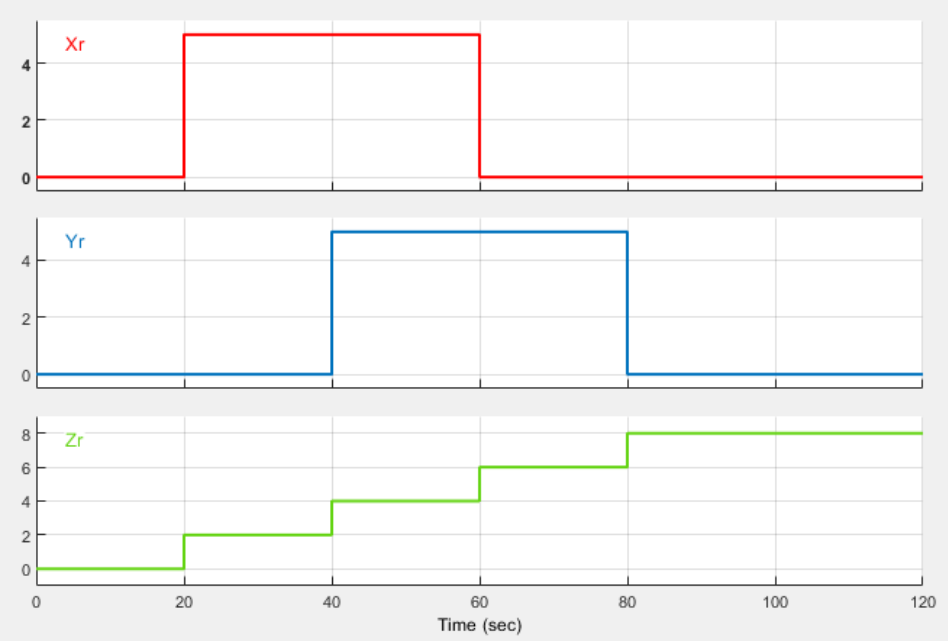

Figure 4.14: Waypoints generation signals with "Signal Builder" Simulink block

The results obtained from the simulation are shown below, first in the "Only Propellers" case and later in the "Normal" case.

"Only Propellers" case

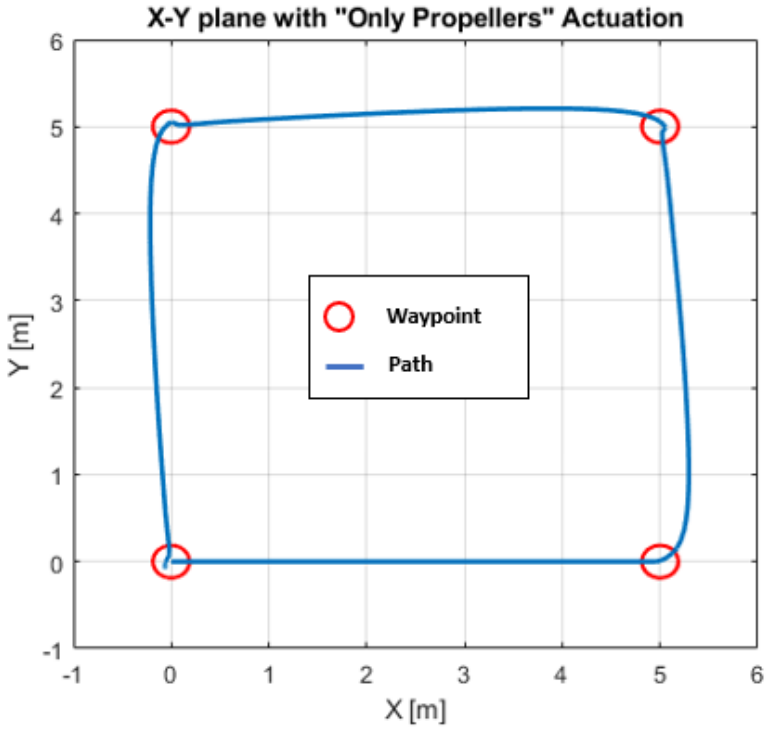

Figure 4.15: Trajectory of the Robotic Fish in the X-Y plane and with "Only Propellers" Actuation

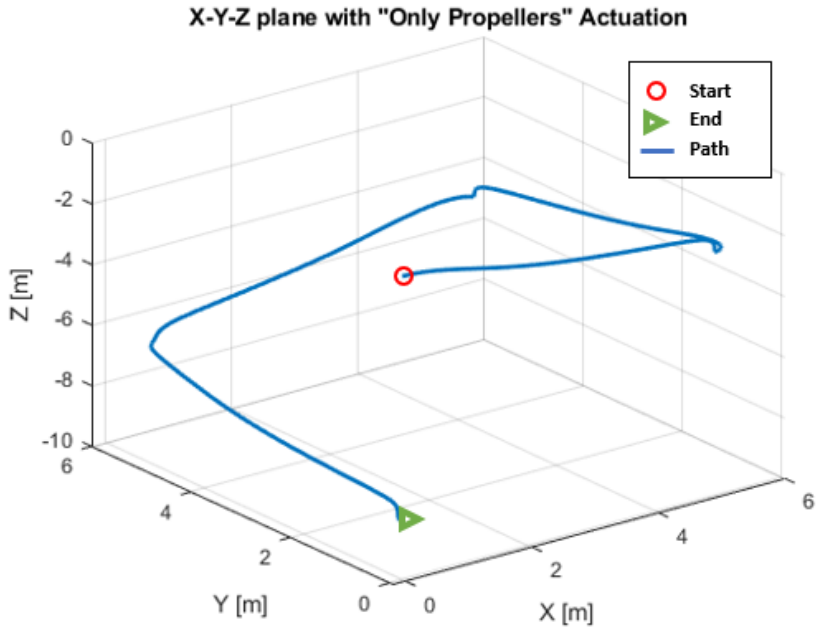

Figure 4.16: Trajectory of the Robotic Fish in the X-Y-Z plane and with "Only Propellers" Actuation

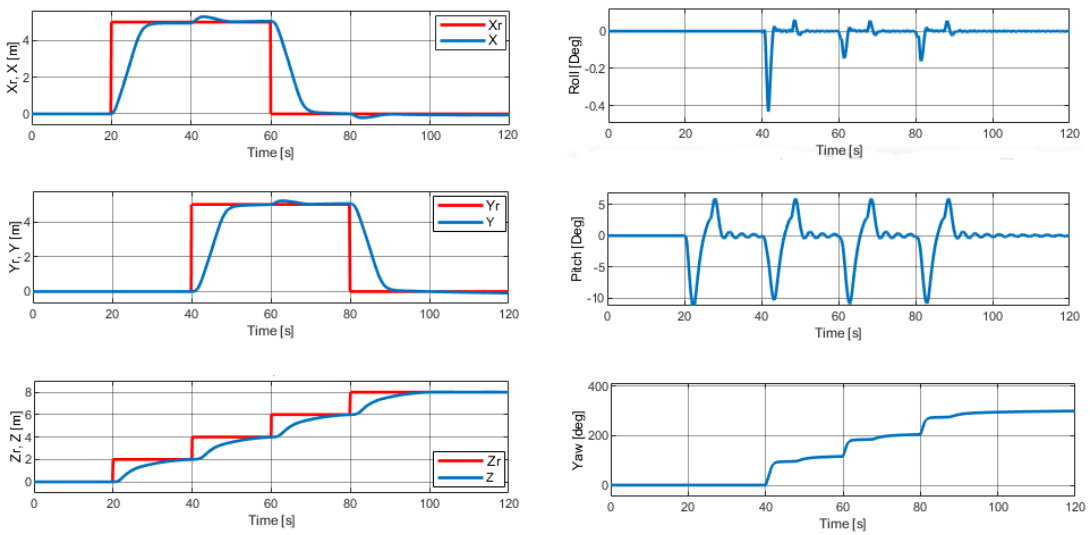

Figure 4.17: Robotic Fish position and attitude during the path with "Only Propellers" Actuation.

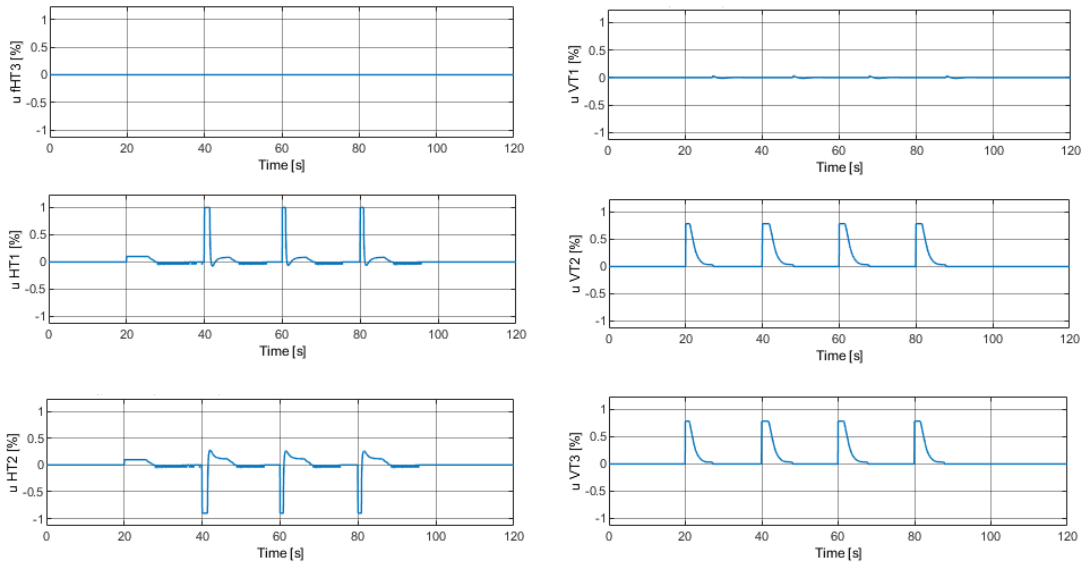

Figure 4.18: Actuator's control signals during the path with "Only Propellers" Actuation

"Normal" case

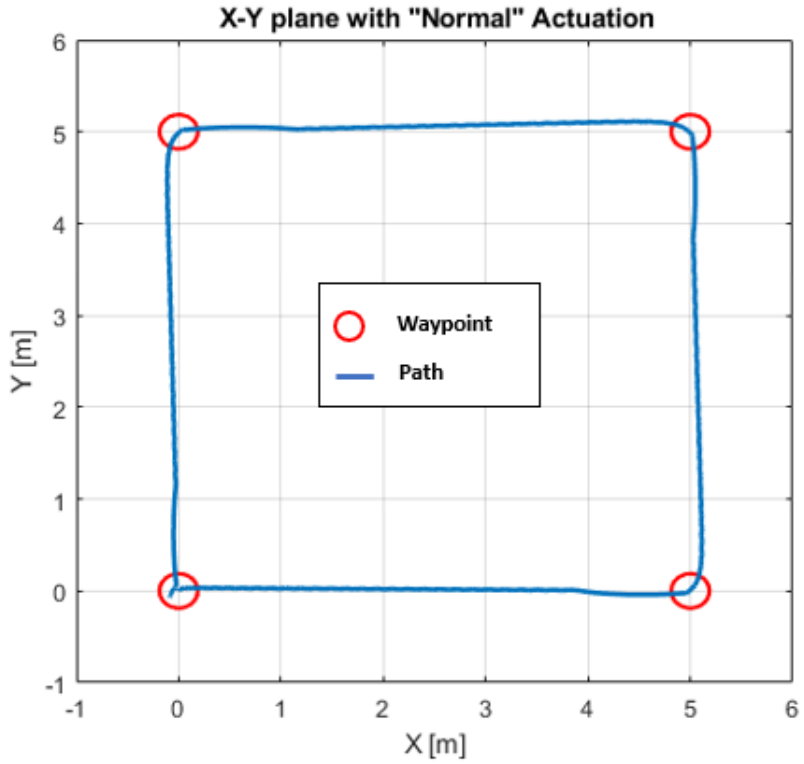

Figure 4.19: Trajectory of the Robotic Fish in the X-Y plane and with "Normal" Actuation

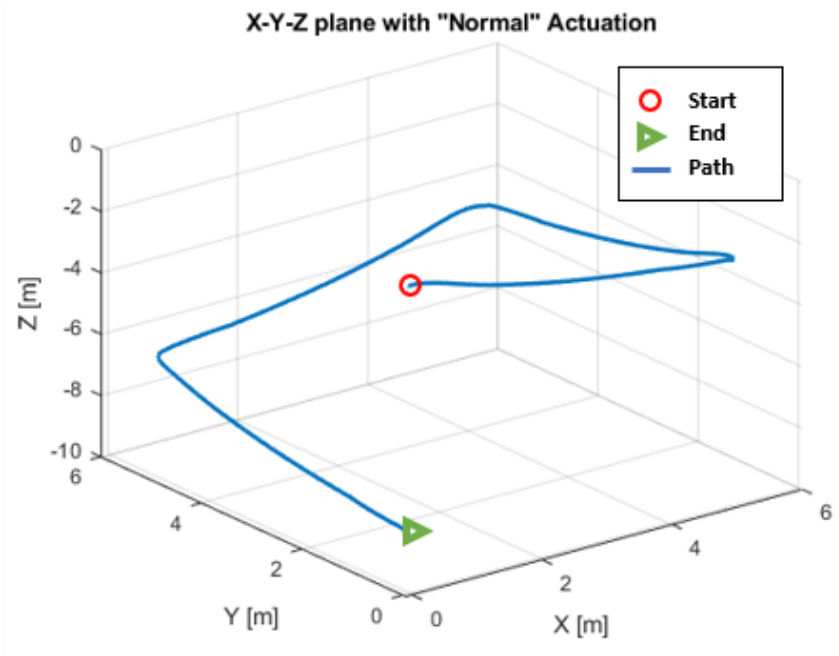

Figure 4.20: Trajectory of the Robotic Fish in the X-Y-Z plane and with "Normal" Actuation

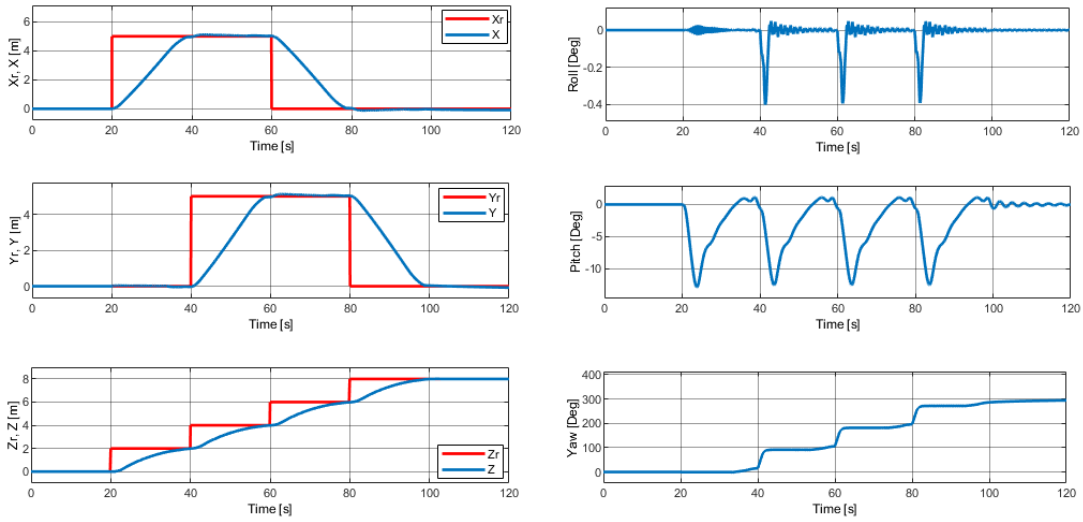

Figure 4.21: Robotic Fish position and attitude during the path with "Normal" Actuation

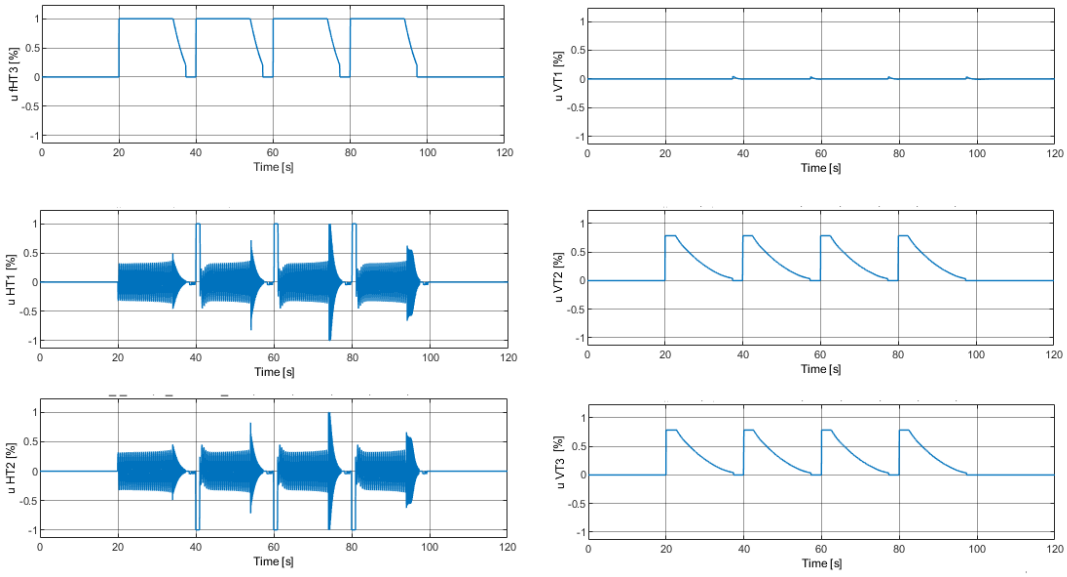

Figure 4.22: Actuator's control signals during the path with "Normal" Actuation

in Figure 4.22 it is possible to notice that the command signals of the lateral propellers (uHT1 and uHT2) present considerable oscillations. This behaviour is due to the fact that the propellers try to compensate the oscillations of the Yaw which are caused by the caudal fin, when it is turned on. In our case, this behaviour of the propellers does not affect the surge motion, but we must also consider that in the mathematical model, the body of the robotic fish has been approximated to a cylinder of radius R and length L. As a future work we could think of implementing a proper mathematical model for the robotic fish and therefore to better analyse this condition of the propellers presented above.

Chapter 5.

GUIZZO 6.0 Virtual Underwater World

The main topic of this thesis is to develop a simulator, in the Simulink environment, of the biomimetic robot's navigation, guidance and control system. This simulator was used to derive simulation results presented in Chapter 3 and Chapter4.

The model includes the non-linear model of the robotic fish with 6 DOF and the propulsion system, described in chapter 3; it also includes the vehicle's NGC system, presented in chapter 4. To further understand the behaviour of the marine vehicle analysed, a virtual underwater world has been developed with GUIZZO 6.0 model in a virtual underwater environment.

This chapter describes the virtual world implemented for the biomimetic robot, going to analyse the "Virtual underwater world" block of the NGC system simulation software shown in Figure 5.1.

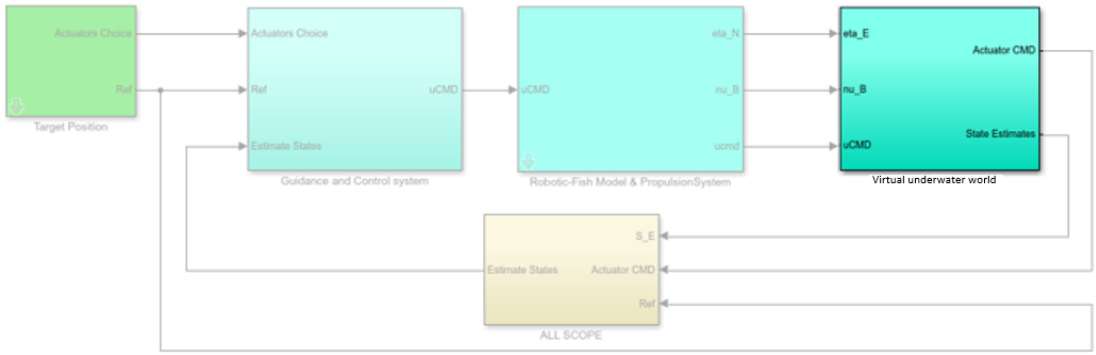

Figure 5.1: GUIZZO 6.0 NGC system simulation software Simulink block diagram.

5.1 Virtual Underwater World

As previously mentioned, in order to test the NGC system and to have a better view of the biomimetic robot's performance, the simulation model has been enhanced with the introduction of the virtual world.

During the Erasmus Internship at the University of Limerick department, CRIS (Centre for Robotics & Intelligent System), a virtual world with a realistic underwater environment was provided by Senior Research Fellow, Edin Omerdic. This virtual underwater world was developed with the model of FALCON and was provided with different objects, in order to evaluate manoeuvring capabilities and performance of the vehicle [37]. The provided virtual world was then adapted for the GUIZZO 6.0, replacing the model of the vehicle FALCON with that of the fish and modifying, also, the underwater environment.

As mentioned in chapter 2, the GUIZZO 6.0 3D model was build using CATIA software. To import this model into virtual world, it was necessary to convert it into a file with WRL extension, which is used for Virtual Reality Modelling Language (VRML) file format. VRML files are known as "worlds", which is what WRL stands for.

After replacing the VRML file of the biomimetic robot with that of the FALCON model, the changes to the virtual environment were made directly in the MATLAB software, using the 3D World Editor (native VRML editor), which is included in the Simulink 3D Animation product.

Once the final virtual underwater world was obtained, it was connected to the simulation software of the robotic fish NGC system.

Simulating, GUIZZO 6.0 simulator generates signals data of the vehicle's dynamics and kinematics (vectors $\eta(t)$ and $v(t)$). By connecting the Simulink model to a virtual world, this data can be used to control and animate the virtual underwater world. The connection between the Simulink model and virtual underwater world is implemented in the simulator software block "Virtual underwater world" (Figure 5.2). A brief description of individual components is given in the following.

5.1.1 – "Underwater world"

The block "Underwater World" (block 1 in Figure 5.2) provides the GUI interface to output signals from Simulink to the virtual underwater world. This block writes values from its ports to virtual world field specified in the Block Parameter dialog box, (Figure 5.3), which can be open selecting SimulationBlock parameters in the Virtual Reality Display (Figure 5.4).

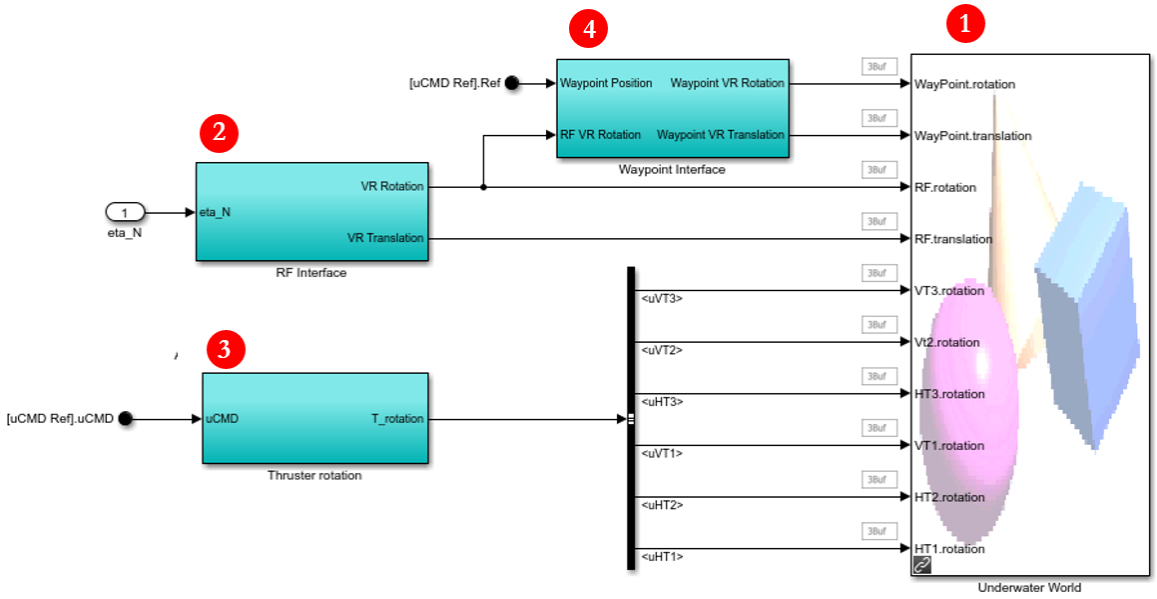

Figure 5.2: Connection between Simulink model and virtual underwater world

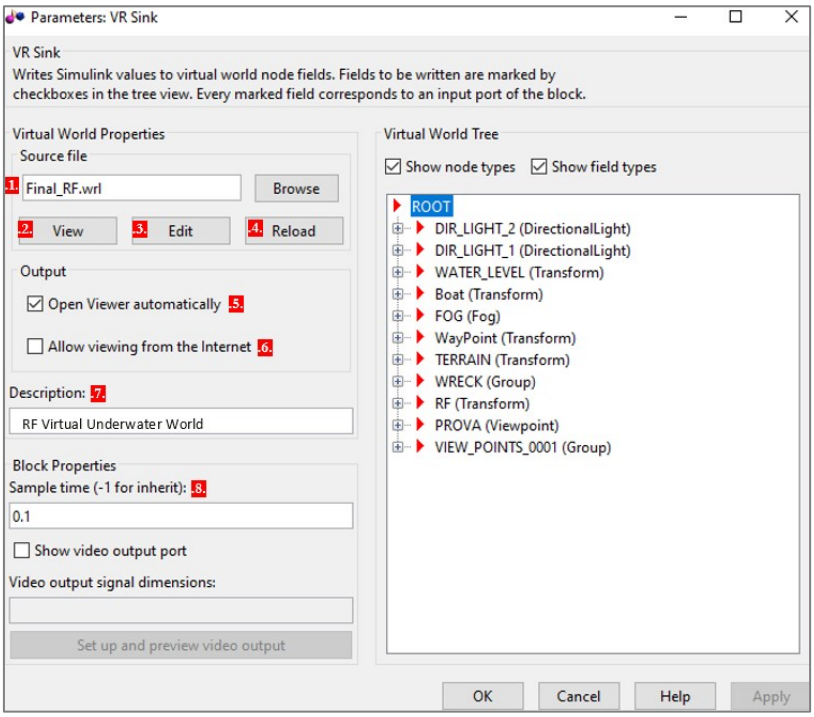

Figure 5.3: Block parameters dialog box "Underwater World"

- **Source file**: asks to insert the VRML file name .1. of the virtual world. The View button .2. allows viewing the world in the Virtual Reality Toolbox viewer or a Web browser. The Edit button .3. launches an external VRML editor, and the Reload button .4. reloads the world after the changes are made. By default, the full path to the associated .wrl file appears in this text box. If only the filename is entered in this box, the Virtual Reality Toolbox assumes that the file resides in the same directory as the model file.
- **Open VRML viewer automatically** .5.: this checkbox, if it is checked, allows to display the virtual world after loading the Simulink model.
- **Allow remote access to world** .6.: allows to view the virtual world on a client computer, or, if it is not checked, the world is visible only on the host computer.
- **Description** .7.: the inserted text will be displayed in all virtual reality object listings, in the title bar of the Virtual Reality Toolbox viewer, and in the list of virtual worlds on the Virtual Reality Toolbox HTML page.
- **Sample time** .8.: Enter the sample time or -1 for inherited sample time. Lower sample time improves the quality of animation but decrease simulation speed. The default value is 0.1s.
- **VRML Tree**: shows the structure of the VRML file and the virtual world itself.

Figure 5.4 shows the Virtual Reality Display. It is the Virtual Reality Toolbox Viewer, which displays a virtual scene with control panel at the bottom.

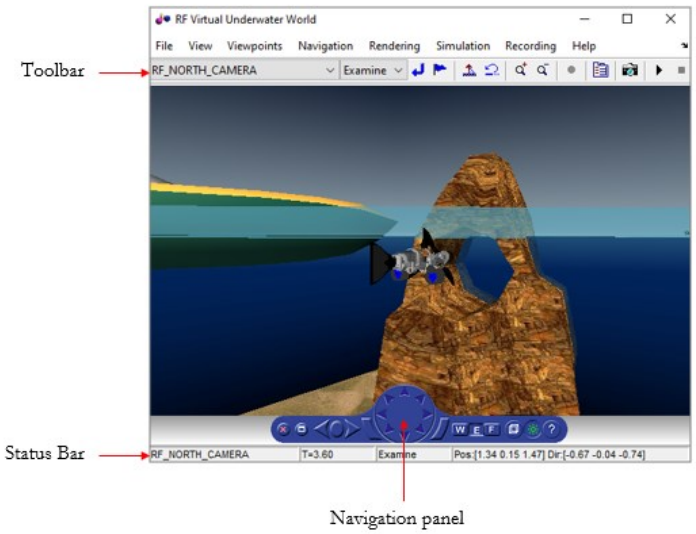

Figure 5.4: Virtual Reality Display.

5.1.2 "RF Interface"

VRML uses the right-handed Cartesian coordinate system $\{VR\}$, which is different from the MATLAB graphics coordinate system. VRML uses system in which the x-axis points to the right, y-axis points upward and z-axis places objects nearer or further from the front of the screen. Each rotation in VRML requires four parameters (three coordinates of principal axes unit vector and principal angle). Because of this, quaternions are a natural way for attitude representation of objects in a virtual world.

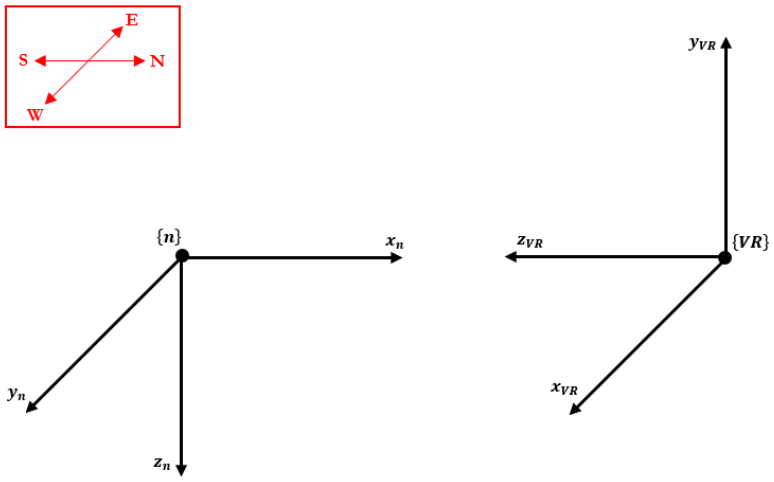

Figure 5.5: coordinate frames $\{n\}$ and $\{VR\}$.

Origins of $\{n\}$ and $\{VR\}$ were chosen to coincide. Position vectors $\boldsymbol{\eta_1} = [x_n \quad y_n \quad z_n]^T$ and $\boldsymbol{\eta_1}^{\boldsymbol{VR}} = [x_{VR} \quad y_{VR} \quad z_{VR}]^T$ are related by

$$-x_n \rightarrow +z_{VR}$$
$$+y_n \rightarrow +x_{VR}$$
$$-z_n \rightarrow +y_{VR}$$

As mentioned before, in VRML orientation of an object is given by a four-parameter vector, which are three coordinates of principal axes unit (a, b and c) and principle angle (ϑ). Thus, the orientation vector in $\{VR\}$ frame is defined as:

$$\boldsymbol{\eta_2}^{\boldsymbol{VR}} = [a \quad b \quad c \quad \vartheta]^T$$

To calculate the robotic fish's attitude quaternions were used, in fact, the orientation expressed in $\{n\}$ frame is given by $\boldsymbol{\eta_2} = \hat{\boldsymbol{q}} = [q_0 \quad q_1 \quad q_2 \quad q_3]^T$. This facilitates the calculation of the vector $\boldsymbol{\eta_2}^{\boldsymbol{VR}}$, which components are obtained as follows:

$$a = q_2$$
$$b = -q_3$$
$$c = -q_1$$
$$\vartheta = 2\,cos^{-1}(q_0)$$

The block "RF Interface" (block 2 in **Figure 5.2**) performs transformation of $\boldsymbol{\eta_1} \rightarrow \boldsymbol{\eta_1}^{\boldsymbol{VR}}$ and $\boldsymbol{\eta_2} \rightarrow \boldsymbol{\eta_2}^{\boldsymbol{VR}}$. The implementation of this block is shown in Figure 5.6.

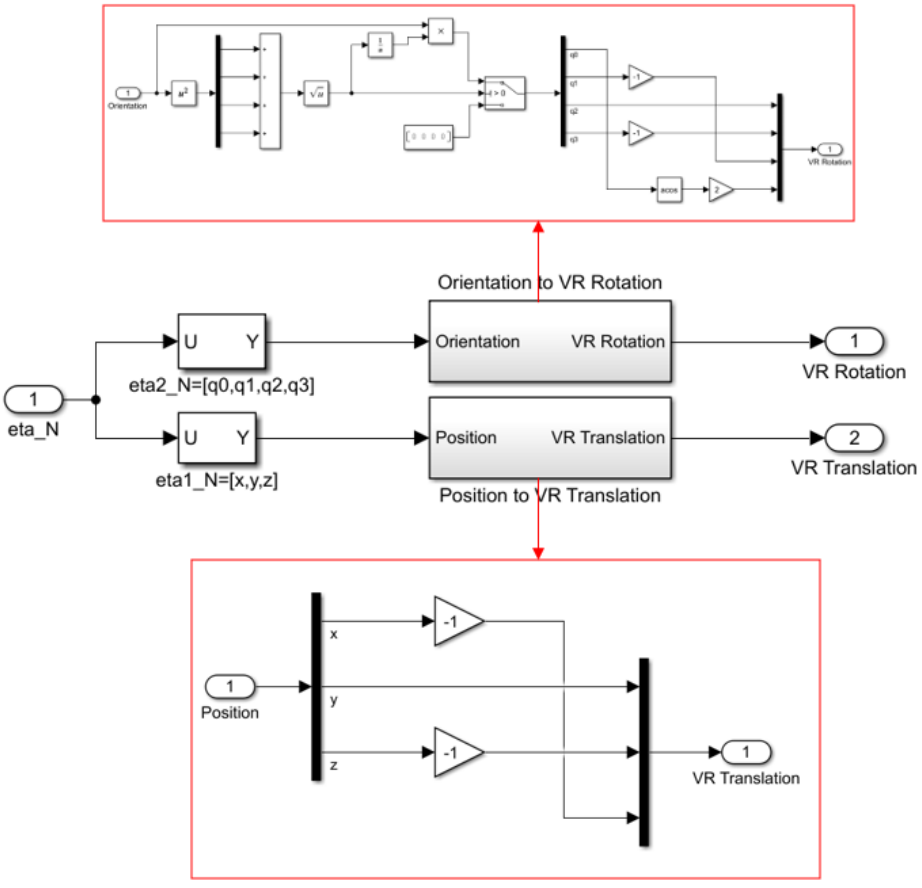

Figure 5.6: "RF Interface" block diagram.

5.1.3 "Thruster Rotation"

This section briefly analyses the "Thruster Rotation" block (block 3 in Figure 5.2). This block generates signals to animate rotation of propellers blade and the motion of the three fins. The velocity of propellers blades and the motion of the fins in animation depends on the performance of the host computer: faster the computer, faster the animation. An in-depth description for the caudal fin's animation is reported below.

To animate the caudal fin, it is necessary to provide the virtual underwater world with the fin's angle of rotation with respect to its vertical axis. Thus, the rotation vector $\boldsymbol{HT3_{rotation}} = [0 \quad 0 \quad 1 \quad \theta]^T$ is provided to the "Underwater world".

To reflect reality, the robotic fish's caudal fin is considered to perform a sinusoidal motion, therefore a sine wave function is used to calculate the fin's rotation angle θ.

This function will have the following characteristics: a constant width, $A = 15°$; an oscillation frequency f, which is equal to the caudal fin oscillation frequency given by f_uHT3 control signal (introduced in chapter 2, and ranges from $0\ Hz$ to maximum of $2\ Hz$); an offset θ_0 which is equal to caudal fin's steering angle (described in chapter 2 and ranges from $-60°$ to $60°$).

Moreover, caudal fin's sinusoidal motion requires a fluid transition when a change of speed, and therefore a change of the frequency, occurs. This fluid transition is obtained by cancelling the phase shift due to the change in the oscillation frequency.

As result, the sine wave function used to calculate caudal fin's rotation angle θ is given as follows:

$$\theta = A\ sin(2\pi t f_1 - (2\pi t(f_1 - f_0) + \varphi_0)) + \theta_0$$

Where f_1 is the new frequency, f_0 is the previous frequency and φ_0 is the previous phase of the sinusoidal wave.

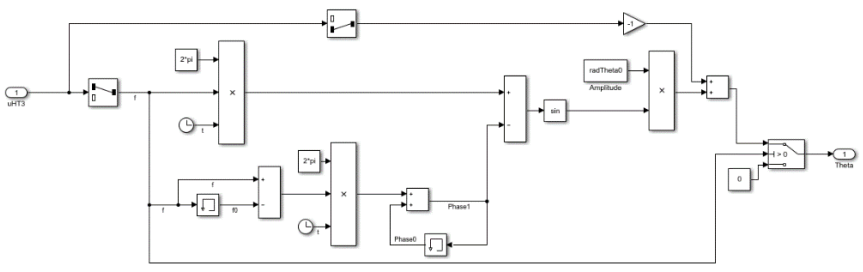

Figure 5.7: Implementation in Simulink of the Sine wave to calculate fin's angle of rotation θ.

5.1.4 "Waypoint Interface" block and Viewpoints

The "Waypoint Interface" block (block 4 in Figure 5.2) has the same implementation as the "RF Interface" block. In fact, the block is used to generate the translation and rotation signals in the coordinate system $\{VR\}$ of a sphere of radius ε. This sphere was inserted for a purely visual purpose; it indicates the position of the reference that the robotic fish must reach. Therefore, the block "Waypoint Interface" does nothing but transform the position of the reference from the coordinate system $\{n\}$ to that of the VRML $\{VR\}$. Figure 5.8 shows the Virtual Reality Display in which the robotic fish is in the initial position and must reach the reference which is indicated by the green sphere.

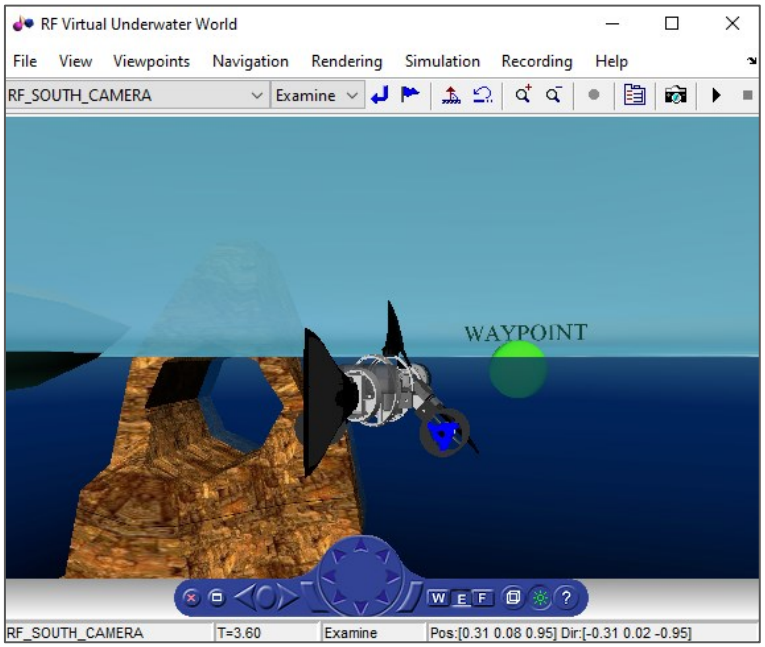

Figure 5.8: Virtual Reality Display with waypoint sphere.

Lastly, as regards the virtual underwater world, a brief description is given regarding the viewpoints that characterize virtual reality. In order to better visualize the scene, there are five different viewpoints located in different places around the robotic fish. These viewpoints move together with the vehicle, so that the distance between each viewpoint and the robotic fish remains constant over time. The orientation of the viewpoints, on the other hand, is fixed in $\{E\}$. A sixth viewpoint is inserted, however, inside the fish to have a front-view of the scene. This is a body-fixed viewpoint, bounded to the vehicle which gives the picture like an on-board camera. The position of this viewpoint was chosen such that the small part of the front side of the vehicle is visible.

The different viewpoints are shown in Figure 5.9 and listed below:

A. RF_NORTH_CAMERA: visualize the scene from the front of the vehicle.
B. RF_SOUTH_CAMERA: visualize the scene from the back of the vehicle.
C. RF_WEST_CAMERA: visualize the scene from the west-side of the vehicle.
D. RF_EAST_CAMERA: visualize the scene from the east-side of the vehicle.
E. RF_UP_CAMERA: visualize the scene from the up-side of the vehicle.
F. RF_INSIDE_CAMERA: on-board camera, visualize the front-view.

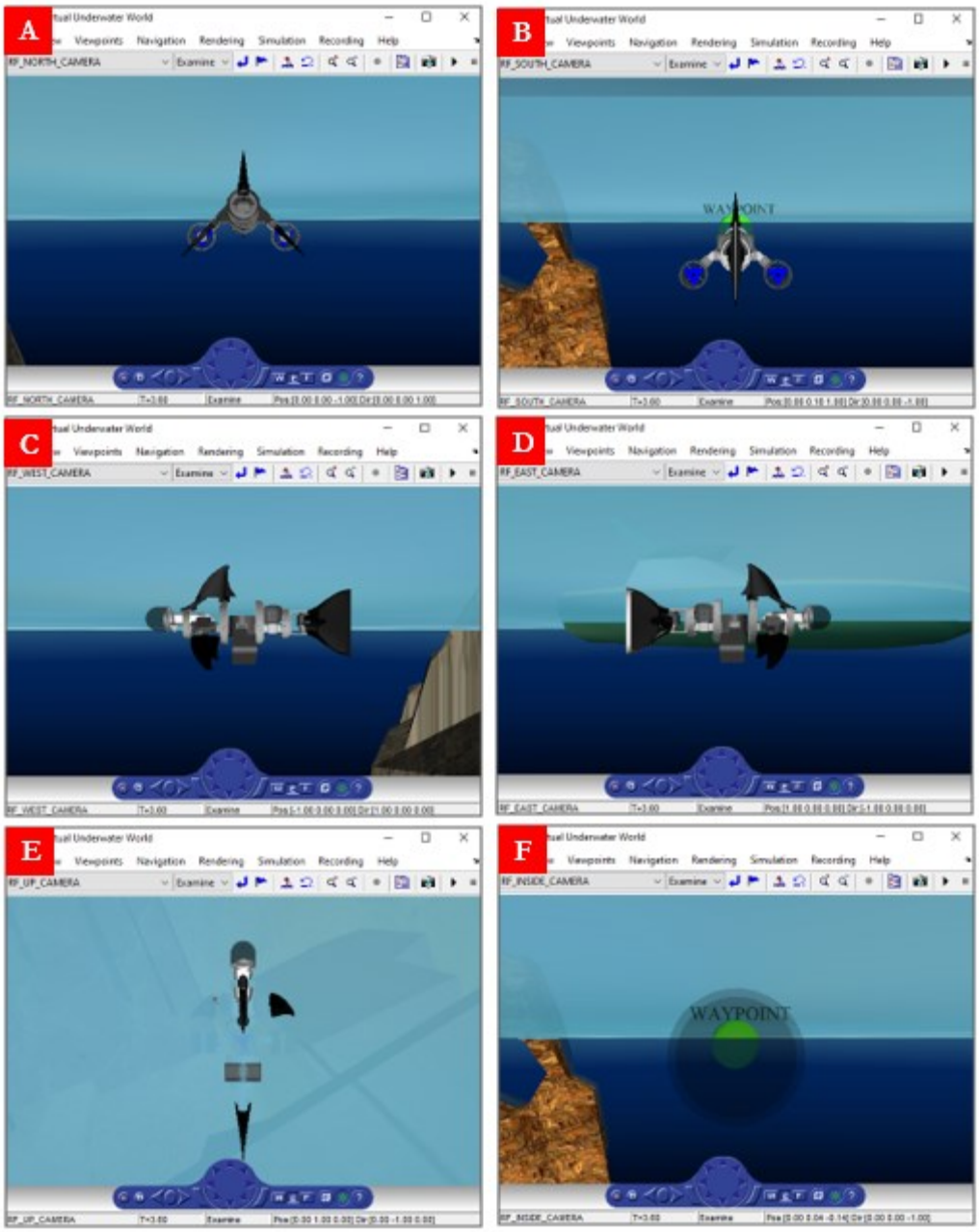

Figure 5.9: Virtual Reality Display with different viewpoints

Chapter 6.

Concluding remarks

As mentioned in the introduction, two goals were presented in this paper: the first is to develop a simulation environment with a three-dimensional graphical interface for the robotic fish GUIZZO 6.0. The second, however, is to design and implement in the simulator a guidance and control system suitable for the vehicle mentioned above.

The prototype of the analysed vehicle was, therefore, described starting from a general description of the biomimetic robots and consequently analysing the 3D drawing of GUIZZO 6.0 model and then proceeding to the description of the mathematical model and the propulsion system implemented in Simulink.

Afterwards, the realization and implementation in the simulator of the vehicle's guidance and control system was reported, and finally the results obtained by the simulation software were reported and discussed.

One of the possible future work that can be done, is to introduce in the simulator disturbances due to the environment in which the robot is accomplishing its mission. For example, ocean currents and wave's mathematical model may be implemented in the simulator, in order to validate the guidance law and control system developed. Furthermore, a non-linear control law, such as Sliding mode or Backstepping control, can be introduced instead of using classic PID, making the whole system more reliable.

Certainly, another future work is the field test of the guidance and control system proposed with a real model of GUIZZO 6.0. In this way it is possible to analyse the energy consumption of the two different types of propulsion systems with which GUIZZO 6.0 is equipped.

Appendix A

GUIZZO 6.0 Parameters

Parameter	Value	Units	Description
m	3.259	Kg	Mass
I_x	0.*0268*	$Kg \cdot m^2$	X axis inertia
I_y	0.0512	$Kg \cdot m^2$	Y axis inertia
I_z	0.043	$Kg \cdot m^2$	Z axis inertia
ρ	1000	Kg/m	Seawater Density
c	0.14	m	Caudal fin Mean Chord
S	0.014	m^2	Caudal fin Area
R	0.05	m	Body Radius
L	0.55	m	Body length
θ_0	15	deg	Oscillation Amplitude
S_{fin}	0.017	m^2	Fin platform Area

Table A.1: Physical parameters

Parameter	Value	Units	Description
$c_{d,f}$	0.5		Drag Weight
$c_{d,t}$	$[0.8 - 1.2]$		Drag Weight
$X_{\dot{u}}$	$0.1m$	Kg	Added Mass
$Y_{\dot{v}}$	$\pi\rho R^2 L$	Kg	Added Mass
$Z_{\dot{w}}$	$\pi\rho R^2 L$	Kg	Added Mass
$K_{\dot{p}}$	0	$Kg \cdot m^2$	Added Mass
$M_{\dot{q}}$	$\pi\rho R^2 L^3/12$	$Kg \cdot m^2$	Added Mass
$N_{\dot{r}}$	$\pi\rho R^2 L^3/12$	$Kg \cdot m^2$	Added Mass
A_f	πR^2	m^2	Circle Area
A_t	$2\pi RL$	m^2	Cylinder Surface
$X_{u\|u\|}$	$\rho A_f c_{d,f}/2$	Kg/m	Cross-flow drag
$Y_{v\|v\|}$	$\rho A_t c_{d,t}/2$	Kg/m	Cross-flow drag
$Z_{w\|w\|}$	$\rho A_t c_{d,t}/2$	Kg/m	Cross-flow drag
$K_{p\|p\|}$	0	Kg/m	Rolling Resistance
$M_{q\|q\|}$	$\rho A_t c_{d,t} L^3/16$	Kg/m	Cross-flow drag
$N_{r\|r\|}$	$\rho A_t c_{d,t} L^3/16$	Kg/m	Cross-flow drag

Table A.2: Added mass and damping coefficients for a cylinder

Parameter	Value	Units	Description
c_{L}	0.5	n/a	Fin lift coefficient
$\mathrm{x_{fin}}$	0.11	m	Fin axial position
$\mathrm{y_{fin}}$	0.11	m	Fin axial position
$\mathrm{z_{fin}}$	0.075	m	Fin axial position
$\mathrm{a_2}$	3.6	Kg	
$\mathrm{a_1}$	-0.026	$Kg \cdot m^2$	
$\mathrm{a_0}$	-0.163	$Kg \cdot m^2$	
$\mathrm{b_2}$	8.952	$Kg \cdot m^2$	
$\mathrm{b_1}$	-0.359	m^2	
$\mathrm{b_0}$	0.012	m^2	
$\mathrm{c_2}$	51.81	Kg/m	
$\mathrm{d_2}$	33.01	Kg/m	
ϕ_{surge}	0.59	Kg/m	
ϕ_{sway}	0.44	Kg/m	
ϕ_{yaw}	0.53	Kg/m	

Table A.3: Bio-inspired Thruster Parameter (Caudal fin, Pectoral fins)

Parameter	Value	Units	Description
$\mathrm{K_{HT1}}$	11.2	N/rpm	HT1 Thrust coefficient
$\mathrm{K_{HT2}}$	11.2	N/rpm	HT2 Thrust coefficient
$\mathrm{K_{VT1}}$	11.2	N/rpm	VT1 Thrust coefficient
$\mathrm{r_{HT1}}$	$[0 \quad -0.11 \quad 0]^{\mathrm{T}}$	m	HT1 point of attack
$\mathrm{r_{HT2}}$	$[0 \quad 0.11 \quad 0]^{\mathrm{T}}$	m	HT2 point of attack
$\mathrm{r_{VT1}}$	$[0 \quad 0 \quad -0.03]^{\mathrm{T}}$	m	VT1 point of attack
$\mathrm{e_{HT1}}$	$[1 \quad 0 \quad 0]^{\mathrm{T}}$		HT1 Thrust direction
$\mathrm{e_{HT2}}$	$[1 \quad 0 \quad 0]^{\mathrm{T}}$		HT2 Thrust direction
$\mathrm{e_{VT1}}$	$[0 \quad 0 \quad 1]^{\mathrm{T}}$		VT1 Thrust direction

Table A.4: Propellers Thruster Parameter (HT1, HT2, VT1)

Bibliography

[1] Lantos B., and Márton L., "Nonlinear control of vehicles and robots". Springer Science & Business Media, 2010.

[2] Wang W. H., Engelaar R. C., X. Q. Chen, and J. G. Chase, "The state of art of underwater Vehicles - Theories and Applications". In Mobile robots: state of the art in land, sea, air, collaborative missions, I-Tech Education, 2009.

[3] Sfakiotakis M., Lane D. M., Davies J. B., "Review of fish swimming modes for aquatic locomotion". Oceanic Engineering, IEEE Journal of, 1999.

[4] Webb P. W., "Forms and functions in fish swimming". Science America, 1984.

[5] Breder C. M., "The Locomotion of Fish". Zoologica, 1926.

[6] Tonello A., "Control and guidance systems for the navigation of a biomimetic autonomous underwater vehicle," MS Thesis, Università degli Studi di Padova,2011.

[7] Barrett D. S., "The design of a flexible hull undersea vehicle propelled by an oscillating foil". MS Thesis, Department of Ocean Engineering, Massachusetts Institute of Technology, 1996.

[8] Anderson J.M., P. A., "The vorticity control unmanned undersea vehicle (VCUUV): an autonomous robot tuna". Draper Technology Digest, 2000.

[9] Atherton E., TS1166-ROBO, "Autonomous fish: swarms, surveillance, and swimming". Boston Engineering, 2009.

[10] Kumph J. M., "Maneuvering of a robotic pike". MS Thesis, Department of Ocean Engineering, Massachusetts Institute of Technology, 2000.

[11] Hirata K., Takimoto T., Tamura K., "Study on turning performance of a fish robot". In Proceedings of the First International Symposium on Aqua bio-mechanisms,2000.

[12] Hirata K., National Maritime Research Institute of Japan, Welcome to fish robot home page, 2000.

[13] Nakashima M., Ono K., "Development and experiment of two-joint dolphin robot". Neurotechnology for biomimetic robots, 2002.

[14] Nakashima M., Takashi Y., Ono K., "Threedimensional manoeuvrability of the dolphin robot". Bio-mechanisms of swimming and flying, 2004.

[15] Dogangil G., Ozcicek E., Kuzucu A., "Design, construction, and control of a robotic dolphin". Proceedings of the International Conference on Robotics and biomimetics,2005.

[16] Liu J., "Modelling and online optimisation of robotic fish behaviours". PhD Thesis, University of Essex, 2007.

[17] Hu H.,"Biologically inspired design of autonomous robotic fish at Essex". Proceedings of the Fifth IEEE UK and RI Chapter Conference on Advances in cybernetic systems, 2006.

[18] Liang J., Wang T., Wang S., Zou D., Sun J., "Experiment of robofish aided underwater archaeology". Proceedings of the International Conference on Robotics and biomimetics, 2005.

[19] Wang T., Wen L., Liang J., Wu G., "Fuzzy vorticity control of a biomimetic robotic fish using a flapping lunate tail". J. Bionic Engng, 2010.

[20] Clapham R. J., Hu H., "iSplash-II: Realizing Fast Carangiform Swimming to Outperform a Real Fish". Robotics Group at Essex University, 2015

[21] Katzschmann R. K., DelPreto J., MacCrurdy R., Rus D., "Exploration of underwater life with an acoustically controlled soft robotic fish" Science Robotics, 2018.

[22] Kato N., "Control performance in the horizontal plane of a fish robot with mechanical pectoral fins". IEEE J. Oceanic Engng, 2000.

[23] Georgiades C., German A., Hogue A., Liu H., Prahacs C., Ripsman A., Sim R., Torres L. A., Zhang P., Buehler M., Dudek G., Jenkin M., Milion E., "AQUA: an aquatic walking robot". Proceedings of the IEEE/RSJ International Conference on Intelligent robots and systems, 2004.

[24] Licht S. C., "Biomimetic oscillating foil propulsion to enchance underwater vehicle agility and maneuverability". PhD Thesis, Massachusetts Institute of Technology, 2008.

[25] Licht S., Polidoro V., Flores M., Hover F. S., Triantafyllou M. S., "Design and projected performance of a flapping foil AUV". IEEE J. Oceanic Engng, 2004.

[26] Festo, AquaRay, 2007.

[27] Yu J., Hu Y., Huo J., Wang L., "An adjustable scotch yoke mechanism for robotic dolphin". Proceedings of the International Conference on Robotics and biomimetics, 2007.

[28] Hu Y., Wang L., Yu J., Huo J., Jia Y., "Development and control of dolphin-like underwater vehicle". Proceedings of the American Control Conference, 2008.

[29] Guo J., "Guidance and control of a biomimeticautonomous underwater vehicle". Advances in unmanned marine vehicles, 2006.

[30] Zhou C., Tan M., Gu N., Cao Z., Wang S., Wang L., "The design and implementation of a biomimetic robotic fish". Int. J. Advd Robotic Systems, 2008.

[31] Scaradozzi D., Palmieri G., Costa D., Zingaretti S., Panebianco L., Ciuccoli N., Pinelli A., and Callegari M., "UNIVPM BRAVe: A Hybrid Propulsion Underwater Research Vehicle", International Journal of Automation Technology, IJAT, 2017.

[32] Costa D., Palmieri G., Palpacelli M. C., Panebianco L., and Scaradozzi D., "Design of a BioInspired Autonomous Underwater Robot". Journal of Intelligent & Robotic Systems, 2017.

[33] Fossen T. I., "Marine Control System-Guidance, Navigation and Control of Ships, Rigs and Underwater Vehicles". Marine Cybernetics, 2002.

[34] Costa D., "Development of biomimetic propulsive system in multiphysics environment". PhD Thesis, Università Politecnica delle Marche, 2017.

[35] Ciuccoli N., "Intelligent system for the exploration of structured and complex environments". PhD Thesis, Università Politecnica delle Marche, 2019.

[36] Stuelpnagel P. "On the Parameterisation of the Three-Dimensional Rotation Group". SIAM Review, 1964.

[37] Omerdic E., "Thruster Fault-Tolerant Control: Thruster Fault Diagnosis and Accommodation System for Underwater Vehicles". 2009.

[38] Antonelli G., "Underwater Robots". Springer, 2014
[39] Fossen T.I., "Guidance and Control of Ocean Vehicles". West Sussex UK, John Wiley & sons Ltd, 1994.
[40] Locke A. S., "Guidance". D. Van Nostrand Company, Inc, 1955
[41] Bryson A. E. Jr., Ho Y. C., "Applied Optimal Control". Blaisdell, Waltham, MA, USA, 1969.
[42] Nazaroff G. J., "An optimal terminal guidance law". IEEE Trans. Automat. Contr, 1976.